Novel Patterning Techniques for Manufacturing Organic and Nanostructured Electronics

by

Jianglong Chen

M.S. Materials Science and Engineering
Massachusetts Institute of Technology, 2003

Submitted to the Department of Materials Science and Engineering in partial fulfillment of the requirements for the degree of

Doctor of Philosophy

at the

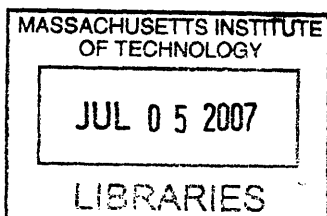MASSACHUSETTS INSTITUTE OF TECHNOLOGY

June 2007

Signature of Author: _____
Department of Materials Science and Engineering
May 11, 2007

Certified by: _____
Vladimir Bulović
Associate Professor of Electrical Engineering and Computer Science
Thesis Supervisor

Certified by: _____
Harry L. Tuller
Professor of Ceramic and Electronic Materials
Thesis Reader

Accepted by: _____
Samuel M. Allen
POSCO Professor of Physical Metallurgy
Chair, Departmental Committee on Graduate Students

Novel Patterning Techniques for Manufacturing Organic and Nanostructured Electronics

by

Jianglong Chen

Submitted to the Department of Materials Science and Engineering on
May 17, 2007 in partial fulfillment of the requirements for the degree of
Doctor of Philosophy in Electronic Materials

Abstract

Molecular organic semiconductors and nanometer size particles are two new classes of functional materials allowing fabrication of electronic devices on low-cost and large area substrates. Patterning these electronic materials requires the development of unconventional techniques, and the scientific understanding behind the manufacture processes.

We introduce the first-generation Molecular Jet (MoJet) printing technique for vacuum deposition of evaporated thin films and apply it to the fabrication of high-resolution pixelated (800 ppi) molecular organic light emitting devices (OLEDs) based on aluminum tris(8-hydroxyquinoline) (Alq3), and the fabrication of pentacene based organic field effect transistors (OFETs) with narrow channel (15 μm) and asymmetric silver/gold contacts. Patterned printing of both organic and metal films is demonstrated, with the operating properties of MoJet-printed OLEDs and OFETs shown to be comparable with the performance of devices fabricated by conventional evaporative deposition through a metal stencil. This MoJet printing technique is reconfigurable for digital fabrication of arbitrary patterns with multiple material sets and a high print accuracy of better than 5μm, and scalable to large area substrates. Analogous to the concept of "drop-on-demand" in Inkjet printing technology, MoJet printing is a "flux-on-demand" process and we show it capable of fabricating multi-layer stacked film structures, as needed for engineered organic devices.

We present the concept and the applications of the second-generation MoJet printing technique. Using this technique, we demonstrate patterned molecular organic semiconducting thin films directly printed by a three-step local evaporative deposition, in conjunction with using the HP thermal InkJet printing technology. This MoJet printing technique can be applied to pattern solution-processable molecular organic thin films, providing flux-on-demand in an ambient environment.

We develop an Inkjet assisted micro-contact printing technique for the patterning of colloidal semiconductor nanoparticles. Active OLEDs incorporated with a uniform thickness layer of colloidal nanoparticles are fabricated by using this Inkjet printing plus stamp transferring technique. The material usage efficiency is largely boosted.

To our knowledge, these three novel patterning techniques presented in this study provide for the first time unprecedented capabilities for manufacturing organic and nanostructured electronic devices.

Thesis Supervisor: Vladimir Bulović
Title: Associate Professor of Electrical Engineering and Computer Science

Acknowledgements

I am grateful to my thesis supervisor, Prof. Vladimir Bulović, for his guidance and inspiration. He is always willing to share his knowledge, expertise and excitements with the fellow group members. And his advice always leads me to the right direction. Special thanks to my thesis committee members, Prof. Marc Baldo, Prof. Angela Belcher and Prof. Harry Tuller. They have suggested improvements to my thesis and given me many insightful comments despite of their very busy schedules.

I would like to acknowledge my collaborators in this study. Valérie Leblanc has spent countless hours making MoJet printhead chips and testing them in the clean room, without these MEMS chips the MoJet project wouldn't be possible. The director of MEMS@MIT center, Prof. Martin Schmidt, introduced me to Prof. Bulović and the LOOE group, and has frequently offered insights about the MoJet project and shared his "real world" experience at the MoJet weekly meetings. Sung Hoon Kang joined the MoJet I project at a very early stage and assisted with assembly of the Mojet I printer and characterization of the MoJet I printhead. Jennifer Yu 's "down to the details" attitude in studying the PDMS stamp is the key to the successful demonstration of QD-LED devices. Jonathan Halpert and Hao Huang in Prof. Bawendi's lab provided me very valuable quantum dot solutions and relevant information whenever needed; Annie Wang in Prof. Akinwande's lab helped me access the probe station that I could test the pentacene transistors.

I would like to thank the entire LOOE group for your encouragement and stimulating discussion, and all the fun of doing the rotation between team Kora and Ookami. I also thank Hewlett-Packard scientists, Dr. Paul Benning, Dr. David Schut, Dr. Peter Madilovich and Dr. Murali Chapalara, and the Imaging and Printing Group (IPG) in Corvallis, for their great support financially, technically and morally.

Lastly I must thank my family for giving me their love and full support. At MIT it is hard to be both a graduate student and a good spouse at the same time. I thank my family, especially my wife Liling, for their unselfish sacrifices that made my thesis possible.

Contents

Chapter 4. Second generation Molecular Jet printing technique

Chapter 5. Inkjet printing nanocrystal solutions

Chapter 6. Inkjet assisted stamping nanocrystal OLED

Appendix

List of Figures

11

List of Tables

Preface

The method of printing, one of the four great inventions of ancient China (together with compass, gunpowder and papermaking), was first conceived before the 6th century, and later spreaded through the Silk Road to Middle East and Europe, where it was further developed in the 15th century. Since the invention of printing technology, it has largely revolutionized how information is stored and shared. Today printing technology has evolved dramatically beyond laying down ink on paper. In this dissertation, implementation of novel printing technologies in the fabrication of electronics and optoelectronics devices by using unconventional ink materials will be illustrated and related research results discussed.

Compared with the long studied conventional ink for printing graphic arts and texts, the new functional ink materials, including organic molecular solids and nanometer size particles are a new face, promising to enable new paradigms in large area electronics development through printing, with their final applications still largely undefined. Nevertheless , comparing today's printed electronics technologies to the early days of the semiconductor microelectronics industry, many similarities can be identified.

Nowadays silicon transistor based integrated circuit technology and its applications are changing our daily lives in many aspects. Parallel to the research devoted to shrink the transistor size and increasing its switching frequency, considerable attention is also devoted to applications that require large area electronic systems, greater than the size of the largest silicon wafer, e.g. 12" diameter, where the traditional material (e.g. single crystal silicon) and patterning technique (e.g. photolithography) are not seen as the ultimate technical solution. Among the technological alternatives that are being vigorously pursued, organic semiconductors and nano-structured materials have been identified as promising candidates because of their optical and electrical

17

versatility, unrestricted by single crystal structures, their ability to be deposited on wide range of substrates at room temperature, and deposition processes implementable over large areas. However, despite bright future of the organic and nano-structured electronics, their manufacture process is still strongly tied to the development of novel patterning techniques, that can precisely control deposited film thickness with the incremental resolution of less than 10 nm and lateral patterning accuracy of better than 10 μm.

To answer the technology challenge of developing a high resolution printing technology for organic and nanostructured materials, the present dissertation proposes and demonstrates three new printing techniques, and validates these printing technologies with fabrication of active electronic and optoelectronic structures.

The dissertation starts with the general overview of printing technologies in the first chapter, including plate-based analog printing technologies and plateless digital printing technologies. Advantages and shortcomings of each sub-category with regard to the print quality and the system complexity are compared. Due to the weak van der Waals bonding nature in the molecular organic structure, the resulting non-photolithographic patterning techniques in the manufacturing of organic devices are outlined in the second chapter, where the need to develop a solvent-free, high-resolution, digital-fabrication patterning technique is addressed. Solvent-based fabrication is normally used for patterning polymeric devices for its low cost potential, while thermal evaporation method has typically yielded high quality, high purity and therefore high performance molecular thin film devices with multiple-layered structures. In the third chapter, we describe our new Molecular Jet printing technique (abbreviated MoJet) which combines the ease of the direct printing technology with the high quality of evaporated thin film structures to enable deposition of electronic quality molecular films with unprecedented resolution. We

outline the operating principles of the first generation Molecular Jet printing technique, and quantify the parameters that control the profile of deposited films. Results of using this printing technique in vacuum to define molecular organic semiconductor based organic light emitting devices (OLEDs) and organic field effect transistors (OFETs), as well as metal patterns with negligible distortion are discussed, followed by a summary of existing challenges associated with this first generation Molecular Jet technique. In the fourth chapter, we present an alternative printer design, named the second-generation Molecular Jet technique. Performance improvements, including capability of patterning molecular organic thin films in ambient are introduced. The Molecular Jet printing technique as a whole is a promising alternative to manufacturing molecular organic electronics. We then shift our topic to patterning techniques for other unconventional electronic materials, including metal nanoparticles and colloidal semiconductor quantum dots. The main challenge in patterning these new nanostructured material systems is the low material usage efficiency in today's deposition techniques, requiring significant overproduction of sometimes expensive nanostructured materials. In chapter five we demonstrate that the thermal inkjet printing technique can reduce the waste of the printed nanostructured electronic materials. The mechanism of the inkjet printed pattern formation is studied and detailed analysis is provided. In chapter six, we propose a new patterning technique for forming uniform colloidal quantum dot layers by using inkjet assisted microcontact printing (stamping) method. We study the interaction between the ink vehicle and the substrate surface, suggest choices for optimized printing conditions, and demonstrate a light emitting device that utilizes stamp-printed colloidal quantum dots as electrically excited lumophores.

We hope that the present study of patterning these nanostructured functional materials by innovative printing technologies will lead to new insight of some old problems and assist in the

discovery of effective methods for fabrication of large area electronic devices, that are poised to

become ubiquitous with the advent of printing techniques.

Chapter 1. Introduction of printing methods

CONTENTS

1. Overview
2. Analog printing technologies
3. Digital printing technologies
4. Summary

1. Overview

Printing processes in general produce graphic **patterns** (texts or images) by applying **image carrier** with **ink** (dyes or pigments) onto a **substrate** (such as paper) as it travels through a **printer** (or press). The underlined items are five essential elements of a printing process. In analog printing, a gravure cylinder, a press plate and/or a screen can be an image carrier; in digital printing, the image is stored in digital format and must be generated at each output. Here the image carrier becomes a "virtual press plate" by programming the moving path of a printhead. Classifications of well-established printing technologies are shown in **Figure 1-1** [1,2]. Conceptually to most people, printing is only about "ink" and "paper", but it is actually not limited to any particular "ink" or "substrate", especially when patterning of electronic functional materials is involved, which is the central topic of this thesis.

2. Analog printing techniques

Plate based printing is the oldest method to print books and graphics. Four most commonly seen plate based printing techniques are shown in **Figure 1-2.** The original press plates were made out of baked clay or handcrafted wood, later the moving type printing system was invented in 1041 by a Chinese craftsman *Bi Sheng*. The repetition of characters is carried out by inking the plate surface first, where the image area is raised above the rest non-image area, then the paper is

placed atop in contact with the plate and a smooth board presses the paper over the plate. The paper is then peeled off and left to air dry. The plate can be reused to produce the same image repeatedly. Today many letter presses still operate in the same way for printing letterhead, envelope, special invitation etc, all of which are sharing the same underlying working principle that is called "relief printing", similar to what was done over a thousand years ago.
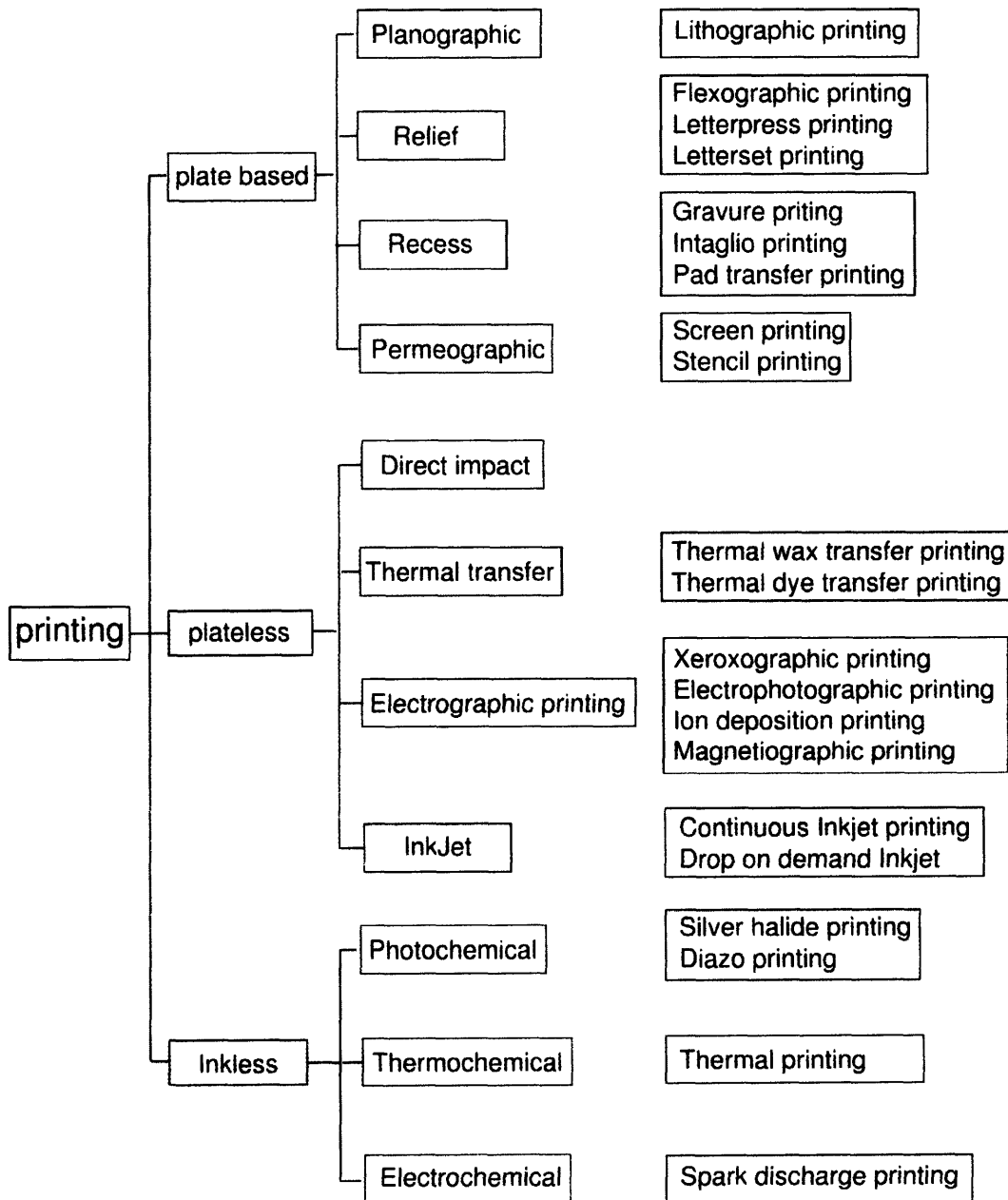
Figure 1-1. Classification of printing technologies

22
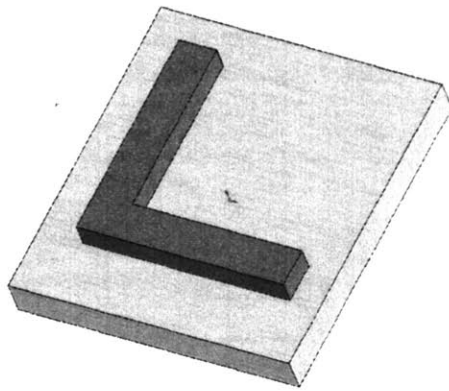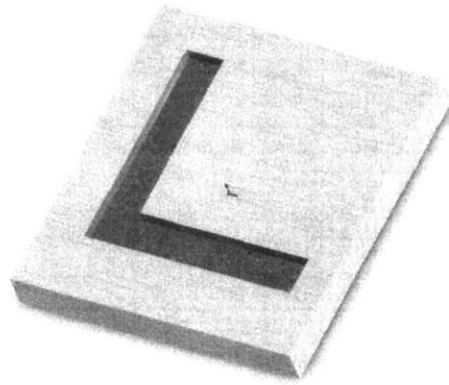
A. Relief printing

B. Recess printing
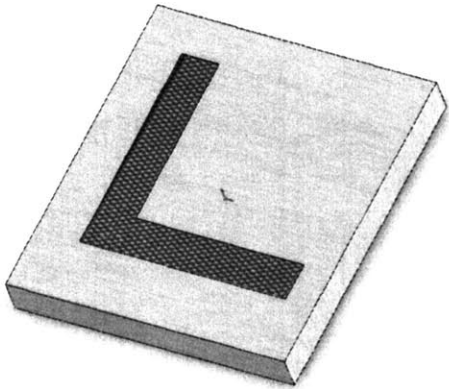
C. Planography printing
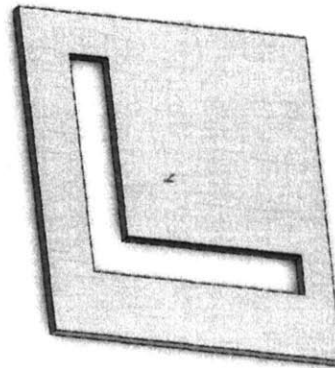
D. Through printing

Figure 1-2. Plates used in analog printing process

Relief printing

Relief printing works by impressing to the paper with only the raised part of the printing surface on a print plate. Ink roller only touches the raised area, the surrounding areas are lower thus don't receive ink. The inked imaged is transferred to the paper by impression and relief.

The press plates are normally made out of zinc, magnesium or copper. Photopolymer films can also be used to make press plates, most often as the wraparound press plates in flexography. The plate patterning is done through photochemical wet etching, similar to the mask-making

process in microelectronic industry, by coating photoresist to the plate surface, doing sequential

exposure and final emulsion in etchant solution.
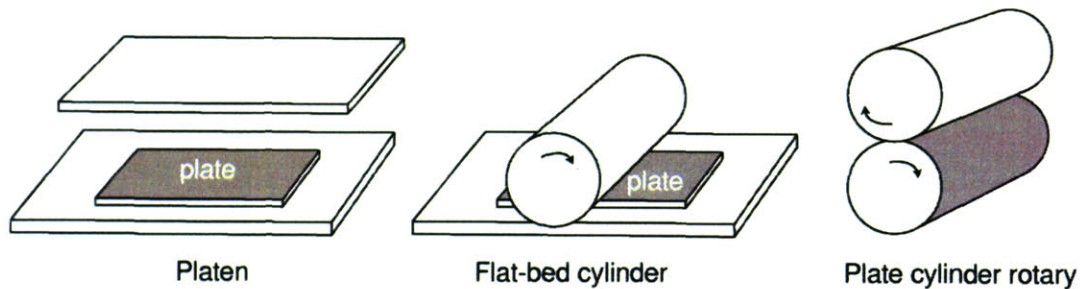
Figure 1-3. Printing methods in conventional plate based printing press
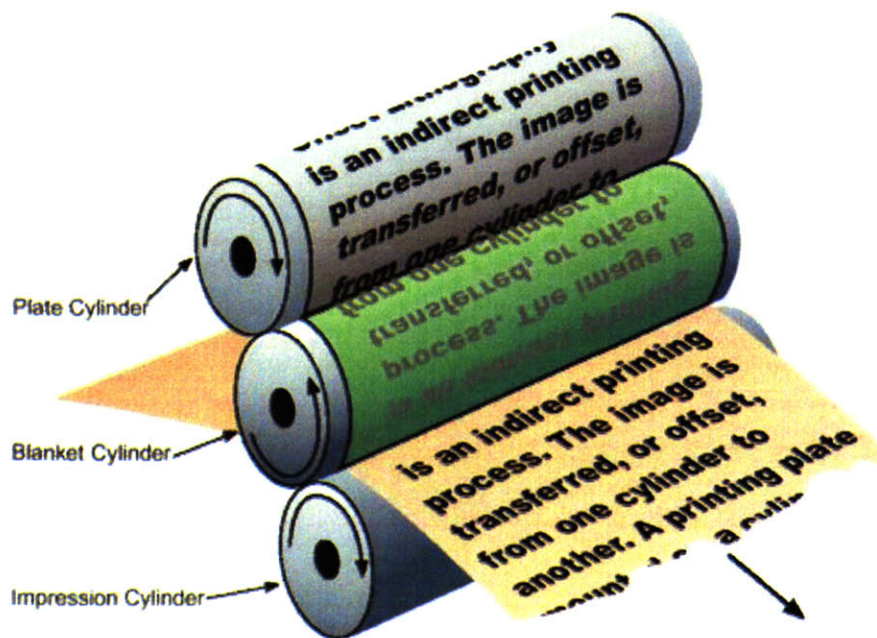
Figure 1-4. Rotary offset printing technique

According to the shape of the plate or the roller, the presses can be three types: **platen press,**

flat-bed cylinder press and **rotary press**, as shown in **Figure 1-3** [2]. In both the platen and the

flat-bed cylinder type presses, plates are mounted on a flat surface, typically for small print runs

such as embossing customized logos or letterheads. Rotary press is the most efficient among

these three types and usually is used for long print runs. It utilizes a plate cylinder and an

impression cylinder. Paper either in individual sheet form or a continuous web from a large roll

passing between two cylinders is pressed to make the printed impression on the paper. Multiple colors can be printed in a single pass by lining up several such press units in series, as illustrated in **Figure 1-4** [3].

As mentioned earlier, flexible (thus curved) relief plates are utilized in flexography, a high-speed and versatile printing process. It is still one of the fastest growing printing processes, which is well suited for printing large area solid colors on a variety of substrates. Typical flexography systems are shown in **Figure 1-5** [3].
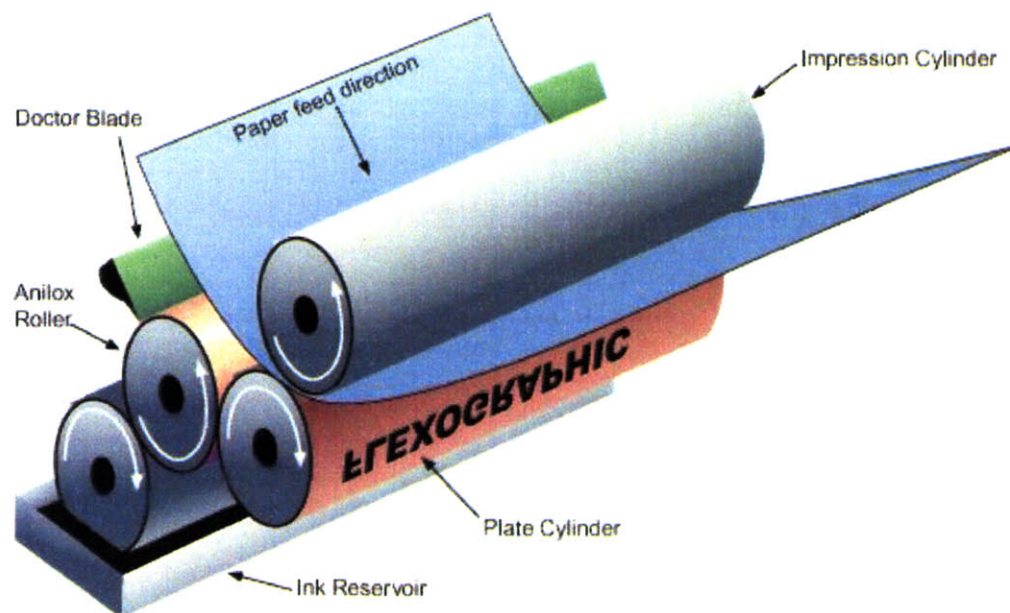
Figure 1-5. Flexography printing technique

Planographic printing

As opposed to print from a raised surface in the relief printing, planographic printing utilizes a flat surface, as shown in **Figure 1-6**. The most widely used technique is called lithography (French autography). The image is formed based on the principle that water and oil do not mix thus separating image and non-image areas. On the printing plate (normally metal zinc or aluminum) the image area is treated with greasy substance that repels water but retains ink; the

non-image area is processed to be still water receptive. After the printing plate is flooded with water, only the greasy area will accept the ink made of oil and the non-image area will remain water covered.
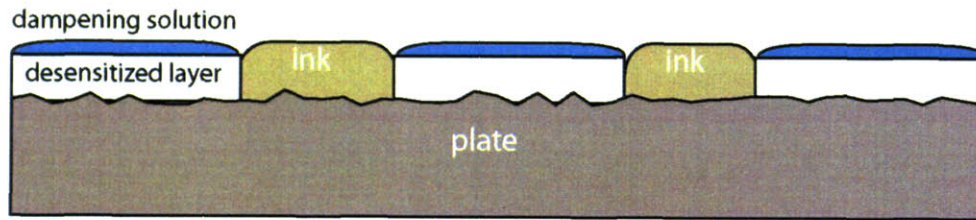
Figure 1-6. Schematic diagram of planograhy

Depending on how images are transferred from the flat plate to the paper, lithography printing can be divided into two categories: direct litho and offset litho. In the offset litho, the image is first transferred onto the surface of a rubber blanket image carrier mounted on a cylinder and then transferred onto the paper. During the transfer the image on the rubber blanket is a mirror image of that on the print plate and the paper.

The making of the litho printing plate is mostly done through a photolithographic process, where the image area is defined by patterning metal plate base coated with negative photopolymer. Instead of etching the metal plate, the exposed areas are coated with hydrophilic substance such as gum Arabic. If the plate is made out of synthetic silicone rubber, in light of its very low surface energy, neither water nor oil ink will wet its surface, which eliminates the need of dampening water during the print. This gives litho printing the advantage of simplicity besides its low cost, high speed and good print quality.

Recess printing

The illustration shows a close-up of the three different varieties of cells used in gravure printing.

The cells shown above are the same in area but different in depth.

The cells shown above are the same depth but different in area.

The cells shown above are different in area and depth.
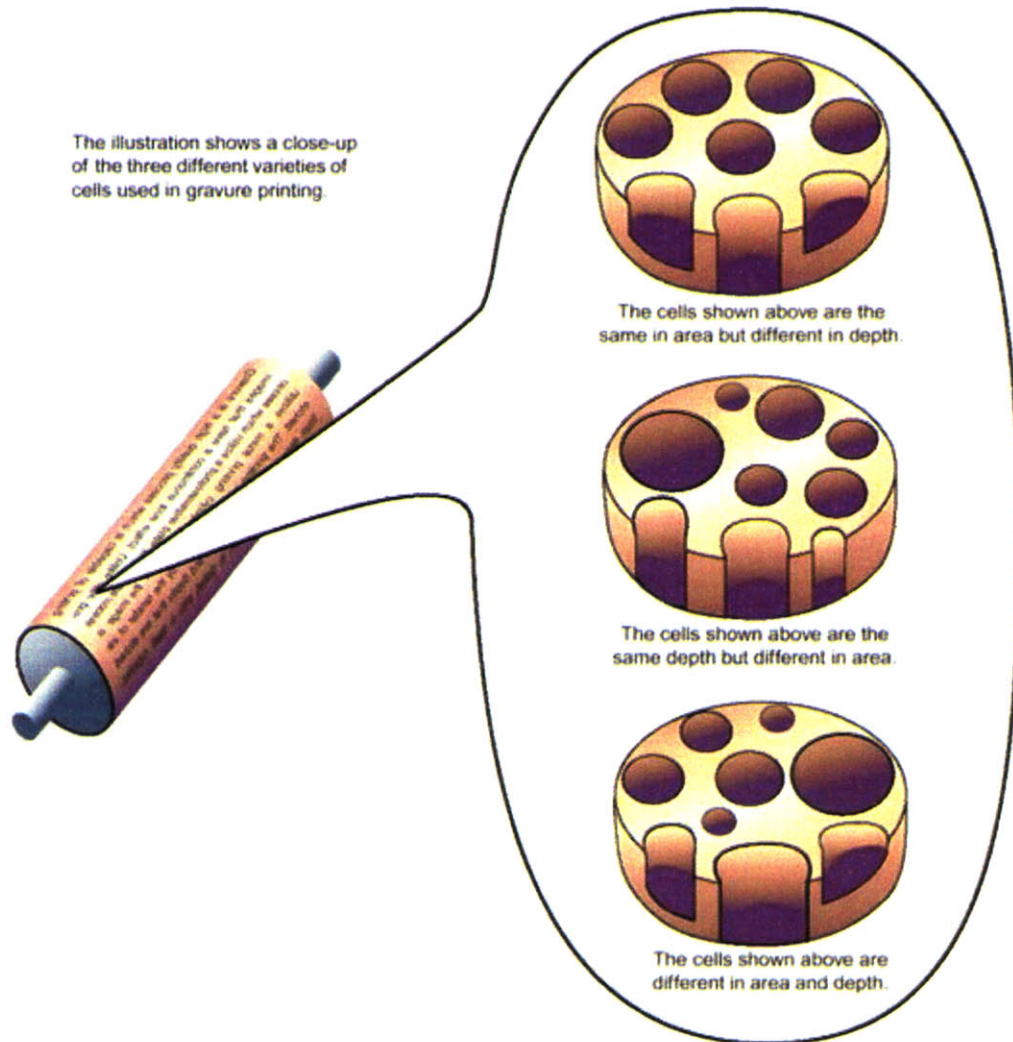
Figure 1-7. Recess printing plate examples

Recess printing operates by a different working principle in which the images are transferred from engraved or sunken recesses in the image carrier, while the unetched areas represent the non-image areas, as illustrated in **Figure 1-7** [3]. This characteristic decouples the surfaces used for making impression and the ink-carrying surface, allowing a long and durable printing run without much degradation. The etched or engraved recess cells also enable the reproduction of continuous tone and high quality images such as a photograph. It is the preferred choice for large volume, high quality printing jobs.

There are several variants in the recess printing method. In the earlier age, a refined printing process called **intaglio** was invented in Germany. Fine art images (usually with tonal effects, like a shadow) are hand carved onto a copper plate surface so that ink can fill into these areas. Originated from the intaglio process, gravure printing uses a similar plate but the volume (depth, or opening size) of engraved cells varies so that the tone of the image can be changed. For example, when a dark tone area is engraved onto the print plate the cells are deeper.

Gravure process with copper cylinder can be adopted onto a rotary printing press, called the rotogravure system. The plate cylinder rotates in the bath of ink and is inked all over; a squeegee type doctor blade wipes off the excess, so the ink only stays in the cells and is then picked up from the press cylinder to the substrate (paper) when the cylinder is pressed against the paper to make a print, as shown in **Figure 1-8** [3]. The process is then repeated many times.
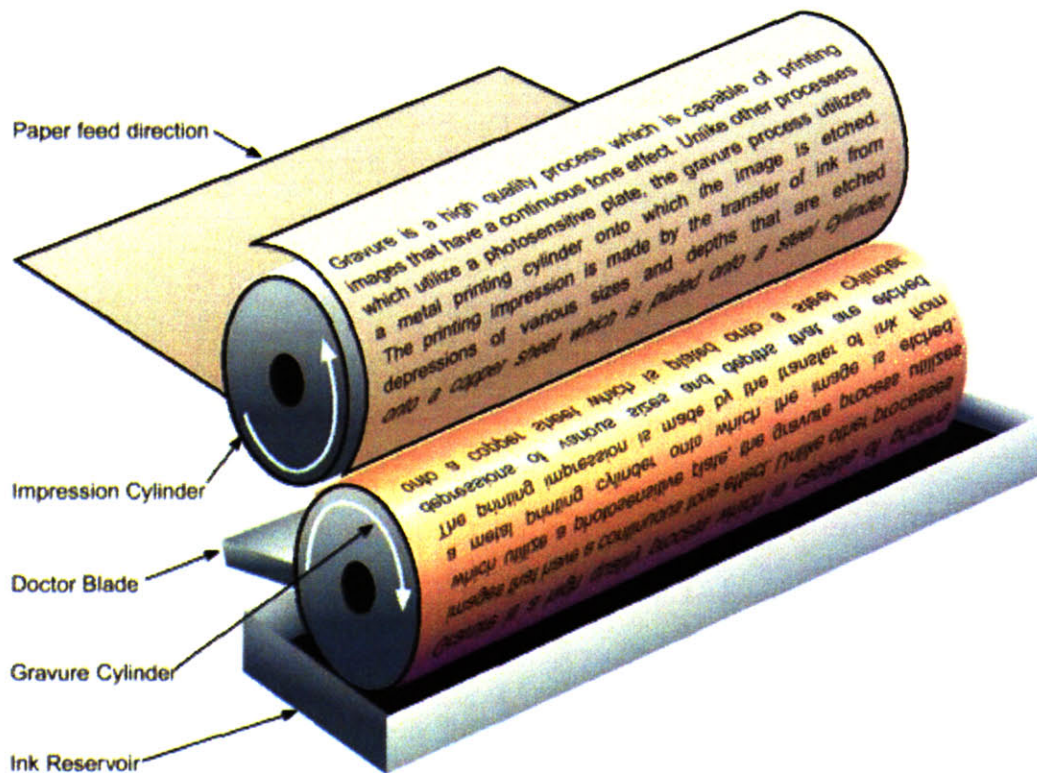
Figure 1-8. Gravure process

The gravure plates are conventionally engraved by using a sensitized medium called carbon tissue to transfer the image onto the plate surface. This gelatin medium is positioned onto the plate and soft emulsion hardens in proportion to the exposure light flux through a continuous tone image (positive transparency shadow mask). After exposure and removal of the paper back, the sensitive layer is developed and the plate is covered with squares of equal size but varying heights. In the next stage the plate is etched in ferric chloride solutions, where the etching is affected by the cover medium. Squares that are etched first are deeper and hold more ink than the shallow ones. Nowadays photoresists replace the carbon tissue, so that the image can be engraved onto the gravure cylinders in a digital manner by a diamond styli or laser beam. The finished copper plates are often electroplated with a layer of chromium so that the friction of the blade doesn't wear off the copper plate. For longer durability than the conventional gravure print, ink cells of the plate are developed with various sizes and depths. In the light density shadow areas the cells are small but deep. This kind of plate-making is most suitable to be digitized by a scanning high-power laser beam. Once the plate is made, the image can be transferred onto the paper directly or through another image carrier cylinder.

Through printing

Unlike other plate based printing, the through printing utilizes a porous medium as the image carrier [4]. The image areas are permeable to the ink to access the substrate, while the non-image areas act essentially as a stencil to block off the ink. Two significant advantages of through printing (represented here by screen printing process) are versatility on choosing print surface and low print equipment cost. As a result, screen printing method is widely used in industrial applications, from dying textile, printing labels, forming contact pads, to printing circuit board.

There are several ways to make a screen printing plate. The desired graphic used to be hand painted onto the screen by the artist. However, for industrial applications, the method has to be highly automatic. The screen is precoated with a layer of photo emulsion layer and then exposed to light through a positive mask where the image areas are opaque. The non-image areas allow light to pass through and harden the emulsion. Then the screen is washed thoroughly to dissolve the image overlay area, leaving a negative screen image on the screen.

The impression of ink onto the substrate is made by using a squeegee to spread the ink and force it through the fine mesh of the screen, which is illustrated in **Figure 1-9** [3]. The simplest setup only requires the print screen with a frame and a rubber squeegee that one person can easily handle. The resolution and the size of image are limited by the mesh count and the frame size. The thickness of ink pressed on the substrate tends to be thicker than those of plate printing methods, which may lead to an additional ink drying step in the printing process.
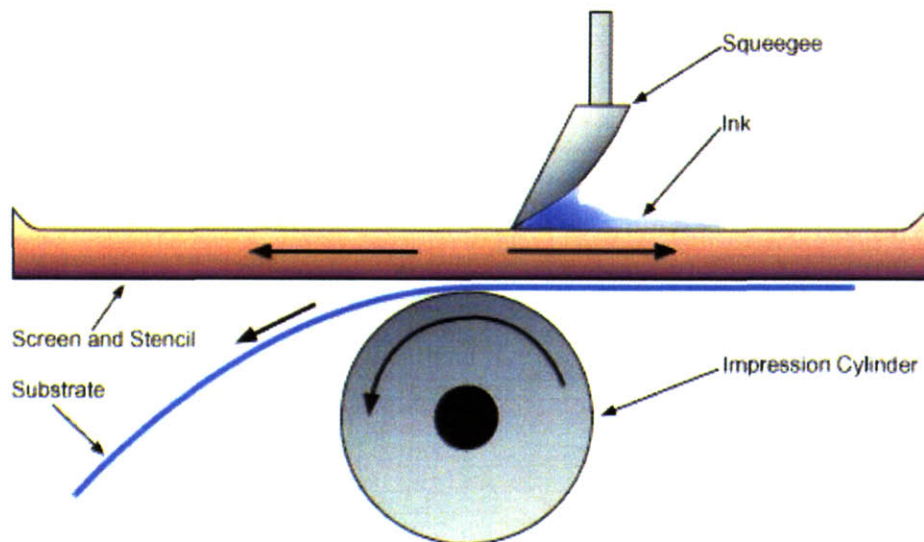
Figure 1-9. Screen printing technique

3. Digital printing technologies

The digital version of graphic and text is discretized into small units such as lines and dots/pixels. Each unit's coordinate and color information is defined by bits. Specific encoding format might vary as a file is created and saved. Our focus here is how to covert the electronic information to hardcopy prints for direct visualization. This requires the printer to be able to reconfigure to generate different outputs.

Impact printer
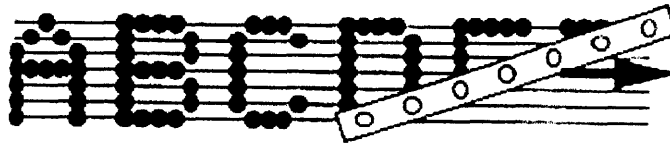
Figure 1-10. Direct impact dot matrix printing

The early accomplishment is the introduction of dot-matrix printer, which forms characters and graphics by direct impact on a carbon ribbon tape using a multiple pin mechanical printhead, shown in **Figure 1-10** [5, 6]. Each pin is addressable to form dots on the paper, as the printhead moves across the slider bar, dots were printed in the pattern of characters. The pin layout on the printhead determines the print speed and resolution. In the early 1980s, Epson released one of the first dot matrix printers, MX-80, which was very popular as the best selling computer peripheral. Dot matrix printer operates by striking the carbon tape against the paper, several pages can be printed simultaneously. This is useful to duplicate invoice copies, for example, in the cashier counter, point of sale terminals (POS) or ATM these days. However, the inherent mechanical impact head makes the printer slow, very noisy, and low resolution. The print head pins eventually wear out after a certain period. Pretty soon the dot matrix impact printer had to hand

over its dominant position to other types of printers. Nevertheless the dot matrix print principle and using the carbon ribbon as ink carrier is adopted for digital printing while the mechanical head is replaced by other more advanced working mechanism.

Thermal printer

Apple introduced the first thermal dot matrix printer Silentype™ that uses a special thermal paper and a heated printhead [7]. The dot matrix characters and graphics are patterned by locally heating a chemically treated paper. The thermochromic dye of the paper changes color when current passes through the integrated thin-film resistors in the printhead to heat up the area in contact with paper and the thermochromic reaction is initiated. Although special paper is more expensive than regular paper, the thermal printer doesn't need any other consumables. One common problem associated with this type of printer is that over time the printed image tends not to last long before fading occurs due to the aging of thermochromic dye. Today, thermal printer is still used to print receipts or invoices in some Point of Sale (POS) terminals that replaces the impact printer due to faster print speed, higher reliability and lower maintenance cost.

Thermal wax transfer printer
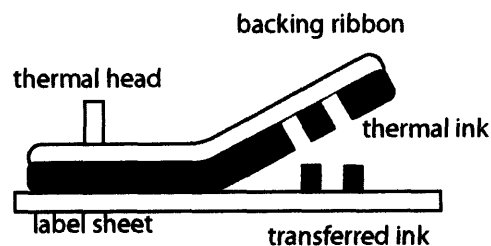
Figure 1-11. Thermal transfer printer [2].

32

Figure 1-11 shows that similar thermographic technology is used in the thermal transfer printer, which prints by melting a precoated ink ribbon and transferring it onto regular paper. The inked ribbon performs essentially the same functions as in the impact printer, except the ink adhesive with wax or resin on the ribbon is transferred by heat and will later stay adhered to the paper after thermal transfer. The mechanical parts are simple and there is no need for liquid ink delivery and clog recovery system. The printer can be compact and lightweight because it requires only the moving mechanism of ink ribbons and print roils. Compared to impact printer, thermal wax transfer printer can operate at higher speed and is less noisy. These days it is still widely used in small format printing such as fax machine or label printer. Its disadvantages include difficult to reproduce levels of grayscale, complexity to print full color (which needs multiple-color ink ribbon) and image being not scratch resistant.

Dye sublimation printer

The basis of dye sublimation printer is the phenomenon known as direct solid-vapor phase transformation, bypassing the liquid state when some dye materials are brought to their sublimation temperatures. This is another type of thermal transfer printer [2, 4]. The most important design factor is to determine and select the right sublimable dyes that do not degrade during and after the heat transfer. Successful development of special dyes is achieved at the beginning of 1990s that marks the dye sublimation printing as a very promising printing method.

The structure of a dye sublimation printer is very much like the previously mentioned thermal wax transfer printer. But the thermal head must deliver higher thermal energy to vaporize the dye. High speed and high-resolution printhead has been realized through the design of highly efficient, rapid heating/cooling rate and high density heating elements inherited from

years of industrial research on thin film technology. The requirement for the supporting sheet is that the sheet should be flexible yet heat-resistant for momentarily high temperatures in the range of 250~350°C. Polyester film is the best candidate for its strength and low-cost. For the dye-receiving sheet (i.e. paper substrate), plain paper can't be directly used due to the compounds inside it can degrade the printhead when in contact with high temperatures. Special print paper has to be used.
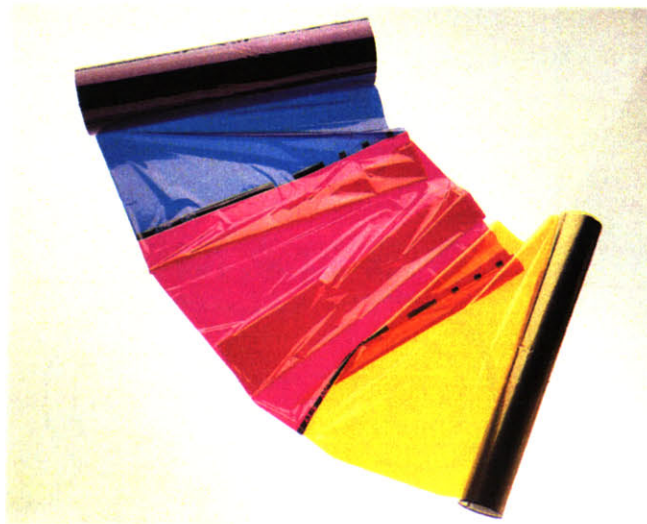
Figure 1-12. Area sequential Xerox Co. dye sublimation ribbon roll

The dye sublimation printer can produce continuous tone, which is achieved by varying the current passing through the heater therefore adjusting the heating temperatures of the heater and fundamentally the flux of dye molecules reaching the paper. Unlike other printers (i.e., inkjet printer), dye sublimation employs non-opaque, subtractive primary color system of cyan, magenta and yellow dyes and layers them on top of each other that is capable of excellent reproduction of colors. The three-color patterning mechanism is either line sequential or area sequential method, as shown in **Figure 1-12.** Known for its high quality colors and continuous

tone output, dye sublimation printer is supreme in digital photographic applications, for example, making instant postcard size photos.

Laser dye transfer printer
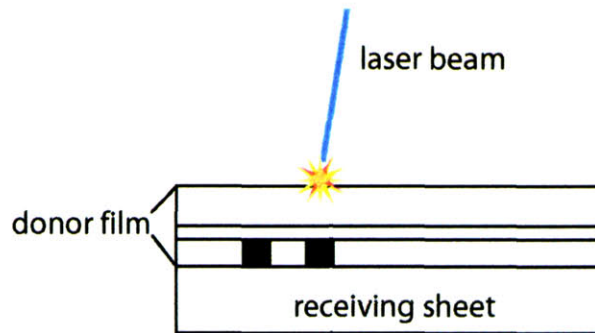
Figure 1-13. Laser thermal transfer printing

A new dye transfer printer is currently being pursued to improve the resolution to a higher level [2, 8]. A relatively high power laser beam as a heating source has replaced the micro heater. A dye sheet called the donor sheet comprises a base in order to convert light to heat and a transfer layer containing a dye-donor layer which is melted by heating and is transferred to the underneath dye-receiving layer (which is supported by another base sheet), shown in **Figure 1-13**. Using the donor sheet and laser drawing, very fine dots and lines can be printed at above 2500 dpi. The image size is primarily determined by the frame size of the donor sheet. And because there is no direct contact between the printhead and the receiving layer, even very delicate organic materials can be directly printed. Although this printing technique has been used to produce color filters for LCD monitors, it is still limited by the reliability of the laser source.

Electrophotography / Laser printer
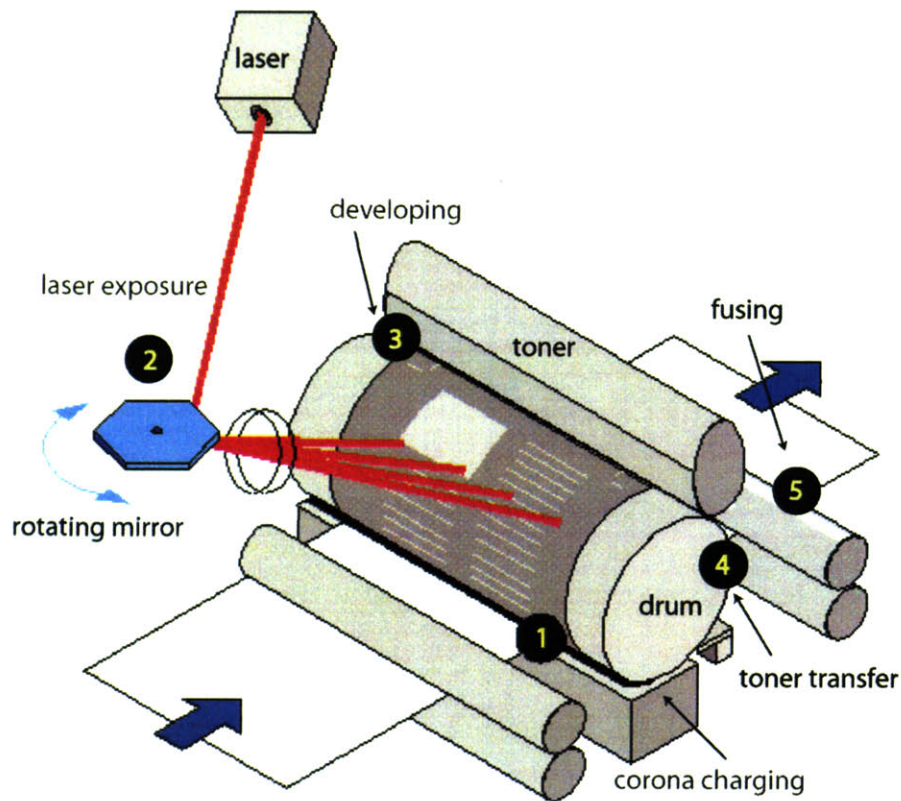
Figure 1-14. Laser printing mechanism [2, 9]

Chester Carlson invented electrophotography that later became the technical foundation of a more than 100 billion dollar document production industry [10]. Electrophotography in laymen's term means creation of writings by electrical charges. The laser printer is such an example. An electrostatic latent image is generated by sequential scanning of a laser beam onto a photoreceptor; then the image is transferred onto a medium (i.e., paper). Because the laser beam can move much faster than a belt-driven scanner head (for example InkJet printhead), a laser printer can print at very high speed, approaching 200 monochromic pages per minute (ppm) and

100 ppm in full color in some high end models. The laser spot is tiny, enabling very fine feature size printing at above 2000 dpi resolution.

The Carlson electrophotographic process is the basic working principle of today's laser printer: charging a photoconductive material coated drum uniformly, exposing an optical image onto it to form a latent image, applying electrostatic force to attract toner particles onto the latent image, transferring the toner image onto paper, fusing, discharging the print drum and cleaning. Although it was invented in 1938, not until another two decades of dedicated work was put on it, did the idea became a reality. The basic seven steps remain the same in the electrophotographic process: charging, exposing, developing, transferring, fusing, discharging and cleaning. We will briefly review the technologies in each step.

Charging

Electrostatic charges are uniformly projected by a charging unit (corona wire or roller), which is a thin wire (or pin) and a nearby grounded shield that can ionize air as high voltage is applied in between. The charge can stay on the surface of a photoreceptor when the photo-conductor is in the dark state.

Laser writing (exposing)

The core component of the laser printer is a photoreceptor, consisting of an aluminum base layer and photoconductor coatings of a charge blocking layer, a charge generation layer and a charge transport layer.

Upon charging the photoreceptor, a laser beam sweeps through a polygon mirror rotor across the photoconductor surface, while the beam intensity is modulated on and off by data stream for the reproduction of digitized image signals. As the photoreceptor drum revolves, a latent image is patterned onto the photoconductor layer (for example, amorphous selenium), the area where laser beam falls onto the photoconductor becomes conductive and dissipate charges, restoring electrostatic neutrality.

Developing

Developing is the process where the exposed surface is in intimate contact with toners (fine ink particles that carry opposite charges) so that the particles are electrostatically attracted to the photoreceptor drum surface where the latent image is written.

In the most common type of toner, dual component toner, the ingredients are a mixture of pigment particles (i.e., carbon black of a few microns in diameter), wax and resin/polymer binder that will attach themselves to the carrying media (carrier beads in many cases) that will carry the fine particles to the electrostaticly patterned drum surface and thereby develop the latent image. Carrier beads are usually a few hundred microns in diameter made of magnetic compounds. Toners and carriers are fed onto a roller surface by magnetic force and then rubbed to the photoreceptor drum; only toners will stick to the photoreceptor and adhere to a latent image.

Transfer to paper

At this point the image is complete with toner on the drum and is to be printed onto the paper. As the paper passes between the drum and the transfer corona, the transfer corona applies an opposite charge (refer to the drum) to the paper. The charged toner then jumps off to the paper.

For color prints this process is done four times (one color at a time) or all at once. Then the paper runs through a charge eliminator to neutralize the electrical charges on the paper.

Fusing

To fix the toner on the paper, the toner layer (primarily the wax and thermoplastic resin powders) must be fused to bond to the paper permanently. Fuser roll and pressure roll are commonly used. Fuser roll is a smooth, soft and non-sticky cylinder with a high-power heating element inside. The paper is temporarily heated up to about 350 degrees Fahrenheit under pressure. When it is cooled down, the image is fixed. There are two issues in this thermal and pressure process: the substrate has to be designed for Laser printer to sustain the fusing temperature which otherwise can melt the substrate (for example, some transparency plastics); the energy to maintain the fusing roll's temperature is wasted at standby. Lower fusing temperature or fast revival speed will be the key to conserve energy.

Discharging and Cleaning

After transferring, the drum is discharged and any remaining toner on the drum surface will be removed by the cleaning device. The quality of cleaning will greatly affect the succeeding print cycles. Rotating brush or wiper blade is usually used. The unused toner is either collected in the waste compartment or routed back for reuse.

During the corona discharge, a small amount of ozone is generated by the high voltage splitting and ionizing oxygen. Ozone is considered a health hazard above certain concentration level thus ozone filters are used to prevent air pollution of the user environment.

InkJet printer

The technical basis of Ink droplet formation is the Plateau-Rayleigh instability [2, 4]. A cylinder shape fluid stream will undergo stretching and necking and eventually break into small spheres of certain radius by virtue of the surface tension where the surface area tends to minimize itself. Although Lord Rayleigh discovered this phenomenon more than 100 years ago, realization and perfection of inkjet printer took about three decades. **Table 1-1** summarizes the development of inkjet printing technique chronologically [2, 4].

Table 1-1. Discovery and development of inkjet printing technology

Year	Milestone
1878	Liquid stream instability described by Lord Rayleigh
1951	First practical Rayleigh break-up inkjet device by Siemens
1960s	A. B. Dick VideoJet and Mead DIJIT products based on continuous ink-jet technology
1960s	Dr. Sweet of Stanford University demonstrated methods of creating droplets of uniform size and spacing.
1976	The IBM 4640 ink-jet printer was introduced as a computer printer
1977	Siemens PT-80 printer first piezoelectric DoD printer
1977	Canon invented thermal ink Jet concept
1984	Canon launched first bubble jet
1984	Hewlett-Packard first 12 nozzle ThinkJet printer with disposable printhead
1987	First Color Inkjet printer by HP PaintJet
1990	Epson developed the first piezoelectric inkjet printer

Inkjet printing belongs to non-impact dot-matrix printing technology, using printheads that dispense ink through a small orifice without directly touching the substrate (paper). Inkjet printing since its debut has been a versatile, reliable and cost-effective method to generate completely digital outputs. **Figure 1-15** reveals the rapid growth of the inkjet printer market in the US [11].
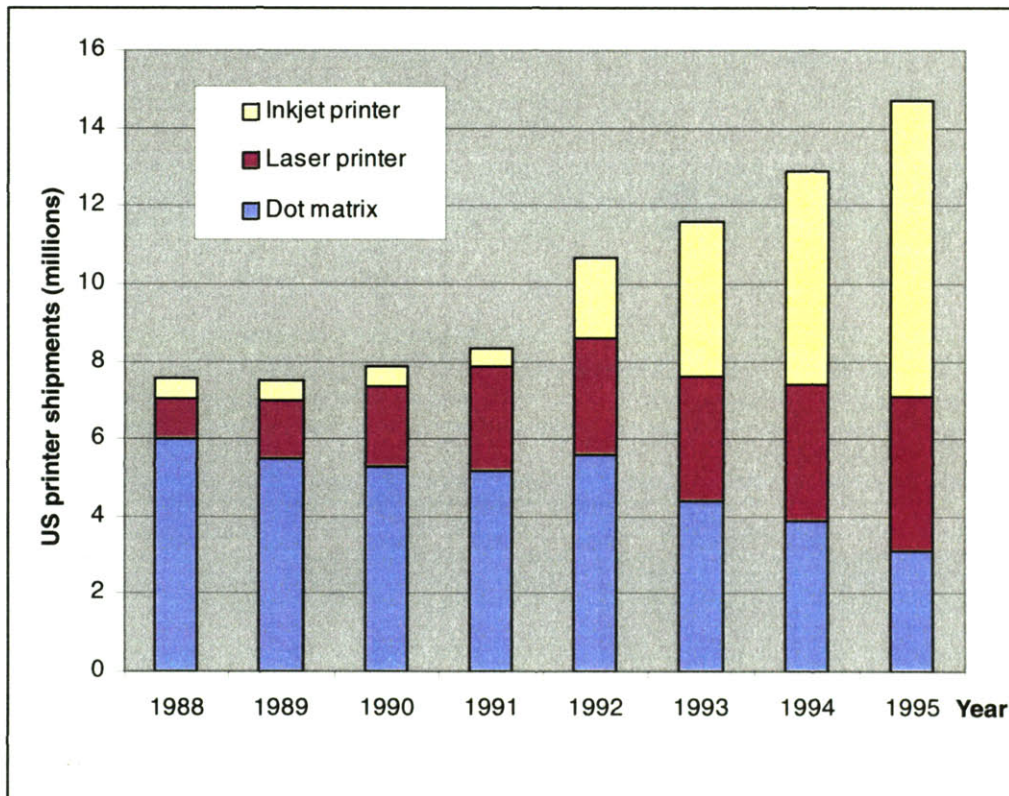
Figure 1-15. US printer shipments show rapid growth of Inkjet printer

Inkjet printer falls under two major categories: continuous or "drop on demand" mode. Continuous inkjet printer is mainly used in industrial marking process where the printhead generates a continuous ink flow that then breaks into a stream of droplets. These droplets are charged and can be deflected by electrostatic force to reach the substrate or a gutter. "Drop on demand" (DoD) is more popular in office or home applications. In DoD mode a droplet is only

41

ejected when it is needed on an imaging area, which eliminates complicated droplet charging and deflection hardware used in the continuous printer. Both the simplicity and reliability are greatly improved so is the performance of inkjet printer, as shown in **Figure 1-16** [12].

Drop volumes are approaching a practical limit
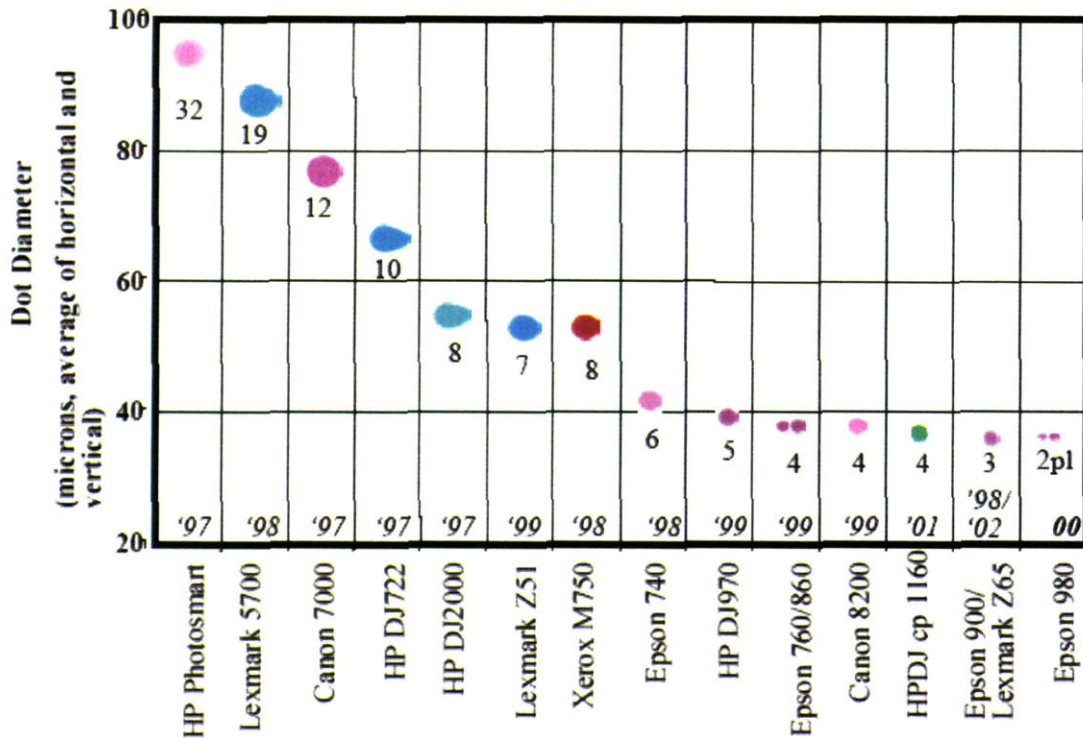
Figure 1-16. Deduction of drop size as Inkjet printing technique advances

Thermal Inkjet and Piezoelectric systems are the two most popular DoD technologies.

Thermal inkjet printers dominate about 3/4 of today's inkjet printer market. In a thermal printer, a pulsed current passes through the heater to generate vapor bubbles, ejecting small drops of ink through orifices and placing them on a medium to form text or images. Piezoelectric printers use a "dimension changeable" piezoelectric material, commonly lead zirconium titanate

(PZT) ceramic. In response to the driving signals, this piezoelectric material will elongate or bend to pump ink through nozzles and deliver drops.

Both methods these days are inexpensive to use, fast operation and highly reliable, and can delivery down to picoliter (pL) size drops for high resolution printing work (for example, printing photos). We will come back to review the technological details of these two DoD inkjet printers in the next chapters. **Table 1-2** provides a quick comparison of these two DoD inkjet printing technologies.

Table 1-2. Comparison between thermal Inkjet and Piezo Inkjet

Technology	Advantages	Disadvantages
Thermal Inkjet	Large nozzle density and high resolution Air bubble or clog tolerance Less or no ink waste	Precise heat flow control needed Sensitive to ink viscosity changes Possible kogation at heater surface
Piezo Inkjet	Tolerate ink viscosity changes Drop size variable by control signals No heating damage to ink	Sensitive to trapped small bubbles Regular ink flush required Large nozzle spacing

1.4. Summary

In the past few decades, rapid development of computer technologies has tremendously redefined the concept of "printing". Analog printing originated from centuries ago when fire and gouges were used to carve clay or wooden plates, however, today's digital printing technologies have evolved far beyond that. The reproduction of graphics and texts is no longer constrained by first making a printing plate. The concept of "digital printing" is based on the ability to compose and store data files and output them in a form of inking material (dye, toner, etc) at a quality level comparable with the analog printing. And a new bread of printer – digital printer was born in lieu of this new concept.

Because digital printing technologies are based on different working principle, some benefits are unique with digital printing over conventional printing:

Convenience: Digital contents are easier to transmit, store and share, if necessary, via the Internet, phone line or satellite. Users don't need to prepare a printing plate before the print to be processed, they can even print at their home with a personal printer. A good example is the photo print over the Internet that has become a rapidly growing business.

Flexibility: Users can manipulate contents by using software on their computer for every document or application. Images can be cropped, texts can be edited, and color balance, brightness or contrast can be adjusted. It allows each print job (for example, greeting cards) to be personalized. Because the print no longer relies on a printing plate, large banner or blueprint covering almost any size (however that might require further assembly to create the final image) can be printed. This otherwise will be very difficult with conventional printing approaches.

Instantaneity: With digital printing, there is no need to wait for the plate preparation. Digital processing is always ready to print and can print application "on-demand". Instant print offers visual feedback when timely service is critical, and provides interactive capability to refine the print products, as was the case in printing and refinement of text and images incorporated in this dissertation.

Cost saving: digital printing is highly automatic and simple, for short runs it eliminates the need of manual operation and personnel cost; there is less material waste, for instance, plate making, stock and transportation; last but not the least, saving on delivery time also create value to the users.

Conventional printing (e.g. offset printing) still remains the right choice for applications that need large volume (hence the high setup cost will be lower on per copy basis) and extremely fine quality. It is however impractical to print for short runs with conventional printing methods. Digital printing offers similar printing quality and is very competitive in the arena of very short runs (1,000 copies or less).

Digital printing, represented by the DoD Inkjet printing, offers remarkable features and functionalities that are close to or even exceed analog printing technology. The digital printing business is growing strongly, getting bigger every day. Started as a disruptive technology (in reference to the conventional printing technologies), digital printing has become the dominant technology in the personal printing market. Innovators and manufacturers are working together to move it beyond the computer based desktop application. This dissertation considers the potential of use of printing techniques in development of new manufacturing tools for tomorrow's digital fabrication of electronic components and systems. It is envisioned that digital printing tool are poised to enable a whole new level of innovation and integration that can drastically change the concept of printing and revolutionize the way in which things beyond paper prints are made.

Reference

[1]. ISO TC130: Graphic technology/WG1: Terminology, International Organization for Standardization, Geneva, Switzerland.

[2]. N. Ohta, M. Rosen, Color desktop printer technology, CRC Press, Boca Raton (2006).

[3]. http://glossary.ippaer.com

[4]. H. Kipphan, Handbook of print media, Springer, Berlin 2001.

[5]. http://www.infosight.com/mtrfp.htm

[6]. http://www.atariarchives.org/epson/chapter_1.php

[7]. http://apple2history.org/history/ah13.html

[8]. E. V. Patton, C. D. DeBoer, Direct digital color proofing using laser-induced dye transfer, Proc. SPIE 1912, 261 (1993).

[9]. http://www.answers.com/topic/laser-printer

[10]. D. Owen, Copies in Seconds, Simon & Schuster, New York 2004.

[11]. S. K. Yoder, "How H-P used tactics of the Japanese to beat them at their game", Wall Street Journal, Sept. 8, 1994, pp. 1, A9.

[12]. R. Beeson, Desktop Inkjet Products Performance Study. IS&T Non-Impact Printing Conference # 18, San Diego 2002.

CHAPTER 2. Patterning organic and nanostructured devices

CONTENTS

1. Overview

Organic semiconductors have a weak van der Waals bonding nature, with the bonding strength only on the order of few kT at room temperature. This presents both an advantage and disadvantage. A weak intermolecular bonding force tends to jeopardize the device functionality if the fabrication is directly subject to traditional patterning process used in microelectronics industry; on the other hand, the molecular functional materials are not picky about the choice of substrates so that many low cost substrates (glass, plastic or metal sheets) might get an opportunity to be adopted as a part of device structure. An interesting aspect of organic electronics arises as the concept of flexible electronics, which might extend their applications in new fields, for example, wearable electronics or ubiquitous printed electronics.

Material development for organic device applications has been divided into two groups since the early eras of research: molecular organic semiconductors or conjugated polymeric organics. Devices based on molecular organics typically consist of multiple stacked layers of thin films, each around 100 nm thick, with each layer dedicated to a unique function at a thickness around

100 nm; Solution processed polymeric devices tend to have fewer number of discrete layers partially due to the difficulties in choosing proper solvents in the subsequent fabrication steps that do not affect the previously coated layers.

Gen	Substrate size mm	Number of panels from given substrate		
		22" wide	30" wide	46" wide
3	650 x 660	2	0	0
3.5	650 x 830	2	1	0
5	1100 x 1300	8	3	2
7	2120 x 2320	32	15	6
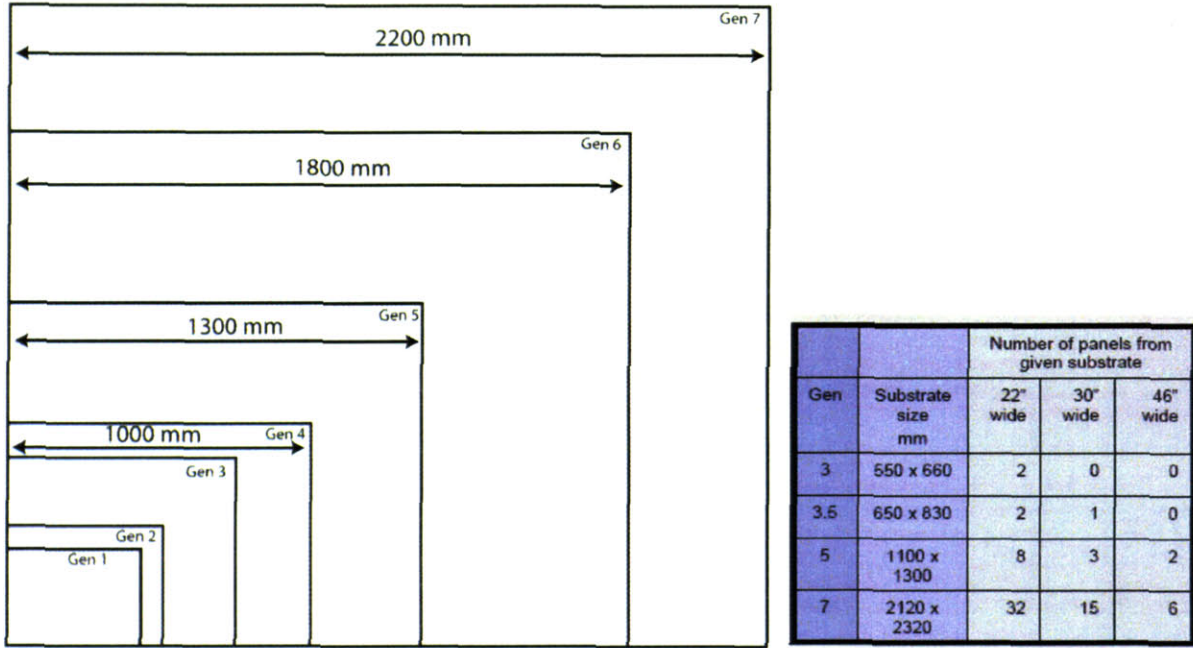
Figure 2-1. Flat panel display mother glass generation

In terms of substrate size, organic electronic technology is in a transition from small-scale research and development environment to large-scale mass production. Production efficiency is the key to drive down the cost of manufacturing. An example we note that high definition flat panel displays whose production has been on the rise. In **Figure 2-1** [1] we draw the substrate sizes of generation 1 through 7 of flat panel display mother glass. Currently only a few patterning techniques can accommodate the largest (Gen 7) substrates. As the organic device performance improves, scaling-up of the patterning process and decreasing the cost of organic materials become more important [2, 3].

A few particular issues that arise in patterning of organic semiconductor layers are listed below. Although relatively weak molecular bonding forces in organic semiconductors can broaden the choice of substrates, they also render conventional microelectronic processing techniques incompatible with the organic thin films [2-7], necessitating the development of novel device fabrication approaches.

- ❑ Freedom of choice of material set

- ❑ Patterning fine feature size on the order of ten microns

- ❑ Scalability to large substrate size

- ❑ Precise alignment of sequential patterns on the substrate

- ❑ Production yield on par with standard semiconductor processing technologies

To date many novel organic semiconductor patterning methods have been proposed and many of them have been successfully demonstrated at lab production scale. However, currently only three types of pattering techniques, namely shadow mask pattering, Inkjet printing (InkJet) and Laser Induced Thermal Imaging (LITI), are mature enough to dominate most of the manufacture-tool market. In the following sections of this chapter, several depositing techniques for organic semiconductors are reviewed; a few promising methods are discussed; followed by a brief outline of some emerging patterning techniques. Advantages and shortcomings of these patterning techniques are summarized in the last section and some thoughts are offered on new applications and future research directions.

2. Vacuum thermal deposition and shadow mask patterning

Basis of thermal deposition
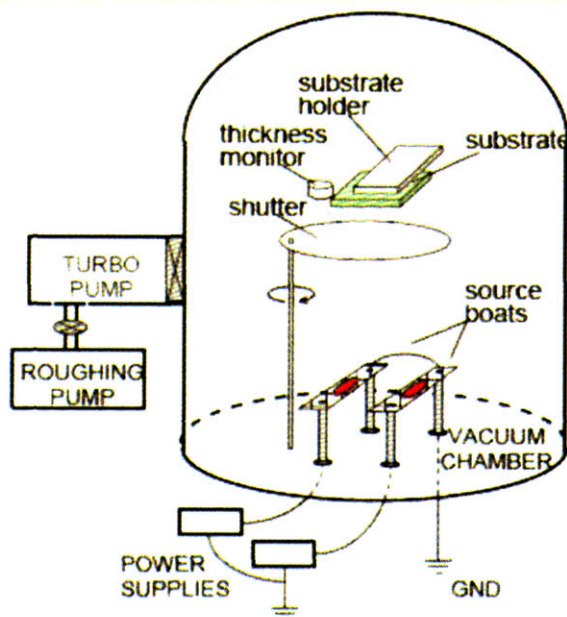
Figure 2-2. Vacuum thermal evaporation chamber and process

Vacuum thermal deposition is traditionally used to deposit multiple layer structured molecular organic devices. The process scheme is depicted in **Figure 2-2** [8]. In this method, the source materials are placed inside a heating container, either a boat or a Knudsen crucible. The substrate sits above, averted to face the heating source. Deposition takes place inside a chamber that is evacuated to reach high vacuum of $\sim 10^{-6}$ Torr. Source materials are heated to attain a desired vapor pressure with the source temperature above the boiling/sublimation point but below the thermal decomposition temperature. The deposition process is monitored by a quartz thickness microbalance located near the substrate and controlled by adjusting the resistive heating current to achieve a stable evaporation rate. In high vacuum, impurities incorporated into the organic thin films can be kept at a low level to allow the deposition of a high purity thin film. The long mean free path at the reduced chamber pressure allows the source molecules travel in a

"straight line" manner within the chamber and the deposition is directional, as opposed to conformal coating in some other types of deposition (e.g., Chemical Vapor Deposition).
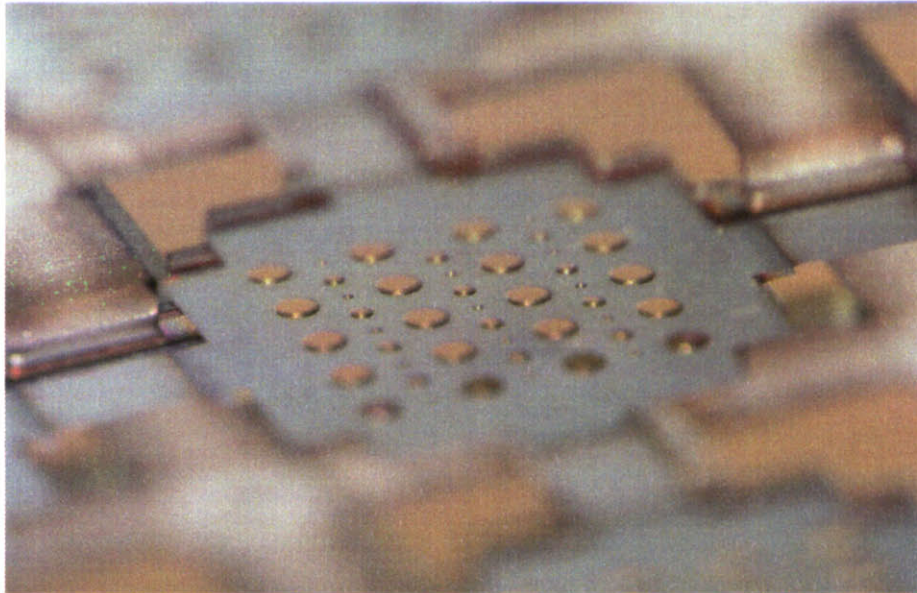
Figure 2-3. Part of a metal stencil mask to pattern circular features

In vacuum thermal deposition, the patterning of evaporated/sublimed molecular materials is accomplished through a shadow mask, also referred to as a metal stencil mask. The main advantage of this technique is that it allows simple one-step, non-contact patterning of deposited thin films. This is in contrast to photolithography, where several process steps require organic thin film exposing to chemical solutions, which can damage the organic thin films. An example of a metal shadow mask stencil is shown in **Figure 2-3**.

Shadow mask patterning is a mature technique normally used in combination with the vacuum thermal evaporation process. The advantages of deposition using this method include high purity in molecular organic thin films and capability to directly pattern deposited metal films. During the deposition, source materials also indiscriminately deposit on the walls of the chamber and the non-open areas of the mask. The fraction of material that reaches through the apertures to the substrate is less than 5% [9], which is a very low material efficiency. The

regular maintenance cost is also high. Most of the time, the metal mask, as well as the evaporation chamber, requires cleaning after extended use to remove materials that accumulate on the mask surface.

The shadow mask stencil is commonly placed unsupported in a horizon position to receive vapor flux. The weight of the mask itself can exhibit some degree of sagging by gravity, distorting the patterns. This becomes more severe as the mask size increases. The tension by the mask frame also poses another problem similar to the gravity. Vertically in-line deposition system has been developed to minimize this patterning distortion. [10]

3. Spin-coating deposition

Spin coating or spin casting is a fluid based deposition process in which source material dissolved in a carrier fluid is spread over a fast rotating substrate. As the solvent evaporates from the substrate, the dispensed material forms a thin layer across the substrate by the centrifugal forces. Spin coating has long been a popular production technique, and is used in today's microelectronics industry. In particular for coating photoresist layers, this is an essential step in the photolithographic process even on substrates with complicated geometries and features [11]. Practical application of the spin coating process in the fabrication of organic devices also includes dispensing charge injection materials (e.g. PEDOT) or colloidal nanocrystals that might be incorporated in an OLED structure.

The final thickness of the spun-coated layer largely depends on the nature of the fluid (e.g. viscosity, surface tension, material loading concentration, etc), the substrate (temperature, surface wettability, etc) and the spin parameters (acceleration rate, final angular speed, duration and exhaust rate, etc). Emslie *et al.* studied the final contour and film thickness after spreading

and showed that spinning increases uniformity of the initially non-uniform fluid profile. The morphology of the solution is given as equation 2-1 and **Figure 2-4** [12]:

$$h(t) = \frac{h_0}{(1 + 4Kh_0^2 t)^{\frac{1}{2}}} \tag{2-1}$$

a.

b.

Film thickness
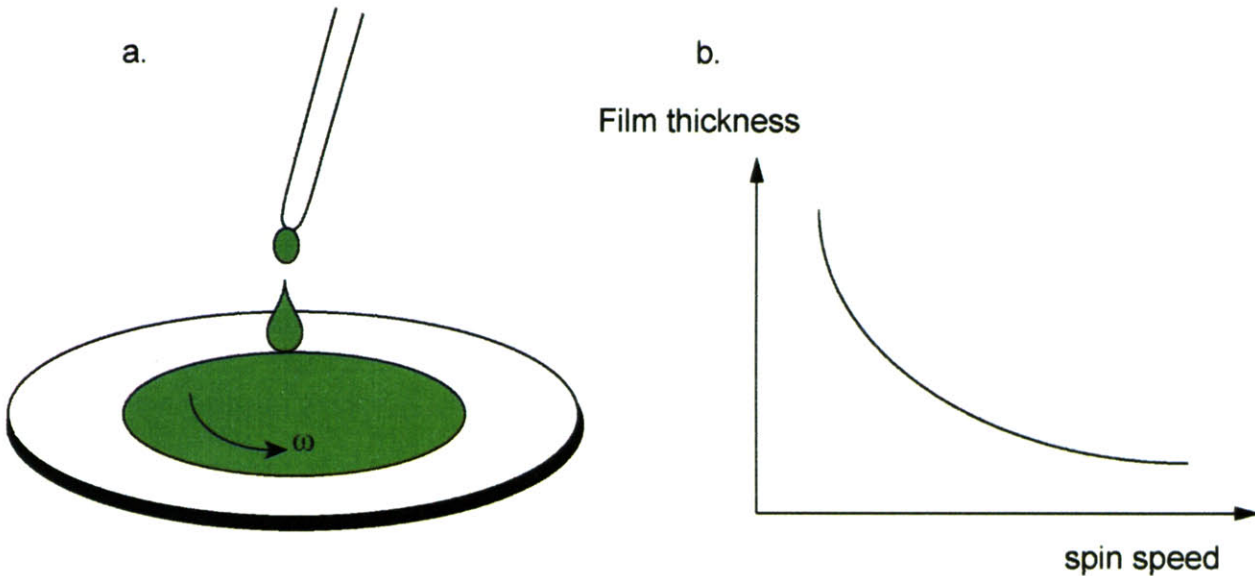
spin speed

Figure 2-4. (a). Spin coating process and (b). film thickness vs. spin speed

where h(t) is the time dependent contour of the fluid; K is a fluid related property, where

$K = \frac{\rho \omega^2}{3\eta}$, ρ is the density of fluid, η is viscosity, and ω is the angular velocity.

The spin rate is usually in a range from 1500 to 6000 rpm and the final film thickness can vary from a fraction of a micron to a few microns. If the rotating plate is infinitely long, all the dispensed fluid will be utilized; however, in reality the substrate size is finite, most of the fluid (>95%) will end up being spun off the substrate, therefore spin coating is a very inefficient process when measured by material usage.

Since spin coating is used only for dispensing fluid, it is good for blanket deposition, but has to rely on another technique, for example photolithography, for patterning. However, conventional photolithography patterning technique is not fully compatible with the fabrication

of organic devices [3]. The organic under layer may not be impervious to photoresist resin, solvent, and the subsequent developing steps in aqueous solutions. Exposure of photoresist to ultraviolet (UV) radiation induces chemical reaction in the exposed area but the UV light could penetrate into the organic layers and break fragile intermolecular bonds, creating charged defects or traps.

Despite its simplicity, low cost and technical maturity, the inefficiency in material usage and the lack of direct patterning compatibility has constrained spin coating technique from further improvement in the fabrication of more complicated organic device structures. The solution could lead to a path of synthesizing more robust organic materials, or as in chapter 5, the inkjet printing technique can be used to dispense source materials where they are required to dramatically increase the material efficiency.

4. Inkjet deposition

Starting as a disruptive technology for digital printing, inkjet technology has been drastically improved in the past decade. Two primary configurations are developed to generate ink drops on demand. Depending on the mechanism of how ink is ejected from the nozzle, inkjet printing can be either thermal inkjet or piezoelectric inkjet. Inkjet printer is used for patterning soluble materials, ranging from the desktop platform of a letter size printer to the monstrous size of an industrial signage printer to accommodate Gen. 8 mother glass [13].

Thermal inkjet structure

The only moving part is the ink fluid itself in thermal inkjet printheads. **Figure 2-5** illustrates the structure of a thermal inkjet printhead and the 4 steps involved in the thermal inkjet printing process [14]. The thermal inkjet printhead consists of a firing chamber, a thin film heater to

generate bubbles and an ink-refill channel. The size of the inkjet orifice is on the order of several microns.

| 1. Bubble Nucleation | 2. Bubble growth | 3. Drop ejected | 4. Drop break off |
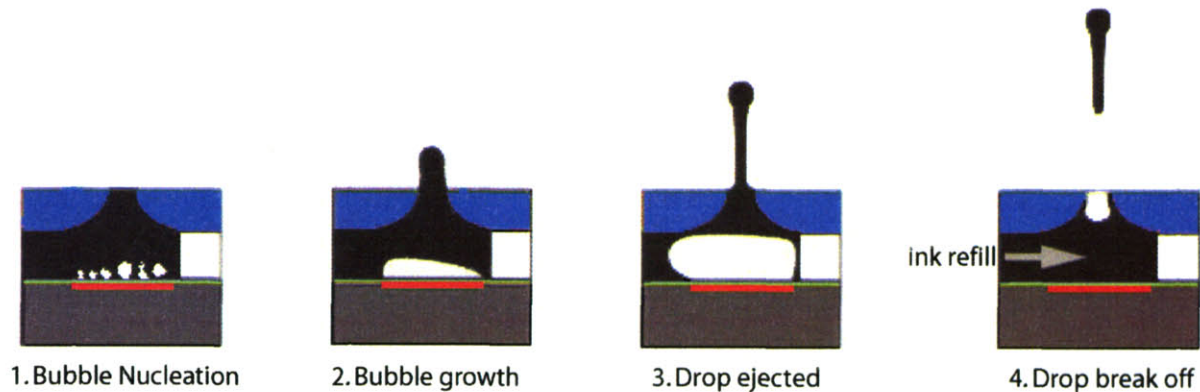
Figure 2-5. Thermal inkjet printing process

Bubble nucleation

An electrical current is supplied for a few microseconds to the thin film heater to raise its temperature to above 300 °C at 10-100 °C/μsec rate – during this time the surface energy density can reach values higher than those on the surface of the sun (temperature ~ 6000K) within 1 milliseconds [15]. At a rapid heating rate, ink fluid near the heater surface will undergo a change beyond the boiling state to become a so-called superheated metastable state, and vaporized bubbles begin to nucleate at the heater surface. The superheated fluid phenomenon occurs in a thermodynamically non-equilibrium fashion, which is in contrast to an equilibrium process (boiling) where seeds of vaporized bubbles have sufficient time to nucleate on the heater and the phase transformation is continuous. At such a rapid heating rate, only the high temperature nucleation sites contribute to the bubble formation, giving very consistent energy transfer to the ink and thus highly repeatable and precise control of the ink drop volume. The heating and nucleation processes take place in merely a few microseconds so that heat conduction from the heater to the ink only occur within 0.1 micron into the ink, about 1% volume of the ink reservoir.

The vapor bubble once formed will have much lower thermal conductivity than the liquid and hence insulate the heater, causing no further heating to the rest of the ink (about 99% of the volume). The timing of the heating current has to be controlled precisely to prevent any potential decomposition or burning of the ink resulting in a contaminated coating layer onto the heater, which might lead to early failure of the printhead. Because of this potential heating induced damage to the ink, speculations have been raised, at first, to question if thermal inkjet printer can be used for dispensing ink with low thermal budget (for example, ink that contains biological entities which might not survive the heat). However during the author's private communication with the thermal inkjet manufacturer, the answer is affirmative that today's thermal inkjet technology doesn't constrain the choice of such ink.

Bubble expansion

The bubbles grow and expand to fill the ejection chamber. During this rapid expansion the bubbles act like an energetic piston to induce pressure increase inside the chamber momentarily above 10 atmospheres, causing a certain volume of ink (about half of the chamber size) out of the printer nozzle. Some ink is forced back into the refill inlet that can help dislodge particles or air bubble trapped inside the channel. Dimensions of both the nozzles (tiny orifices) and the inlets are optimized to maximize the jetting efficiency while maintaining a rapid ink refill.

Ink drop ejection

As the vapor bubble grows and reaches the maximum volume, the expansion can induce a body velocity to the ink and cause a jetting motion out of the nozzle at ~10 meter/second. Immediately the bubble collapses and acts like a pump piston to stroke backward. The nozzle meniscus starts to retreat into the jetting chamber. This causes the jet of ink to elongate and break

off into a separate stream leaving out of the nozzle. It takes another 100 microseconds for the drop to reach the print medium surface.

Satellite drops, often times, can be seen as secondary droplets following the primary droplet, initially as a long tail of the jet breaking off into multiple drops by capillary instability (Rayleigh instability). The printing image will blur due to the satellite drops impacting a slightly different locations from that of the primary droplet. The breaking off of the tail indicates that surface tension forces of the ink are no longer capable of holding that amount of ink together.

Ink refill

Once the bubble collapses the nozzle meniscus is retracted deeply into the chamber and creates a negative pressure inside the chamber to draw ink from the ink reservoir through the refill channel into the firing chamber. Surface tension of the ink causes the meniscus movement to act like a fluid mechanical oscillator. With the energy supplied from the heater this oscillation will occur continuously to cause volumetric displacement of the ink drops (jetting).

Piezoelectric printer

Piezoelectric materials serve as energy transducers to change dimensions and generate acoustic force in response to the driven electric fields. The working principle of the piezoelectric printer is based on ink fluid's incompressible properties, namely small displacement of the piezoelectric material can be enlarged by driving a large diaphragm to produce a large displacement of the ink droplet over a small area, resulting in a large jetting chamber, bulkier design of the ink cartridge and less line density of nozzles compared with the thermal inkjet type printhead. Piezoelectric printheads operate in either elongation, bending or shear mode (see **Figure 2-6)** [16]. In the elongation mode, the piezoelectric actuator is bonded to a diaphragm at one end which pushes the ink. This dimensional change is only on the order of one micron; In

57

the bending mode, the piezoelectric transducer is bonded along its length to the diaphragm. When the jetting signal is applied to the piezoelectric element, the diaphragm will bend about 0.1 micron to eject an ink droplet. In the shear mode the piezoelectric material is deformed by an electrical field perpendicular to the polarization.
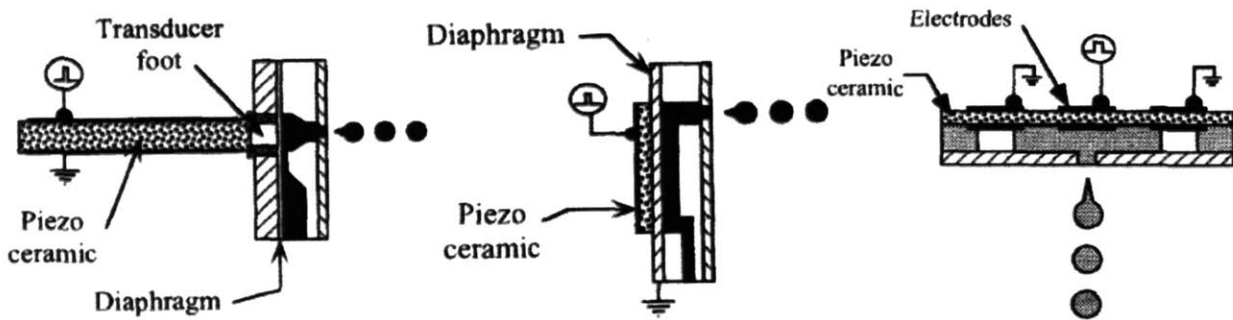
Figure 2-6. Operation mode of Piezo inkjet (a). Elongation mode (b). Bending mode (c). Shear mode

A unique property of the piezo printer is reflected in the variable jetting volume when the driving voltage and waveform changes. The drop volume is not determined by the firing chamber dimension as in the thermal inkjet printer. A bipolar pulse and higher driving voltage amplitude can deflect the diaphragm more and eject higher drop volumes.

Another significant difference between the piezo printer and the thermal inkjet printer is that ink is not heated in the piezo printhead, which may be able to eliminate some concerns on printing functional ink containing heat sensitive materials.

A key disadvantage of piezo printer is associated with its lower tolerance to trapped air bubbles in the ink channel. Piezo printers are based on the simple principle of fluid incompressibility. Trapped air bubbles are more compliant so that jetting performance will degrade with these bubbles. One solution is to regularly purge through the ink channel but a large quantity of ink will be wasted for the cleaning procedure. Some other disadvantages of the piezo printer also include lower nozzle density due to the dimensional requirement of the jetting

chamber and diaphragm, and higher fabrication cost because of more complicated printhead structure.

Ink composition
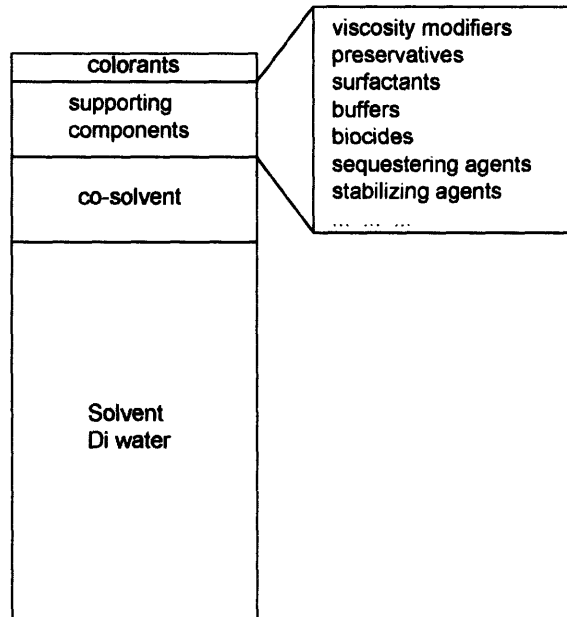
Figure 2-7. Water based ink compositions

Most inkjet printers, either thermal or piezo type, use fluid inks to print images. Solid inks can be dispensed in certain situation where they are heated first to transform them into liquid inks before printing. Whether solid or liquid state, inks are always composed of a delivery vehicle and colorant. Various additives might be present in the ink components to modify the ink properties. Among these properties, viscosity and surface tension are the two most important control factors to ensure precise drop volume, jetting velocity and trajectory.

Figure 2-7 shows the typical main ingredients in aqueous ink solution. Inexpensive DI water is used as the main solvent. Additives such as glycol are used to keep the viscosity unchanged despite water loss to or absorption from the ambient; surfactants are to modify the ink surface tension; cosolvents such as alcohol or polymer are to stabilize dyes or pigments in the ink, or

alter the ink's wettability on the paper; buffering agents help obtain a proper pH value; and preservatives are added to extend the ink's storage and shelf lifetime.

Colorants are the most complex functional ingredient to offer vivid images, which might be in the form of either dye molecules or pigment particles.

Dye based inks contain molecules that can optically absorb light at certain wavelengths, and physically can dissolve in the ink vehicles. Water-soluble dyes are the most common and generally provide the widest color gamut for printing color images. The dimension of dye molecules is on the order of a nanometer. They can be easily absorbed into the paper fiber. However, fading might occur after a long exposure to light, moisture or oxygen in the environment. Dye molecules can also be oil-based for specific requirements.

Pigment based inks use tiny particles of solid color about 100 nanometers in size, thousands time larger than single dye molecules. While dye based colorants are soluble to form the ink, pigments are not "dissolved" in the solvent vehicle. Instead pigment particles exist as a stable suspension solution with dispersant agents. Black inks for printing texts have long been using pigment suspensions but using color pigments in photographic applications is still very limited. Pure color pigments are made of plastic polymers that are ground to very fine sizes and then coated with a dispersing chemical to help pigment particles obtain a light static charge that keep the suspension stable. Over the time the pigment would eventually clump together to form a sludge that will clog cartridges and nozzles, a phenomenon that is referred to as the "pigment crash". Despite the reduced printing reliability as compared to the dye solution based inks, pigmented inks can offer much higher durability or fade resistance once printed. And well-suspended pigment solutions are compatible with both piezo printer and thermal printer, as even the largest single pigment particle diameter is still 100 times smaller than the inkjet nozzle.

Inkjet printers also work with non-aqueous vehicles, such as volatile organic compounds, or alcohols, but are limited to chemicals that are not corrosive to the printhead, packaging sealants and nozzles. Therefore inkjet printing technology has been adopted for the patterning of a wide range of functional inks made of organic materials and nonstructural materials. Successful implementations include printing conductive polymers [4, 17], Light Emitting Polymers (LEP) [17, 18], Organic Transistors [4, 19], as well as nanocrystals [20, 21] that will be addressed later in more details.

Inkjet printing Light Emitting Polymers
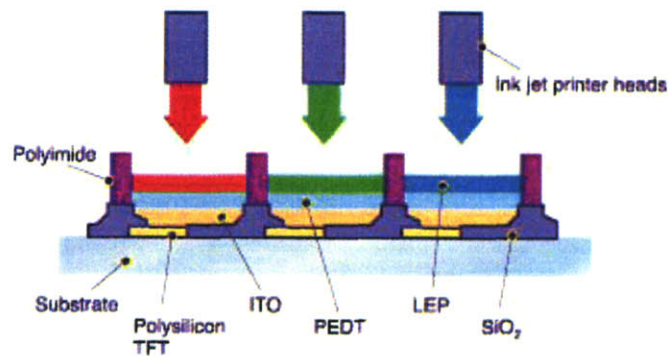
Figure 2-8. Inkjet printing LEP

The substrate is prepared like a printing plate with hydrophilic/hydrophobic surface areas. The key is to form subpixel well with polyimide dams/ribs to confine the inkjet drops. The polyimide dams are fabricated with conventional photolithography, and then the substrate is treated with oxygen/CF_4 plasma to make an array of alternating features consisting of hydrophilic ITO bottom and hydrophobic polymer dams. When a drop of PEDOT is placed inside the well, it will wet the exposed ITO but repel the polyimide dams. The result is well-defined, flat layer of PEDOT after the solvent evaporates. LEP with different emission wavelengths will then be jetted into these wells accurately and form the emission layer. Up to

61

120 ppi active matrix full color displays have been demonstrated by Litrex using this method, as shown in **Figure 2-8** [22].

Inkjet printing organic materials and nanostructured materials is suited for large area and flexible substrates with high throughput by multiple nozzle arrays and with high material efficiency of virtually no waste materials. Technological challenges for the inkjet patterning functional materials have been addressed in some recent literatures [7, 23]. In particular they include:

1. Solvent compatibility: printing multiple layer structures is limited to the choice of solvent and solubility.

2. Thickness uniformity: Surface tension, solute aggregation at the drop edge and drying of solvent can lead to thickness non-uniformity, so called coffee ring effect.

3. Resolution: Size of jetted drops upon impacting onto the substrate often limits inkjet printing feature size smaller then 10 micron, unless an additional step of patterning the substrate is used.

4. Optimization of ink: Choice of vehicle solvent and other additives are critical to generate perfect print features. Slow evaporation rate of solvent will determine if an extra baking step is required, which might degrade the ink's functionality. Fast drying solvent on the other hand can cause clogging of the nozzle during printing.

All these challenges can potentially reduce the yield or the lifetime of the printed devices and increase the manufacturing cost [24]. Therefore special attention should be paid to the design of the printer and the printing process.

5. Laser thermal transfer deposition

Thermal transfer printing is one of the mainstream printing technologies that has been introduced in the previous chapter, represented by the dye sublimation printing technique. A variety of conventional thermal patterning techniques have been applied to the patterning of organic materials [25]. Among them, laser thermal patterning can be characterized as using a laser for highly local heating to release inking materials from a donor sheet (sometimes called a ribbon) and transfer them onto a substrate, as summarized in **Table 2-1** [26].

Table 2-1. Laser Thermal Transfer Methods

Acronym	Full name	Transfer layer materials
LITI	Laser Induced Thermal Imaging	OLED materials, inks
LAT	Laser Ablative Transfer	Inks, conductive polymers
MAPLE DW	Matrix Assisted Pulsed Laser Evaporation Direct Write	metals, inorganics, LEPs
LIFT	Laser Induced Forward Transfer	metals, ceramics
SUFTLA	Surface Free Technology by Laser Ablation/Annealing	Semiconductor devices

Among them, Laser Induced Thermal Imaging (LITI) was developed by 3M for use in the patterning of OLED emitters, organic thin film transistors, and color filters, etc [27]. The printing scheme is illustrated in **Figure 2-9** [6], which encompasses a plastic donor sheet laminated with a series of organic semiconductor donor layers (polymer or molecule), a large format laser exposure system and a receptor (substrate). The donor film is constructed of a PET substrate, an absorptive layer to convert light to heat (usually a carbon black absorber), an interlayer to protect the donor layer from thermal and chemical damage and a transfer layer containing organic semiconductors (polymer or small molecule). The donor film is in close contact with the receptor, a Nd:YAG laser (beam size ~ 30 microns) impinges onto the back of

the donor sheet, light is converted to heat, vaporizing the donor material and adhering it onto the substrate instantly.
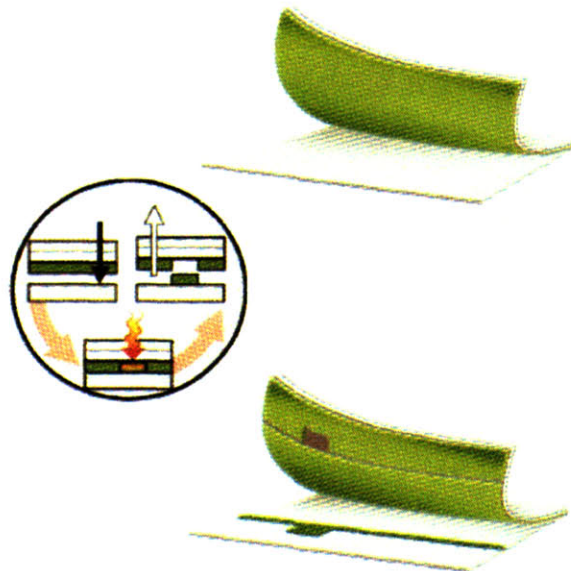
Figure 2-9. Schematic illustration of LITI printing technique

LITI has the unique ability to pattern multiple layers of polymer or small molecule organics in a single step without the issue of solvent compatibility. And the patterning area is scalable to accommodate larger size mother glass.

A potential shortcoming of LITI is that the donor sheet is required in the printing. Control of the thin film thickness uniformity again is critical over a large area; the donor sheet is discarded once it is used for transfer patterning, even though the transferred area represents less than a third of the coated surface area. Another potential drawback of LITI is the use of high power excimer laser system, which could be costly to operate and maintain.

6. Organic Vapor Phase Deposition and Vapor Jet Printing

Organic Vapor Phase Deposition (OVPD) was invented by the Forrest group at Princeton University and jointly commercialized by Universal Display Corporation and AIXTRON AG [28]. The basis of OVPD is a process that utilizes an inert carrier gas stream such as dry argon or

nitrogen to pick up and transport organic vapor from vapor source cells to a hot walled reactor to deposit on a substrate (sitting on a cooling stage) thin layers of organic materials that have low sublimation points and sufficiently high vapor pressure at temperatures less than 400°C. When the hot organic vapor stream reaches the cold substrate, organic molecules which are heavier than the carrier gas molecules will condense on the substrate surface into a solid film [29-33], as depicted in **Figure 2-10**. The mechanism is similar to the process of Chemical Vapor Deposition.
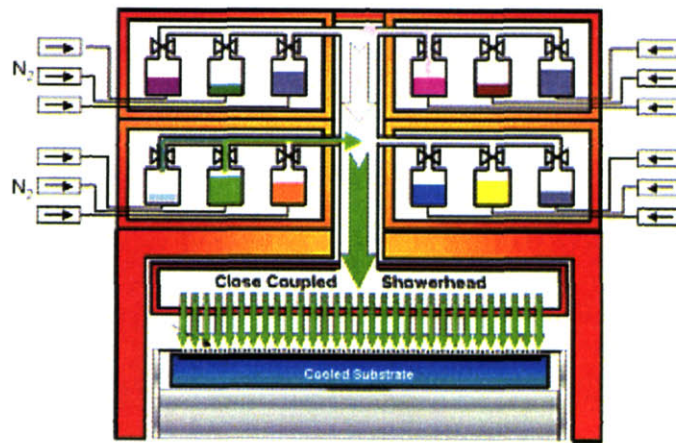
Figure 2-10. OVPD process

Characteristics and advantages of OVPD are listed as the following:

1. Hot walled deposition chamber can avoid undesired deposition of organics on the walls, thus the chamber is self-cleaned and deposition only occurs at the cool substrate surface leading to high materials use efficiency (>50%);

2. Transport and deposition of organic vapors are decoupled, allowing precise distribution control of the source vapor to form uniform layer on large substrates;

3. High purity carrier gas can minimize impurity incorporation during the film deposition while enables doping in the organic films.

OVPD is aiming as a replacement technique for vacuum thermal deposition. But it still must use a patterning technology to fabrication full color OLED displays. If a shadow mask is used for

65

patterning the organic layers, it will still result in lower material use efficiency and high maintenance cost due to the shadow mask. Furthermore, heat transfer from hot walls to the substrate on the cooling stage will require careful design and selection of the chilling system that must be powerful enough to keep the substrate cool. Lastly integration of OVPD system to other deposition schemes, e.g. vacuum chambers for metal deposition, can remain a problem to separate vacuum and non-vacuum environments yet still couple them together to enable transfer of samples from one process chamber to another.

The Organic Vapor Jet Printing (OVJP) system combines OVPD with a microscopic orifice (10~20 um) to achieve high-resolution dispensing. In OVJP, organic vapor is generated and mixed with a hot and inert carrier gas, forming a collimated vapor jet through the nozzle, and then condensed on a cooled substrate to deposit well defined thin film patterns. The nozzle size, nozzle-to-substrate gap and working ambient pressure determine the printed pattern quality and profile. OVJP operates in a similar fashion as InkJet. However, OVJP distinctly differs from the wet InkJet process [4, 34] in which it uses a hot inert carrier gas, instead of a liquid solvent. This eliminates solvent incompatibility issues of inkjet printing; unlike vacuum thermal deposition or OVPD, OVJP directly prints molecular organic semiconductors without using shadow masks. A disadvantage, however, still remains in depositing materials with low vapor pressure below 400 °C such as metals.

7. Soft lithography for patterning nanostructured devices

Soft lithography, including microcontact printing, nanoimprinting, cold welding and soft contact lamination, refers to a family of patterning methods using replicated elastomeric stamps, molds or conformal masks to construct patterns of functional materials, akin to conventional printing techniques described in chapter 1 such as flexography or intaglio printing. The term

"soft" is used because of the replication masters usually are polysiloxane and other elastomers [35, 36].

The soft lithography patterning scheme relies on replication of a patterned master to form an elastic stamp, which can then be inked to print high-resolution patterns as fine as tens of nanometers scale. The basis is the formation of an intimate and conformal contact between the inked stamp and the substrate. Soft lithography is well suited for patterning submicron systems; examples include biological applications (bacteria, proteins, DNA, antibodies, etc), optoelectrical applications (nanocrystals, organic molecules, metals, liquid crystals, etc) and high-density information applications (charges, magnetic bits, etc). In particular, organic electronics such as OLED and OFET can be patterned by soft lithography [37-40].

Seth Coe et al. [8] recently demonstrated patterning a quantum dot OLED with the microcontact stamping method (μCP). **Figure 2-11** outlines the process flow chart. The poly Dimethyl Siloxane (PDMS) stamp is molded from a silicon stamp master pre-patterned by photolithography and CVD coated with a layer of parylene. The quantum dot solution is spin-coated onto the stamp to form a monolayer. This monolayer of quantum dots are then μCP transferred onto a half OLED structure. The remaining structures are completed afterwards by thermal evaporation of organic thin films and metal cathode to fabricate a QD-OLED.

Technological limitations are usually related to the "soft" nature of the stamps that makes it very challenging to achieve high placement/alignment accuracy for multiple layer structures over large area.

prepare stamp master

Molded PDMS
Master

stamp release

PDMS stamp

clean substrate

ITO glass

Parylene coating

Parylene coated stamp

spin coat QDs

Parylene coated stamp

deposit HTL

HTL
ITO glass

Parylene coated stamp

μCP QDs

HTL
ITO glass

Parylene coated stamp

stamp release

HTL
ITO glass

Cathode

QD OLED

ETL
HTL
ITO glass
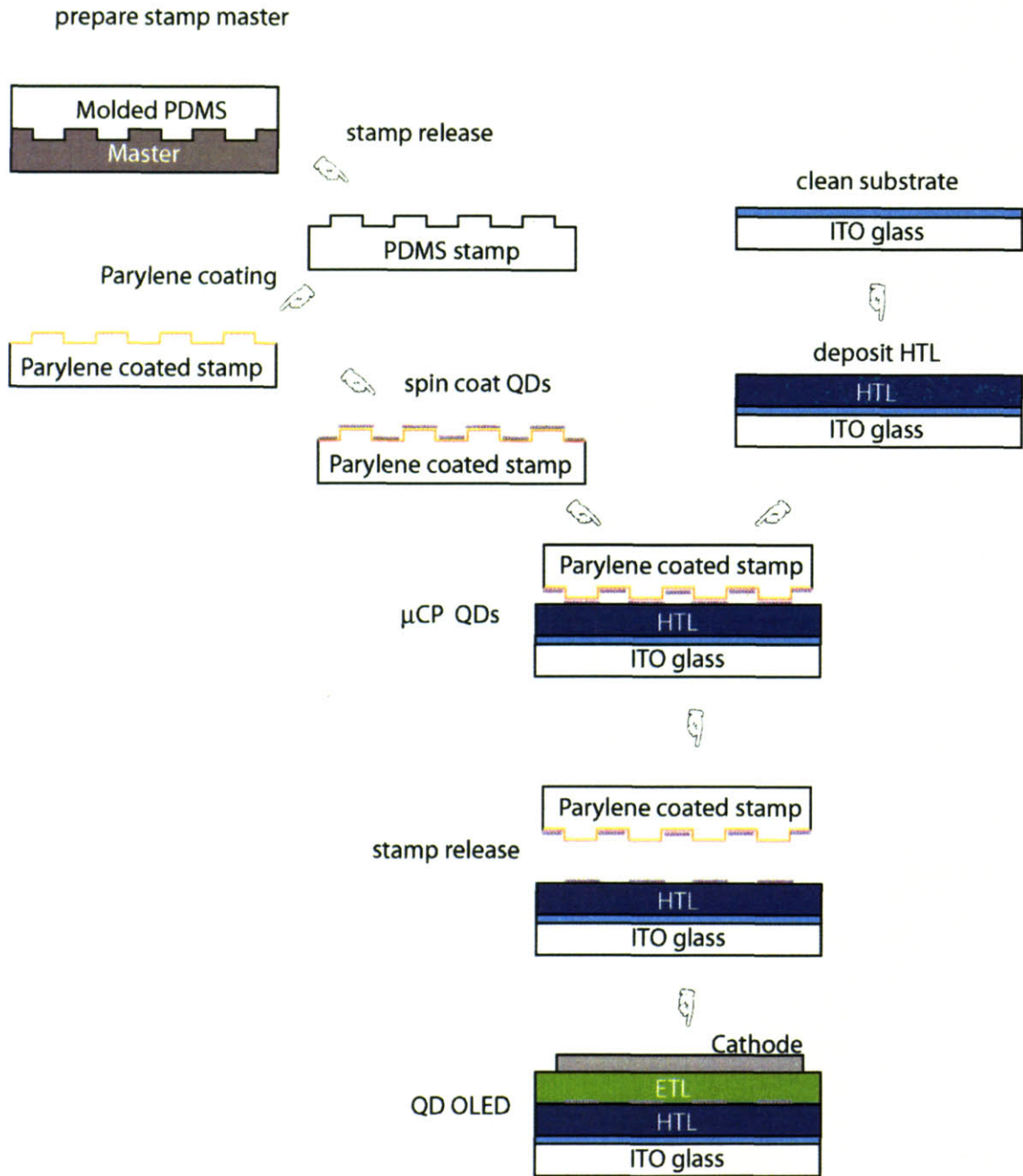
Figure 2-11 μ-contact printing quantum dot OLED flow chart [8]

Reference

[1]. D. Fyfe, Progress Towards the "Big Time", Presention at OLEDs 2005, San Diego, November 2005.

[2]. J. N. Bardsley, International OLED Technology Roadmap, IEEE J. Sel. Top. Quant., 10, 1., (2004).

[3]. S. R. Forrest, The path to ubiquitous and low cost organic electronic appliances on plastic, Nature, 428, 911 (2004).

[4]. H. Sirringhaus, et. al. High resolution inkjet printing of all polymer transistor circuits, Science, 290. 2123 (2000).

[5]. J. A. Rogers, Z. Bao, Printed plastic electronics and paperlike displays, Journal of Polymer Science A 40, 3327 (2002).

[6]. G. B. Blanchet, et al. Large area, high resolution, drying printing of conducting polymers for organic electronics, Appl. Phys. Lett. 82, 463, (2003).

[7]. M. Shtein, PhD thesis, Princeton University 2004.

[8]. Seth Coe-Sullivan, PhD thesis, MIT 2005.

[9]. G. Rorin, Key Challenges for OLED Industry Success, OLEDs 2005, San Diego, November 2005.

[10]. http://www.ipms.fraunhofer.com/en/products/OMS/inline-cluster-e.pdf

[11]. R. G. Larson, T. J. Rehg, Spin Coating, Liquid Film Coating, Chapman & Hall, London 1997.

[12]. A. G. Emslie, F. T. Bonner, and L. G. Peck, Flow of a viscous liquid on a rotating disk, J. Appl. Phys. 29, 858 (1958).

[13]. http://www.litrex.com

[14]. http://www.m600.com/pictures/drucker/tijfunktion-s.jpg

[15]. http://www.hp.com/oeminkjet/reports/techpress_11.pdf

[16]. H. P. Le, Progress and Trends in Inkjet printing, Journal of Imaging Science and Technology 42, 1 (1998).

[17]. J. Bharathan, and Y. Yang, Polymer electroluminescent devices processed by inkjet printing, Appl. Phys. Lett. 72, 2660 (1998).

[18]. Y. Yang et. al. Organic/polymeric, electroluminescent devise processed by hybrid inkjet printing, J. Mater. Sci, 11, 89 (2000).

[19]. H. Sirringhaus, T. Kawase and R. H. Friend, High resolution inkjet printing of all polymer transistor circuits, MRS Bull., 26, 539 (2001).

[20]. D. Huang, et. al, Plastic compatible low resistance printable gold nanoparticle conductors for flexible electronics, J. Electrochem. Soc., 150, G412 (2003).

[21]. S. B. Fuller, E. J. Wilhelm, J. M. Jacobson, Ink-jet printed nanoparticle microelectromechanical systems, J. MEMS, 11, 1 (2002).

[22]. http://www.litrex.com/index.cfm?page=wp1&crid=27

[23]. P. Calvert, Inkjet printing for materials and devices, Chemistry of Materials, 13, 3299 (2001).

[24]. J. N. Bardsley, International OLED Technology Roadmap 2001-2010, U.S. Display Consortium, Japan (2002) or http://www.oled-display.net/oledroadmap.pdf

[25]. J. L. Johnson, *Principles of Nonimpact Printing*, Palatino Press, Irvine 1992.

[26]. M. B. Wolk, et. al. , Laser thermal patterning of OLED materials, Proc. Of SPIE, 5519, Bellingham, WA 2004.

[27]. US patent 6194119, 6144088, 5521035.

[28]. PR Newswire, July 25, 2000.

[29]. http://www.universaldisplay.com/ovpd.htm

[30]. M. Shtein, et al., Drect, mask- and solvent-free printing of molecular organic semiconductors, Adv. Mater. 16, 1615 (2004).

[31]. M. Shtein, et al., Materials transport regimes and mechanisms for growth of molecular organic thin films using low-pressure organic vapor phase deposition, J. Appl. Phys. 89, 1470 (2001).

[32]. M. Shtein, et al., Effects of film morphology and gate dielectric surface preparation on the electrical characteristics of organic vapor phase deposited pentacene thin film transistors, Appl. Phys. Lett., 81, 268 (2002).

[33]. M. Shtein, et al., Mircopatterning of small molecular weight organic semiconductor thin films using organic vapor phase deposition, J. Appl. Phys. 93, 4005 (2003).

[34]. K.E. Paul et al., Additive jet printing of polymer thin film transistors, Appl. Phys. Lett., 83, 270 (2003).

[35]. http://www.wtec.org/loyola/nano/US.Review/04_02.htm

[36]. http://www.nanoterra.com/soft_lithography.asp

[37]. H. Klauk, Organic Electronics: Materials, Manufacturing, and Applications, Wiley-VCH, Weinheim 2006.

[38]. T. W. Lee, et al., Organic light emitting diodes formed by soft contact lamination, PNAS, 101, 429 (2004).

[39]. P. Cosseddu and A. Bonfiglio, Soft lithography fabrication of all-organic bottom-contact and top-contact field effect transistors, Appl. Phys. Lett. 88, 023506 (2006).

[40]. B. Michel, et al., Printing meets lithography: Soft approaches to high-resolution patterning, *IBM J. Res. Dev.*, 45, 697 (2001).

[41]. Z. H. Kafafi, Organic electroluminescence, CRC press, New York 2005.

CHAPTER 3. First generation Molecular Jet printing technique

CONTENTS

1. Background and introduction

A growing interest in organic electronic devices is sustained by continuing demonstrations of striking display applications based on organic light emitting devices (OLEDs) and the promise of organic field effect transistor (OFET) circuits for ubiquitous electronics. To date, however, significant challenges still remain in the fabrication of high definition pixelated OLED patterns, and in the realization of high yields in production of commercial OLED displays. The highest efficiency OLEDs are fabricated using thermal evaporation of molecular materials, with shadow mask patterned sub-pixel features. In order to be used in high-definition full color displays, an acceptable pixel pitch should be less than 250 μm, equivalent to three 40 μm wide red-green-blue sub-pixels placed side by side and separated by less than 50 μm [1]. However, defining 40 μm features through a shadow masking process requires using thin (and, unfortunately, easily warped) metal shadow masks and precisely controlling the separation between the shadow mask and the substrate [2]. There are two requirements that become limiting factors when trying to scale up the mask size beyond Gen3 substrate plates. Alternative methods of micron-scale patterning, such as conventional subtractive patterning by solvent-based photolithography and plasma etching, have not been adopted as they can damage the active organic layers if applied to

directly pattern organic devices, leading to significant degradation in the device performance or even complete failure. Consequently, several additive processes have been proposed and developed for patterning polymeric and molecular organic thin films by directly printing organic semiconductors onto various substrates. These include: inkjet printing [3,4], laser induced thermal imaging (LITI) [5], organic vapor jet printing (OVJP) [6], micro-contact stamping [7] and the molecular jet printing (MoJet) technique presented in this chapter. From the multitude of the proposed patterning techniques, it is clear that no consensus has been reached on the most effective method of OLED patterning; but it is also clear that further improvements in commercial organic devices fabrication are closely tied to the patterning technique, and the ability to scale the technique up to large area substrates.

Among the additive deposition techniques, the most advanced is the inkjet printing process, which has recently been scaled to patterned deposition on Gen 7/8 substrates [8]. Inkjet printing is inherently a solvent-rich technique, restricted to materials that can be solvent processed with suitable viscosity. The inkjet processing also raises the issue of solvent compatibility in multilayer structures and concerns of thickness non-uniformity across deposited films [9]. The complementary, evaporative MoJet printing technology, described in the present work, alleviates these concerns.

The MoJet printing technique enables direct evaporative patterning of low molecular weight organics and metals at high resolution. In the present work, we use the MoJet technique to demonstrate that active organic devices such as OLEDs and OFETs can be directly fabricated with print accuracy and pattern definition of better than 5 μm. Because the MoJet printing scheme is a solvent-free process, it combines the high quality of thermally evaporated thin films with high patterning precision and scalability enabled by micro-electro-mechanical system

74

(MEMS) printing technology. We demonstrate that performance of MoJet printed OLEDs and OFETs is similar to those fabricated by the shadow mask patterning method. However the MoJet printed devices can be patterned at higher resolution on a substrate plate that can be larger in size than GEN 2/3 glass, typical of today's OLED substrates.

2. Experiment design and system setup

The basic experiment design and system setup is described in this section. Results of printing molecular organic semiconductors, high definition OLEDs and OFETs are presented. Discussions on the print pattern formation as well as the performance of printed devices are also included.

2.1. Printing system

The entire printing system is housed inside a vacuum chamber (in **Figure 3-1**) at a base pressure of 10^{-7} Torr.
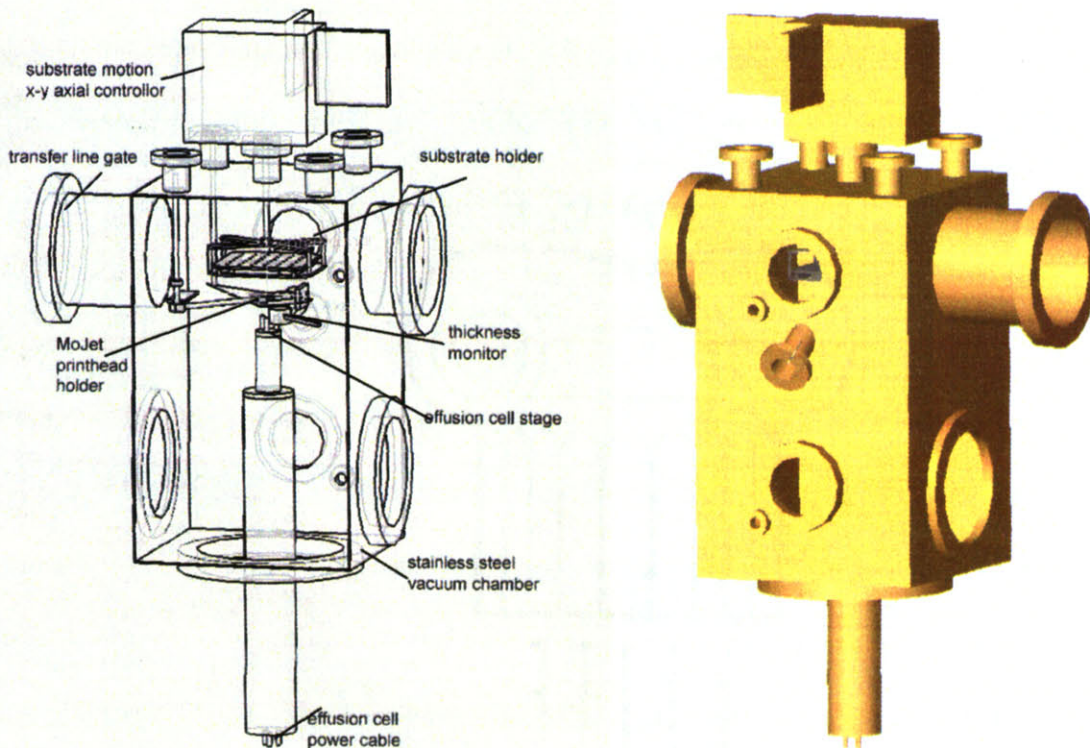
Figure 3-1. Vacuum chamber for the MoJet printing system
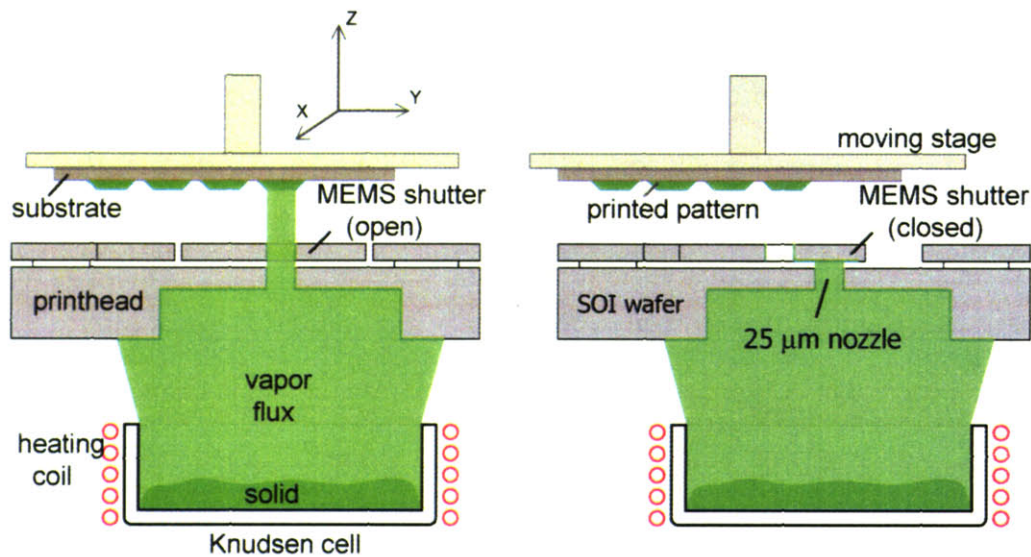
Figure 3-2. Illustration of the molecular jet printing (MoJet) apparatus and process. Vapor flux of the evaporated materials is generated by a Knudsen cell. The flux can pass through the nozzle and reach the substrate to form a deposited pattern, when the micro shutter is open. When the micro shutter is closed, the nozzle is covered and the vapor flux is blocked from reaching the substrate

The MoJet printing system, sketched in **Figure 3-2**, consists of a thermal effusion cell, a silicon MEMS printhead and a computer controlled moving stage. The substrate is mounted to a substrate holder sitting on a fixture above the printhead. The fixture is rigidly connected to a moving stage that can manipulate the substrate's position in X, Y and Z direction. A Luxel Knudsen cell (K-cell) is used to generate evaporated material flux from underneath the printhead. The materials to be deposited are loaded in an alumina or quartz crucible and heated above the sublimation/boiling temperatures. In the experiments described below, aluminum tris(8-hydroxyquinoline) (Alq$_3$), pentacene and silver are individually loaded inside the K-cell crucibles as printing materials. Two distinct source temperature regimes are adopted: for organic material deposition, the heating temperature is below 350 °C; for metal deposition, a much higher heating temperature is required (e.g. 1100 °C for evaporating silver). The printing system operates as a single-nozzle printer. The printed pattern is traced by sending the coordinates of

each pixel to the moving stage controller, which is translated to mechanical movement of the substrate with 2 μm accuracy.

2.2. MEMS printhead
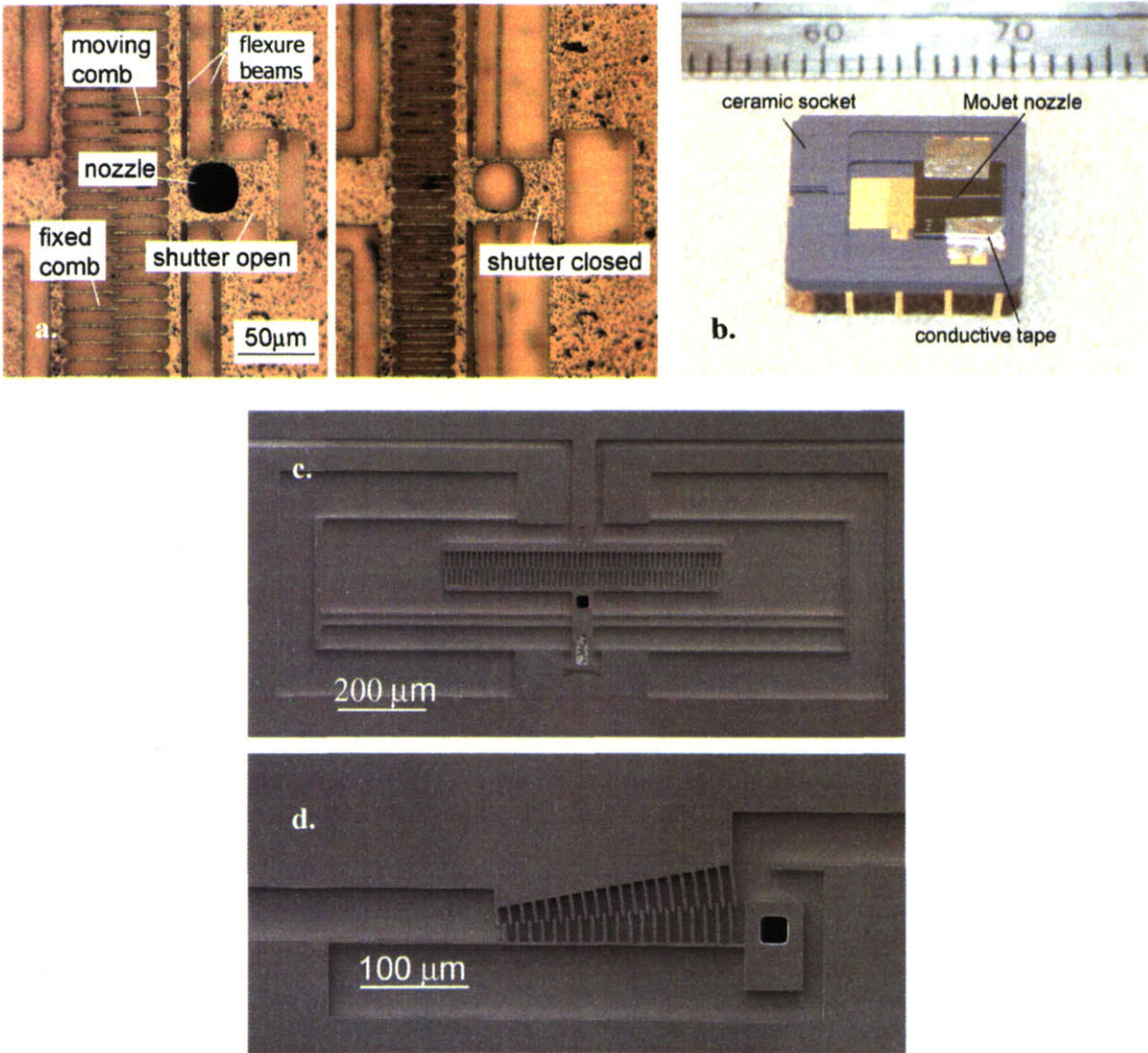
Figure 3-3. MoJet MEMS printheads. (a). Optical microscope images of the printhead, shown with the detailed structure of parts. The micro shutter is actuated by a DC bias. When the shutter needs to be closed, for example during the deposition process while the printhead is moving, a DC bias (30 V for the above structure) is applied across the parallel comb electrodes. The electrostatic force overcomes the tension of flexure beams and pulls the shutter to completely cover the aperture. Once the DC bias is set back to zero, the shutter releases from the closed position and the nozzle is unblocked to allow material flux to pass through. (b) Final packaged device showing the MEMS chip is mounted on a ceramic socket and electrically connected to socket terminals via low profile conductive tapes. (c). SEM image of a symmetric comb drive actuator (d). SEM image of a more compact Zipper actuator.

As shown in the photograph of **Figure 3-3a**, the MoJet printhead is composed of a membrane aperture (nozzle), and an integrated comb-drive-actuated microshutter, which modulates the flux of evaporated materials through the nozzle [10, 11]. The nozzle aperture (e.g. $25 \times 25 \ \mu m^2$ opening size) and the comb-drives are fabricated by deep reactive ion etching of a silicon-on-insulator wafer. The fabricated chip is then mounted onto a custom-made ceramic socket for electrical connection and mechanical support (**Figure 3-3b**). The micro shutter closes when 30 V DC bias is supplied, interrupting the organic flux and preventing organic thin film deposition on the substrate. Two designs of the MEMS printheads have been developed: the first design comes with a long comb-drive actuator and long flexure beams, thus the nozzle packing density is relatively low (**Figure 3-3c**); the second design approach is more compact and may be a more viable alternative in making high density nozzle arrays (**Figure 3-3d**), however, shorter actuator requires higher driving voltage (~90 V DC) compared with the previous design (~30 V DC). Both designs are scalable with little efforts to fabricate multi-nozzle printhead.
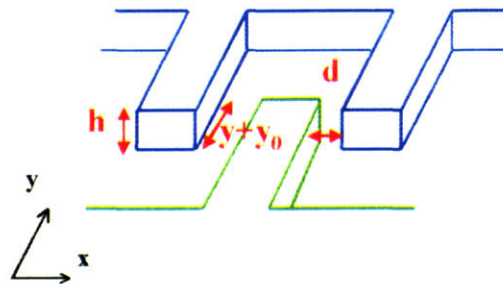
Figure 3-4. Comb drive electrodes

Comb drive electrodes are suspended in air, and essentially behave as a capacitive device (**Figure 3-4**). The capacitance between two electrodes is described as:

$$C = \frac{2n\varepsilon h(y + y_0)}{d} \qquad (3\text{-}1)$$

n is number of pairs, and ε is the dielectric constant of air.

By applying a voltage between the two sets of fingers, the induced electrostatic force between the two electrodes can be described by:

$$F = \frac{1}{2} \frac{\partial C}{\partial y} V^2 = \frac{n\varepsilon h}{d} V^2 \qquad (3\text{-}2)$$

The mobile set of electrodes can be displaced by the electrostatic force and in balance with the folder spinge.

$$ky = F = \frac{n\varepsilon h}{d} V^2 \Rightarrow y = \frac{n\varepsilon h}{kd} V^2 \qquad (3\text{-}3)$$

k is the spring constant of the flexure beam.

The displacement of the mobile fingers is modulated by the applied voltage that increases with the square of the driving voltage. **Figure 3-5** shows that the MoJet nozzle aperture can be modulated from full open to full close as the applied voltage shifts from 0 to 30V.
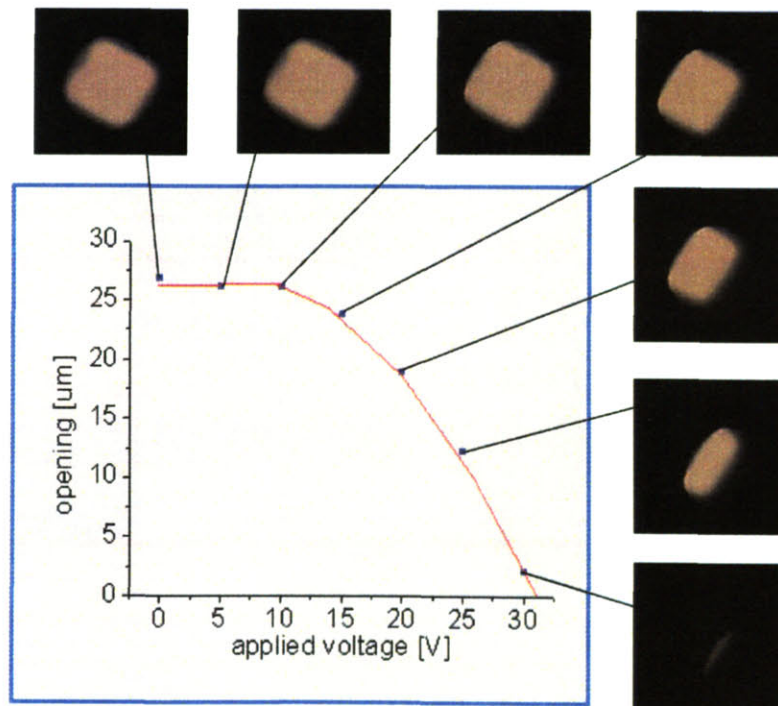
Figure 3-5. Open size modulation of the MEMS shutter by an actuation DC signal

The fabrication process flow is developed by V. Leblanc [10, 11] in **Figure 3-6**. The devices were fabricated starting with an SOI wafer (step 1) with 3 µm buried oxide and 11 µm device layer. A layer of 500 nm of silicon dioxide was thermally grown as the top layer. Photolithography and wet etch in buffered oxide etch (BOE) defined a nested mask for the device layer (step 2). A second photolithography step on the backside using a thick photoresist (AZ P4620) then defined the backside well etched by DRIE in the silicon base layer (step 3). The last photolithography step defined self-aligned apertures on the front that were etched through the device, oxide, and base layers by DRIE and dry oxide etch (step 4). The photoresist was then stripped and the oxide mask was used to pattern the device layer by DRIE (step 5). The wafer was subsequently covered with thin photoresist and diced, then cleaned in an oxygen plasma. Finally, a timed etch was performed on the oxide buried layer in hydrofluoric acid (HF) to release the structure, followed by a cleaning step in isopropanol (step 6).

1. Starting with SOI wafer

2. Pattern front structure

3. DRIE forming membrane

4. Etch through hole by DRIE

5. Forming front features

6. Release moving features

Silicon   Oxide   Photoresist
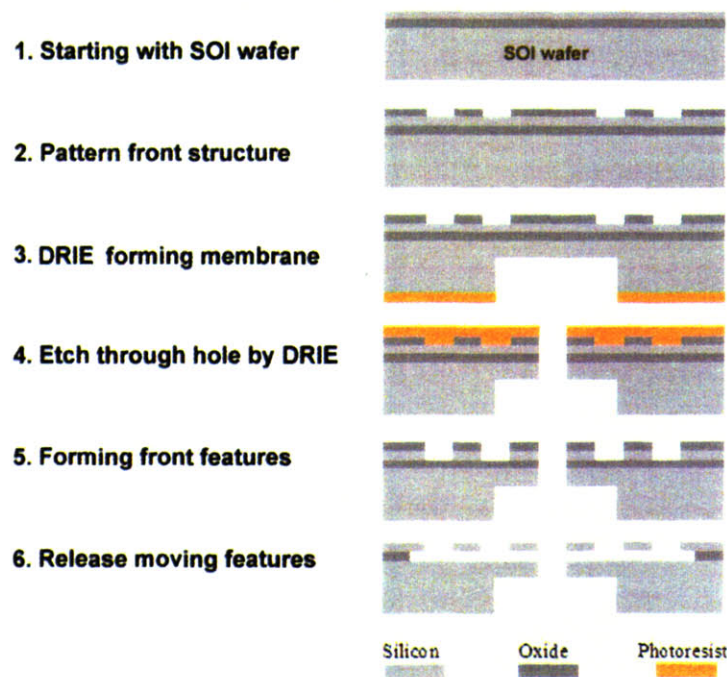
Figure 3-6. Illustration of the MoJet printhead fabrication process

2.3. Pattern profile formation

Figure 3-7. (a). Schematic of the MoJet printing system. Dashed lines represent the trajectory path of evaporated molecules inside a vacuum chamber at pressure below 10^{-6} Torr. When the printhead is separated from the substrate by distance s, the printed pattern will broaden by $2b$. (b). Plot of the pixel size as the function of s and h/D ratio. The size of printed pixel (Alq$_3$ in this case) varies linearly with the separation distance s. This plot shows that by reducing the gap between the printhead and the substrate, and increasing the h/D aspect ratio, produces smaller broadening of the printed pixel.

Figure 3-7a illustrates the schematic of the MoJet printing system situated in vacuum. At a pressure of 10^{-7} Torr, the mean free path of MoJet evaporated molecules is larger than the dimension of the MoJet vacuum chamber. Consequently molecules of evaporated materials travel in straight lines away from the K-cell, with negligible inter-molecular scattering. Under such condition, the printed pixelated pattern is defined by the ballistic trajectory of the jetting molecules. A previous study [2] on vacuum deposition using shadow masking suggests that when the nozzle is centered on the K-cell crucible orifice (of diameter D), the pixelated pattern will form a taper of width b+c. b reflects a broadening of deposited pixel due to separation s between the printhead and the substrate, while c denotes the shrinkage of the top plateau. The taper region p can be quantified as:

$$p = b + c = \frac{D-w}{2h}(s+t) + \frac{D+w}{2(h+t)}s$$

(3-4)

Here h is the source to printhead distance, w is the nozzle aperture size and t is the nozzle thickness. The diameter of the printed pattern is 2b broader than the nozzle aperture size. If $D \gg w$ and $h \gg t$, b is approximately equal to:

$$b \approx \frac{D}{h}s$$

(3-5)

D/h is the aspect ratio determined by the system geometry. Either smaller crucible diameter or longer crucible-to-printhead distance could reduce the printed pixel broadening (**Figure 3-7b**). In our system, the gap s has been the primary controlling factor of pixel shape. We find that the printed pattern broadens by 2b = 7 μm with every 100 μm increment of s. Therefore to define a smaller than 40 μm pixel using a w=25 μm aperture, i.e., the broadening of the pixel should not exceed 15 μm, and s should be maintained at less than 200 μm.
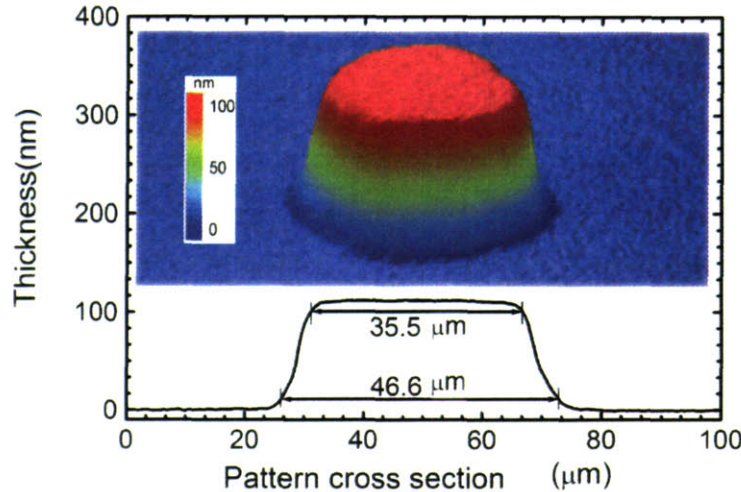
Figure 3-8. Profilometric characterization of a MoJet printed silver pattern. The thickness profile is taken through the center of the circular pattern. Insert is an interferometery optical microscopy image of the silver circular pattern printed at S_0 (zero gap) through a 50 μm diameter aperture. 46.6 μm and 35.5 μm are the diameters measured at 10% and 90% of the height of the pattern respectively.

82

As an example of a MoJet printed pixel, Figure 3-8 shows a circular silver pattern printed through a w=50 μm aperture. The graph shows the trapezoidal cross section of the pattern, and the flat top surface, which is desirable in OLED structures for uniform current and brightness distribution across the pixel.

3. Results and discussion (printing OLEDs and metals)

3. 1. Printing of OLED material Alq3

Aluminum tris(8-hydroxyquinoline) (Alq3) is frequently used as the green fluorescent emitting material in OLEDs, which undergoes direct solid-gas sublimation during evaporation. Stable and high evaporation rate can be achieved during the deposition and its PL spectrum is clearly visible under a fluorescent microscope. Thus, it is an ideal source material chosen for printing with the MoJet printer system. The properties of Alq3 is summarized in **Figure 3-9** [12].
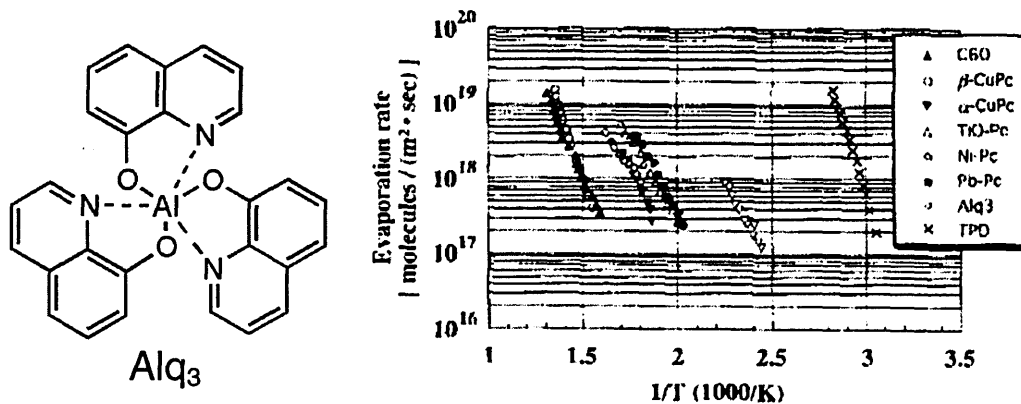
Figure 3-9. Structure and thermal properties of Alq3

Alq3 powder, already purified by zone-sublimation, is loaded inside an alumina crucible in a Luxel Knudsen cell. During the printing, the chamber is pumped down below 5×10^{-6} Torr, the source cell temperature is maintained at about 230 °C and the deposition rate is stable at ~1 nm/sec [13]. The substrate can be manipulated by the moving stage during the printing and the micro shutter can open or close to modulate the Alq3 flux.

Figure 3-10a shows the very first PL image of a printed Alq3 array. The film thickness is about 100 nm for each pixel. This result demonstrates the capability of the printer to print arbitrary patterns by simultaneously moving the substrate. **Figure 3-10b** is the profile of printed patterns, quantified by WYKO surface profiler (from Veeco metrology group) in phase shifting interferometry mode, using a filtered white light band, narrow bandwidth (center wavelength of 632nm). The 3D profile of the printed pattern is shown next to its PL image. The cone shape of pixel profile indicates that the printhead to substrate distance is beyond the optimal value of 200 μm, as a result the taper region dominates the pixel profile.
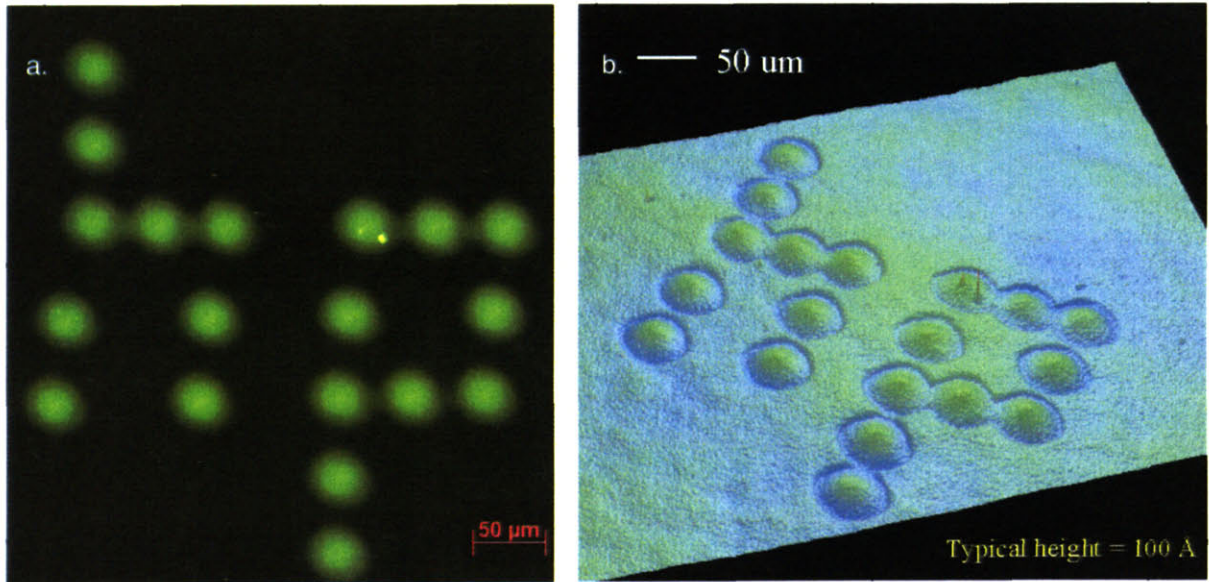
Figure 3-10. PL and 3D profile of the printed arbitrary pattern

The printing speed of the sytem is not constrained by the mechanical modulation frequency of the printhead actuator, which is 6kHz. The rate-limiting step is the sublimation rate of the source materials, which is controlled by the source temperature. For example, we consider deposition of Alq$_3$ thin films at a high deposition rate of 300 nm/sec (achievable at source temperature below 300 °C) [14]. A 30 nm thick Alq$_3$ film can then be printed within 100 millisecond, requiring a mechanical switching frequency of only 10 Hz. In practice, a multiple-

nozzle printhead could be implemented to reduce the printing cyclic time. By using a multiple-nozzle array, both printing speed and patterning area can rise in proportion. A typical XVGA display panel with 1024×768×3 RGB subpixels can then be printed in less than 5 minutes using R, G and B printheads with 800 nozzles at deposition rate of 300 nm/sec and assuming 100 nm thick pixels.

3.2. Printing high resolution OLEDs

The OLED device structure is shown in **Figure 3-11a** together with the chemical structure of molecular materials **Figure 3-11b**. To fabricate the OLED array, first an ITO substrate is sonicated in micro-90 detergent solution and DI water, then degreased by sequential rinses in acetone and isopropanol, and finally treated with oxygen plasma. A PEDOT:PSS solution (Baytron® P VP CH 8000 acquired from H. C. Starck) is spun at 3000 rpm onto the clean ITO surface, followed by a 30 minute post-baking at 100 °C. The sample is then loaded into a vacuum chamber for sequential deposition of organic layers. On top of the ITO anode and the PEDOT:PSS hole-injecting layer (HTL), 30 nm thick TPD hole-transporting layer is blanket deposited. Using the MoJet printing nozzle, an array of 12 nm thick islands of electroluminescent (EL) layer of Alq3 is then printed at 50 um pitch. This is followed by blanket deposition of 30 nm thick TAZ electron-transporting layer (ETL). A magnesium:silver (10:1 mass ratio) layer is deposited in the last step as the cathode.

Electroluminescence images of the printed OLED array are shown in **Figure 3-11c**. Note that each pixel is 30 by 30 micron square, and 30 micron side by side, which is equivalent to a resolution of 800 ppi. At video brightness, the operating voltage is 7.5 V. **Figure 3-11d** shows the energy band diagram of the printed OLED that light was produced from both TPD/TAZ and

TPD/Alq3/TAZ heterostructures. When the EL is taken behind a 470 nm wavelength low pass filter, it clearly shows green light emission from the printed Alq_3 array.
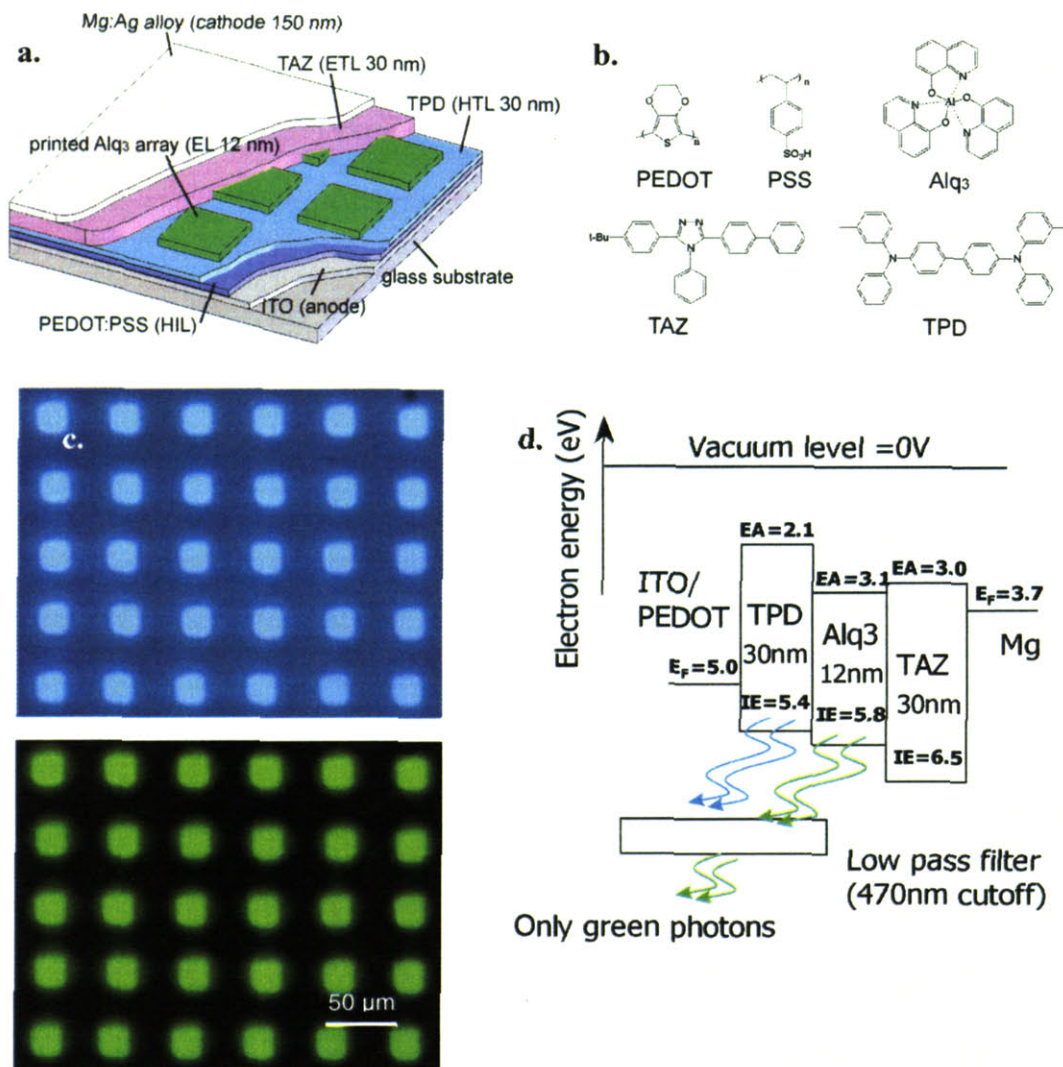
Figure 3-11. (a). Illustration of the layer structure of the printed OLED array. The green electroluminescent layer (EL) layer is directly printed by the MoJet technique. (b). Chemical structures of the materials used: PEDOT (poly(ethylenedioxy)thiophene), PSS (poly(styrenesulfonate)), Alq_3 (tris(8-hydroxyquinoline) aluminum), TAZ (3-(4'-tert-butylphenyl)-4-phenyl-5-(4"-biphenyl)-1,2,4-triazole) and TPD (N,N'-diphenyl-N,N'-bis(3-methylphenyl)-1,1'-bipheneyl-4,4'diamine). (c). Electroluminescence micrograph of the active OLED array at an applied voltage of 7.5V. The top image is the electroluminescent image taken directly under the optical microscope. The bottom image is taken through a 470 nm low pass filter to block the blue electroluminescent light from the TPD film and reveal the green emission of Alq_3 pixels patterned by MoJet. (d). Energy diagram of printed OLED

In this high-resolution printing of an active OLED array, we used a 25 μm nozzle. The size of each printed pixel is 30 μm on 50 μm centers, equivalent to 800 ppi resolution and 500 ppi printed pitch.

3.3. Printer resolution

To demonstrate printing of optoelectronic devices at high resolution, pairs of Alq3 pixels are printed with different center-to-center (cc) distances (in **Figure 3-12**) to determine the resolution limit of our MoJet printing setup, When cc distance is equal to the pixel size (i.e., cc=25 μm), two individual pixels are still resolvable. For shorter cc distance, the two pixels partially overlap (cc=15 μm) or superimpose to become one indistinguishable pixel of larger size (cc=5 μm). The minimal resolvable feature size in MoJet printing technique is thus determined in turn by the nozzle size and the mechanical accuracy of the substrate moving stage (2 μm in our setup).
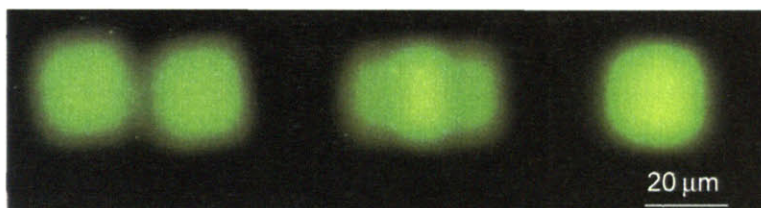
Figure 3-12. Photoluminescence (PL) micrograph of 25 μm×25 μm Alq3 pixels printed on silicon. From left to right, the center-to-center distances between two pixels are varying from 25 μm, 15 μm, down to 5 μm.

3.4. Printing arbitrary metal pattern

The MoJet printing system is also used to directly pattern metals with high melting point, such as silver. Although the setup is similar to printing Alq3, the K-cell crucible has to be heated to 1100 °C before sufficient silver vapor flux is observed. At such a high temperature, the entire printer is exposed to thermal radiation from the K-cell heating source, which can lead to thermal expansion of the printer fixtures and significant distortion of the final pattern printed on the substrates. To reduce the thermal radiation, stainless steel sheets, with an opening in the center

that is smaller than the crucible size are inserted between the K-cell and the MEMS printhead, as illustrated in **Figure 3-13a**.
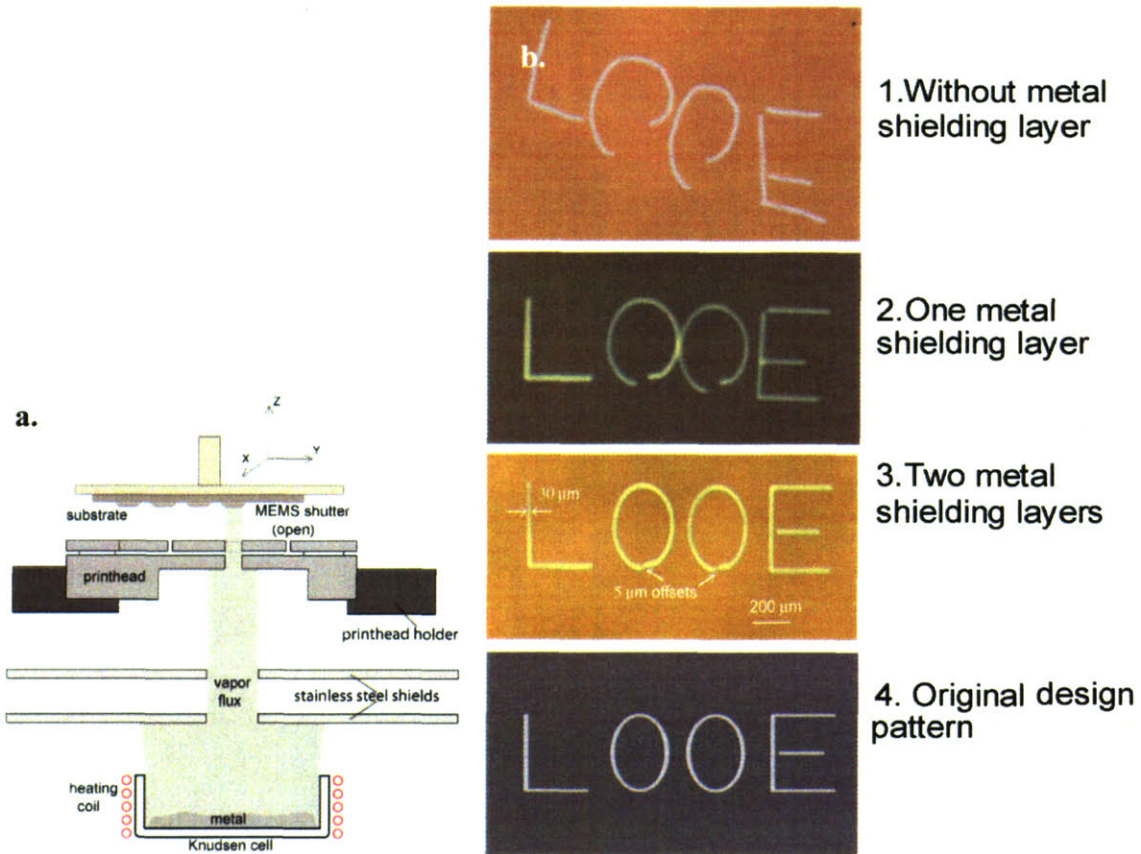
Figure 3-13. (a). Thermal shielding layers inserted in the path of metal vapor flux to limit the inadvertent printhead and substrate heating. (b). 30 μm line width silver pattern MoJet printed on a silicon substrate. Note that plotting of a circular pattern results in ~5 μm offset due to radiative heating of the MoJet printhead by the 1100 ºC K-Cell which causes mechanical distortions arising from thermal expansion of the fixtures.

The shielding layers can allow metal vapor flux to go through while blocking most of the radiated heat. Arbitrary patterns of silver lines of 30 μm width can be plotted on a silicon substrate, as shown in **Figure 3-13b**. Starting without the thermal shields, the printed metal pattern is significantly distorted; Adding metal shielding layers can greatly improve the print quality. The 5 μm offset noticed in the figure is a result of remaining radiative heating, which can be further minimized by applying a reflective coating to the substrate holder fixtures. **Figure**

3-14 shows a set of parallel silver electrodes printed with negligible distortion under such print conditions.
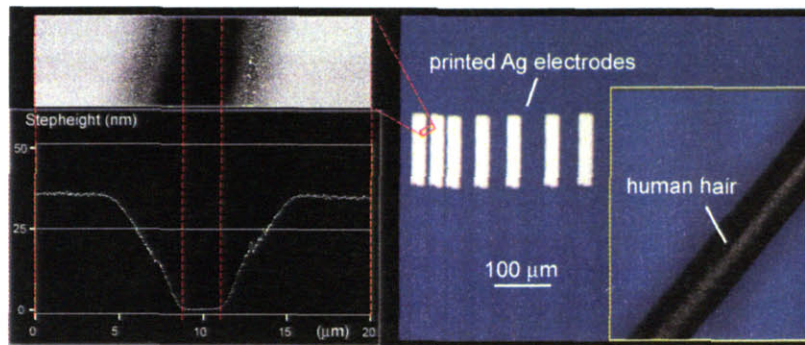
Figure 3-14. Optical microscope image of MoJet printed parallel silver electrodes on thermal silicon oxide with various spacing; a string of human hair is used as a reference (1:1 ratio). AFM image reveals that there is indeed no silver deposited in the 5 μm wide groove between the electrodes

3.5. Metal pattern thickness vs. conductivity
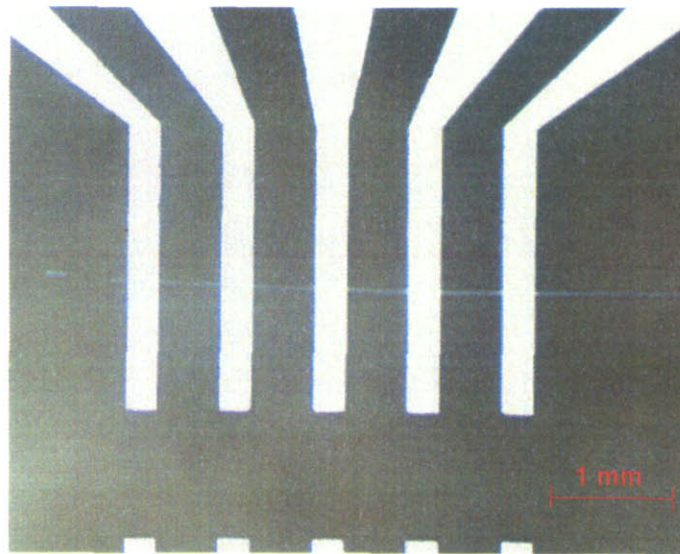
Figure 3-15. Test pattern for 4 probe conductance measurement

The general relationship between the conductance and the thickness of printed silver lines is studied. The effect of conduction electron scattering at grain boundaries, while small in bulk (thick) films and single crystal thin films, is dominant in the polycrystalline thin films. **Figure 3-15** shows a directly drawn 5mm long silver line across four silver contact pads for four probe

measurements. The thickness of the silver pads and line is measured by a Tencor P10 profilometer. Atomic force microscope (AFM) images (**Figure 3-16**) reveal that this silver line is indeed discontinuous microscopically, with grain size on the order of a few nanometers; while the silver contact pads are atomically rough but electrically conductive.
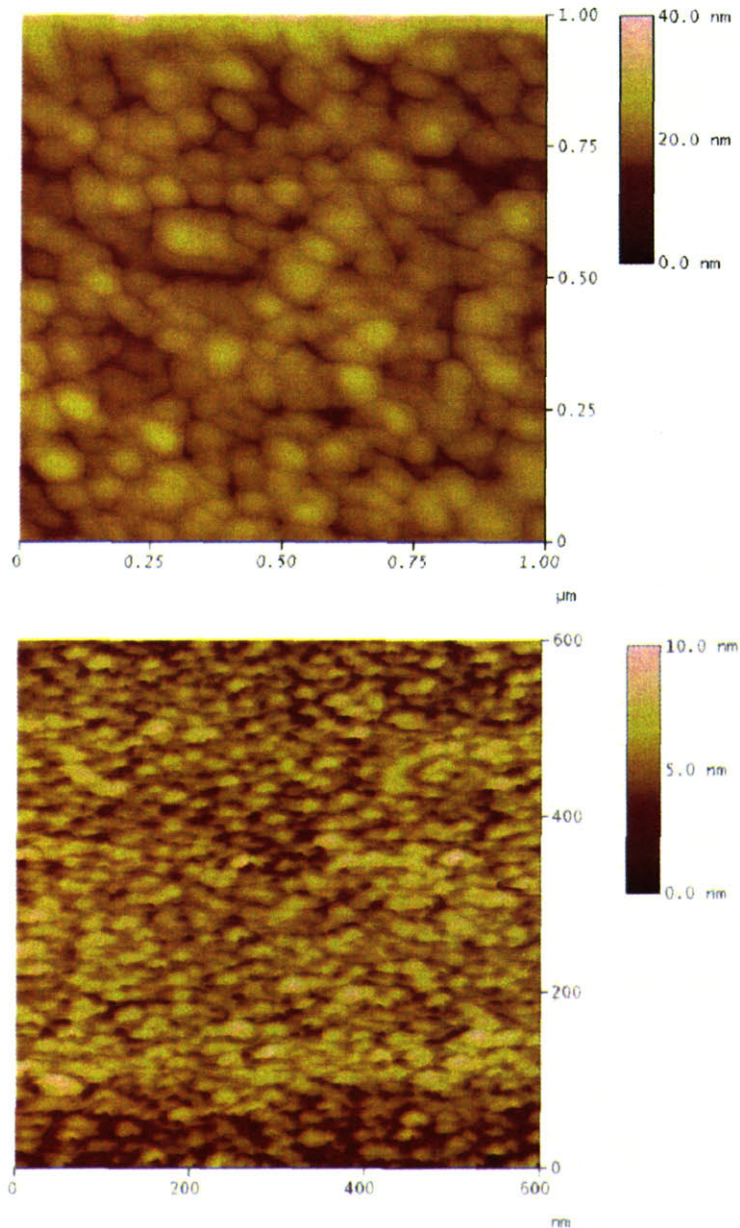
Figure 3-16. Atomic Force microscope images of silver contact pad with thickness of 120 nm and silver line of 6 nm. Average grain sizes of silver pad and silver line are 40 nm and 11 nm.

To determine the relationship between thickness and film conductance, sequential blanket depositions of silver films were made on top of the probe-structured contact pads and the current was measured in situ. It is observed that significant current (~1 mA) shows when the film thickness exceeds 40 nm, in good agreement with ref [15]. To verify this result, silver lines of different thickness (20 nm, 30 nm, and 40 nm) were again drawn and the conductance measurements were performed, as shown in **Figure 3-17**. The result clearly indicates that 40nm film thickness is essential to be sufficiently conductive to pass a milliamp current. Therefore, in the following demonstration, the printed silver patterns are at least 40 nm thick.
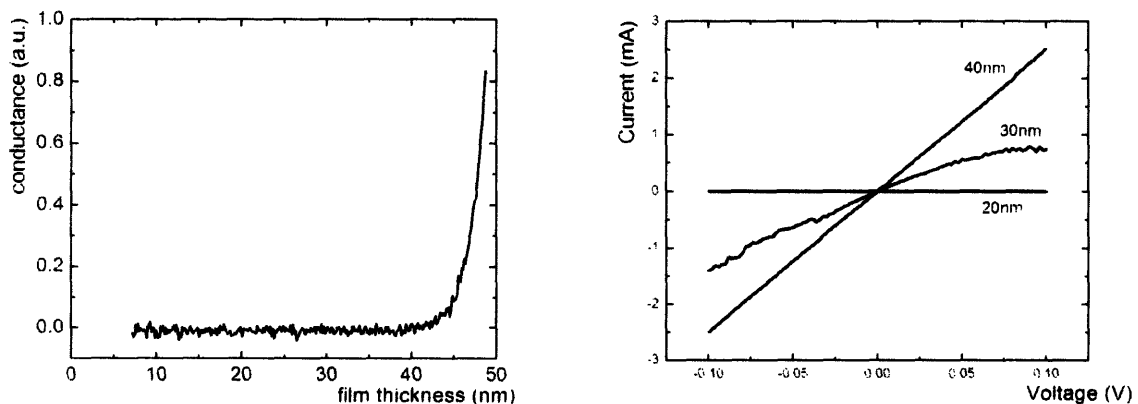
Figure 3-17. Relationship between silver pattern conductance and thickness

3.6. Failure modes of MoJet I printhead

Nozzle clogging issue

During the normal use of the printhead, source materials are deposited not only onto the substrates, but also onto the sidewall of the nozzle aperture and the backside of the shutter. In our tests, even after tens of hours of continuous use at various deposition rates (1-10 Å/s), the opening size of the aperture did not shrink conspicuously from progressive clogging of the nozzle. However the nozzle can still be clogged especially after source materials spit out from

the crucible at high heater temperatures. Chunks of Alq3 might block the nozzle aperture as shown in **Figure 3-18**.
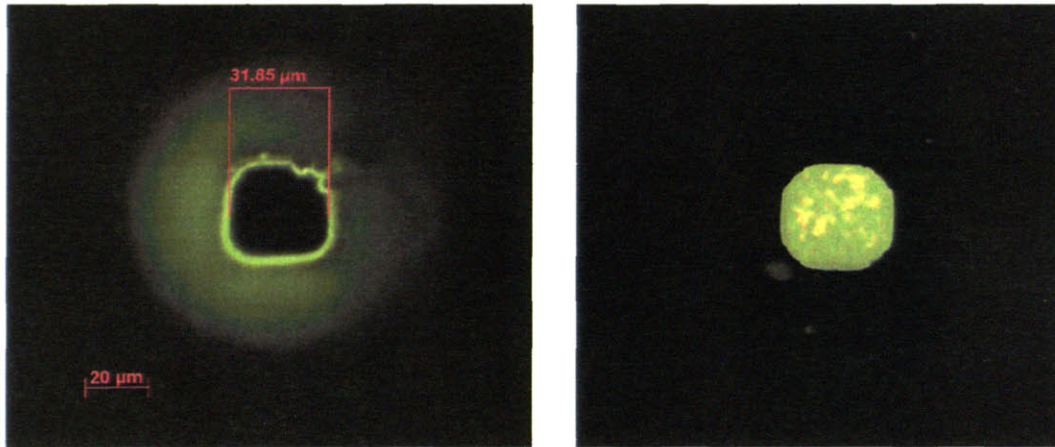
Figure 3-18. PL images of nozzle aperture after continuous use and after being clogged by Alq3. Green emission confirms that alq3 is deposited. The right image shows that chunks of alq3 fill inside the pore and block the flux.

We notice that after prolonged use a thick film of material will accumulate on the backside of the shutter and impede its open/close action, or will clog the aperture to block the vapor flux from getting through. We estimate that in a typical continuous operation, the printhead shutter is in the closed position during less than 1% of the printing time. Since the gap between the shutter and the bulk of the SOI wafer is 3μm, we can deposit 300μm thick film through the printhead nozzle before the material accumulated on the back of the shutter results in shutter stiction.

Damage by impact and stiction

The first generation MoJet printhead utilizes fragile moving parts and operates very closely to the substrate, which can cause severe damage to the printhead when it impacts the substrate. This also affects the printhead cleaning procedures about how the deposited source materials are removed. If wet solvent cleaning is used, the surface tension might bring suspended structures

together and immobilize the moving parts. **Figure 3-19** shows a typical example of damaged printheads during wet solvent cleaning procedure.
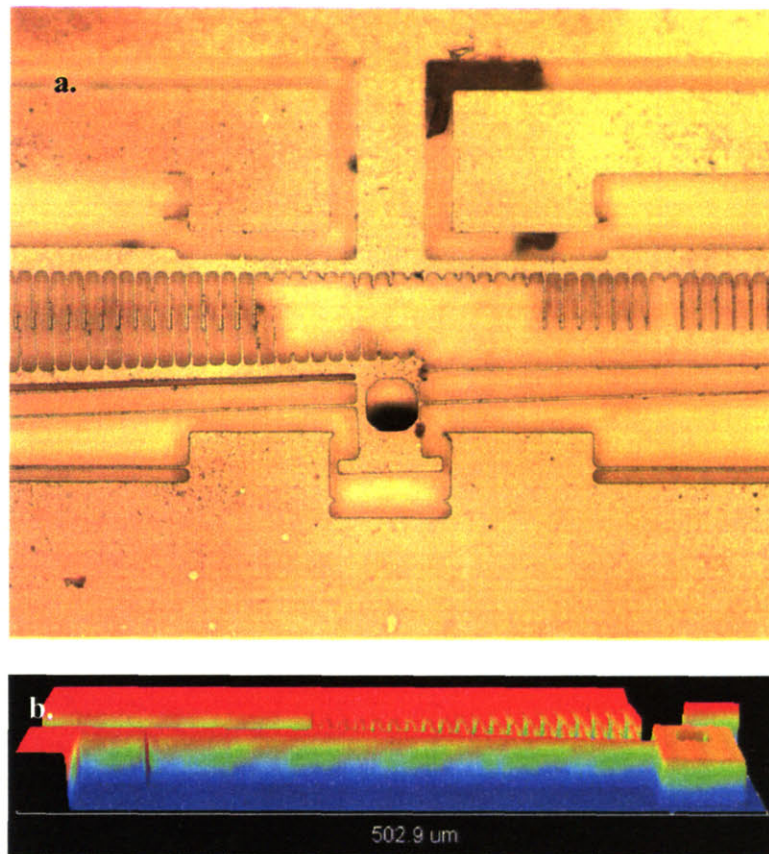
Figure 3-19. Damaged printheads. (a). broken comb drive actuator by sonication in acetone; (b) stiction of the zipper moving comb to the substrate by soaking in acetone

To avoid stiction and clogging, a periodic printhead self-cleaning might be necessary, in analogy to the periodic printhead cleaning routine presently utilized in inkjet printers. The printhead can be temporarily moved to an auxiliary heating station where accumulated materials can be re-evaporated to restore the printhead back to its pristine state. We note that printhead cleaning with wet solvents would be less attractive because of the potential for MEMS devices such as this to experience the 'stiction' phenomena upon drying, which would make the device inoperable. Another solution is to replace the micro-shutter mechanism with a more robust design, as we will describe in the second generation MoJet printhead design.

4. MoJet I Printing pentacene OFET

4.1. Introduction

Research interests in organic semiconductors can be traced back to the late 1940s. However, charge mobility in organic materials remained substantially lower than silicon based devices, possibly because of inadequate purification methods and lack of understanding of the relationships between electrical conduction and structure-property relations in organic solids. This was the case until the emergence of the pentacene organic transistor, whose charge carrier mobility is comparable and in some cases even higher than amorphous silicon. Nevertheless reports of continuous improvement in the organic transistors have maintained research interests. Subsequently organic thin film transistors have been included in the research work of many large companies, to name a few: 3M, Samsung, Pioneer, Philips, Dupont, and Sarnoff.

Although for transistors fabricated on single crystal of pentacene the hole mobility has exceeded 50 cm^2 sec^{-1}V^{-1} [15], charge transport in polycrystalline structured thin film channel and interfacial structure-property effects still pose challenges to achieve elevated and reliable mobilities in thin film pentacene OFET (>1 cm^2 sec^{-1}V^{-1}).
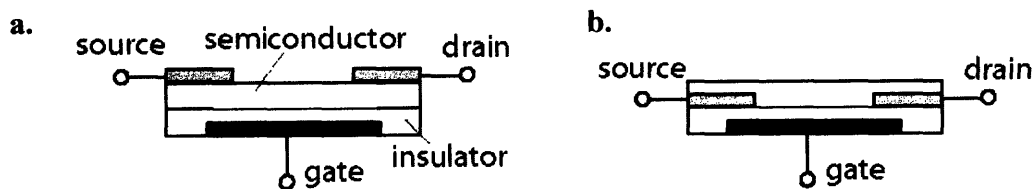
Figure 3-20. OFET device architectures (a). Top contact (b). bottom contact

The structure of OFETs (see **Figure 3-20**) consists of four parts: a thin organic layer as the charge transport channel; two electrodes, the source and the drain contacts, where charges are

injected and collected; a third electrode, the gate, to modulate charge density inside the channel; and a thin layer of insulator to separate the gate and the channel. The structure can have several variants depending on the fabrication sequence of the stacking layers. Because depositing organic semiconductor on top of the insulator is much easier than the opposite due to the week bonding nature between organic molecules, the primary OFET is bottom gated. One of the basic fabrication schemes is to deposit source and drain contact electrodes through a shadow mask on top of a gated channel – the bottom gate top contact structure; Alternatively the semiconducting layer can be deposited on pre-pattern contact electrode as the bottom gate bottom contact device structure. In the bottom contact structure, the electrodes may be patterned by standard microelectronic techniques (e.g., photolithography) to define micrometer size features if the insulating layer is compatible, for example, silicon oxide or parylene. It is more challenging to form top contact structure with micrometer size resolution since the electrodes are mostly defined through a shadow mask. The downside of the bottom contact, however, is that reports have shown that it leads to non-ohmic or higher contact resistance compared with top contacts [17-19].

4.2. Purification of Pentacene

Impurity concentration in electronic grade intrinsic silicon is well controlled under the ppm range by the zone refining technique; intentionally doped elements can drastically change silicon's semiconducting properties, for example, forming n or p regions in a transistor. Organic semiconductors are in general synthesized by wet chemistry. Pentacene was first synthesized by W.H. Mills in 1912 using pyromellitic anhydride and benzene as starting materials and $AlCl_3$ as the catalyst. The mixed products of dibenzoylbenzene-dicarboxylic acids which, upon heat

treatment in concentrated sulfuric acid, underwent an intramolecular condensation reaction with the loss of two water molecules to yield dinaphtanthra-diquinone, further reduction of the diquinone will yield pentacene. [20].

At this stage, pentacene derived from chemical synthesis will undergo purification to separate out impurities (byproducts). The most common method is to re-sublime pentacene because it is insoluble in most organic solvents so that dissolve-crystallization approach will not work. Pentacene sublimation is performed in a thermal gradient environment (e.g. tube furnace) under a reduced pressure and/or inert gas flow, which is often named as "physical vapor transport". The hot boat is kept at around 410°C while the cold end is from 300°C to 200°C. This simple yet effective method relies on the different gas-solid phase transformation temperatures of pentacene and other impurity molecules relating to their molecular weights. Vapor of mixed molecules will travel from the source boat. Light-molecular-weight impurities will travel further and can be collected at the lower temperature end, and heavyweight impurity molecules condense closer to the source. This procedure can be repeated multiple times to obtain higher than 99% purity pentacene. Even at this high purity level, the concentration of impurities is still much higher than silicon and impurities can behave as dopants (shallow or deep traps in the channel) that limit the OFET's performance.

4.3. Energy structure of Pentacene

In conventional semiconductors, n type or p type behavior is dependent on the dopant type, namely the extrinsic dopant determines where the Fermi energy levelr lies in the band gap: if the Fermi level is closer to the conduction band, excess electrons can be promoted from the Fermi lever to the conduction band, the semiconductor is said to be n-type, and vise versa. This

phenomenon is true when there are very few impurities in the semiconductor. In organic counterparts, this is not the case. Pentacene is one of the vast majority of p-type organic materials. **Figure 3-21** shows the energy levels of Au contacts on pentacene by UV photoelectron spectroscopy (UPS), which clearly reveals that the Fermi level in Au is closer to the HOMO level in pentacene [21]. A conducting channel is formed when charges are induced by a gate bias. However, the LUMO level of pentacene is 1.4 eV away from the gold contact electrode's Fermi level, in consequence a substantial energy barrier (a dipole) will form for electron injection, which leads to no visible current passing through the channel when the gate is positively biased. In contrast, the Fermi level of gold is closer to the HOMO level in Pentacene, and the barrier height for hole injection is much lower. When the gate is negatively biased, holes can flow and be collected at the drain with another bias between the source and the drain electrodes. The hole conducting property of pentacene transistor is therefore originated from relative position of its HOMO LUMO levels relative to the Fermi level of the metal contact.
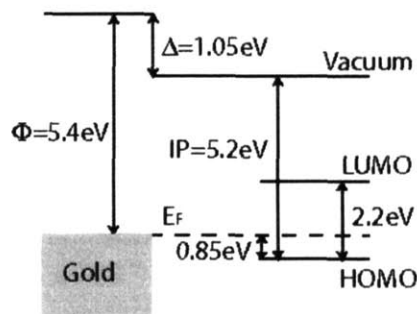
Figure 3-21. Energy level of Au contact on Pentacene

4.4. Charge transport model

The charge transport model for organic thin film transistors is different from the delocalized electron transport in single crystal silicon (band theory). The first class of organic semiconductors are disordered systems, amorphous in nature. Vissenberg's hopping model [22]

97

in particular has been developed to describe charge hopping between localized states. In this model, variable hopping distance and an exponential distribution of traps with semiconductor has been proposed to explain the gate bias power law dependence in the charge mobility and the transistor current-gate voltage curves. The charge hopping is assisted by phonons, as reflected in the temperature dependence of mobility:

$$\mu = \mu_0 \exp[-(\frac{T}{T_0})^{1/\alpha}].$$ (3-6)

In highly ordered molecular crystals, the mobility dependence is still somewhat controversial, i.e. whether the electron state is delocalized or localized. A model derived from multiple trapping and releasing in amorphous silicon [23] has been developed to describe charge transport in this situation. In this model, localized energy levels that act as traps exist in the continuous energy bands. While charge carriers transit within the delocalized levels, they interact with the traps through trapping and thermal releasing. It is assumed that a carrier will be trapped instantaneously once it encounters a trapping site; there is a certain probability that the trapped carrier can be released with the assistance of phonon. The effective mobility μ can be related to the trap-free mobility μ_0 by [24]:

$$\mu = \mu_0 \alpha \exp(-\frac{E_t}{kT})$$ (3-7)

Where E_t is corresponding to the trap depth (distance between trap level and the delocalized band) and α is the ratio of density of energy states in the delocalized band edge to the trap density. For traps distributed at multi-energy-level, the effective mobility will be a sum given the energy distribution and concentration of the traps. Traps inside the molecular crystal arise mostly as a result of structural defects and impurities, such as defects from synthesis, imperfections in the organic crystal structure, oxidized molecules, etc.

Insulator & Interface

The device performance of an OFET is largely affected by the gate dielectric material and the semiconductor-dielectric interface plays a key role. For example, the capacitance of the insulator determines the operation voltage of the transistor. In the bottom gate structure, the morphology of the channel depends on the surface properties of the insulator which provide nucleation and growth sites for the semiconductor layer. Surface modification of the dielectric layer has been demonstrated to flatten the interface and terminate possible unbound bonds that can induce trap states in the channel. Such modification is normally applied by exposing the surface to, for example, silane based self-assembly-monolayer (SAM). This well-ordered monolayer can reduce the nucleation rate, therefore increase the grain size of the semiconductor, as well as decrease the grain boundary density leading to higher charge mobility within the channel [25]. However, recent results [26, 27] show that surface treatment with octadecyltrichlorosilane (OTS) on SiO_2 while dramatically reducing the average grain size of vapor deposited pentacene, can greatly improve the effective mobility to 1.6 cm^2/Vs. .

Contact resistance

When the channel resistance becomes less predominant, to further improve the device performance of OFETs, special attention should be paid to the semiconductor and source/drain interfaces where the contact resistance becomes increasingly crucial in determining the OFET characteristics.
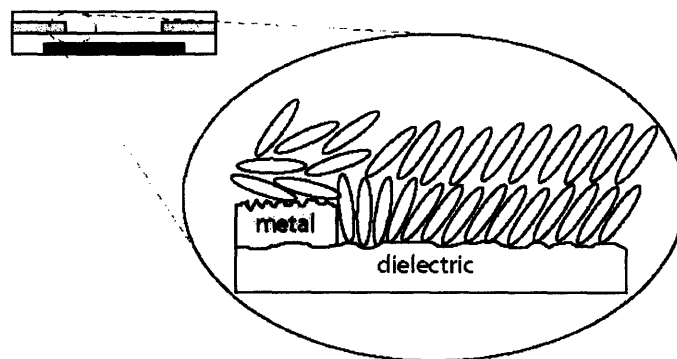
Figure 3-22. Origin of contact resistance at semiconductor metal interface

Top contact electrodes typically have higher performance, which probably is related to lower contact resistance at the Metal-Semiconductor interface. This can be understood that by depositing metal layer on top of the organic layer, metal penetration and the formation of metal clusters heavily dope the semiconductor and creates a large number of midgap states at the MS interface, leading to a substantial reduction of the hole injection barrier [28,29]. At the same time, the conductive channel at the dielectric/semiconductor interface and the contact regions are physically separated, enabling well-ordered channel morphology. Although the top contacts can be patterned with photolithographic technique [30], they are most often done through a shadow mask. The fabrication of bottom contacts is relatively easier. However depositing crystalline layered structure pentacene on metal and dielectric layers will result in different topologies. An electron rich metal surface can couple with π orbital electrons in pentacene which will attract the first few critical monolayers of pentacene film to preferentially lay down flat on the metal surface. **Figure 3-22** illustrates the less ordered structure at the metal electrode surface. Improvement of the ordered structure can be done by overcoating the substrate surface with a Self Assembled Monolayers (SAMs) as a buffer layer to enhance crystallinity of the organic semiconductors at the metal electrode surface. Gate bias induced charges occur within the first few layers (~1nm) of the channel at the SAM-semiconductor interface, which is dictated by the

electrostatics analysis. The development of surface modification and device architecture have contributed to the increasing performance of pentacene based OFET, as shown in **Table 3-1** [31].

Table 3-1. Performance of pentacene OFET

Year	Group	Dielectric layer	Mobility (cm^2/Vs)
1996	PSU	Thermal Oxide	0.62
1997	PSU	TC	0.7
1997	PSU	OTS	1.3
1997	PSU	OTS, TC, double layer	1.5
1999	PSU	OTS, TC	2.1
2000	PSU	OTS, BC	1.7
2000	Necliudov	OTS, TC	1.1
2002	Sheraw	OTS, BC, PVA pattern	1.2
2002	Princeton	OTS, TC	1.6
2003	Infineon	PVP+OTS	3.0
2003	3M	Polysulfonic Acid, TC	3.4
2003	3M	Polystyrene, TC	>5.0
2003	Knipp	OTS	1.1
2004	Choi	PVP + OTS	1.4
2004	Yoneya	Silan SAM, BC	1.1
2004	Schroeder	PVA/PVP, doped TC	2.6
2005	Jang	PVP, BC	1.8
2005	Samsung	Proprietary dielectric	7.0

Operation mode

Pentacene OFET models have evolved. The very first model is borrowed from silicon MOSFET devices, where the transistor can operate in the linear or saturation regions:

$$I_{DS}^{Lin} = \frac{W}{L}\mu C_i(V_G - V_T - \frac{V_{DS}}{2})V_{DS} \approx \frac{W}{L}\mu C_i(V_G - V_T)V_{DS} \qquad (3\text{-}8)$$

C_i is the capacitance of the insulator per unit area;

$$I_{DS}^{Sat} = \frac{W}{2L}\mu C_i(V_G - V_T)^2 \qquad (3\text{-}9)$$

W/L is channel width/length;

In the linear response region, where $V_{DS} \ll V_G$, the drain current is proportional to the charge density in the channel; the threshold voltage V_T is corresponding to the density of non-conductive states (e.g. trapping of mobile charges).

The model developed by Necliudov assumed a gate bias dependent mobility and non-linear contact resistance [32]. To account for the power law dependence on the gate bias, the carrier mobility is defined as:

$$\mu = K(V_G - V_T)^\gamma ,$$

(3-10)

where K and γ are empirically fit.

$$\frac{I_{DS}}{V_{DS}} = (\frac{1}{(W/L)C_i\mu(V_G - V_T)} + R_C)^{-1}$$

(3-11)

R_C is the contact resistance. The voltage drop at the contacts therefore is $I_{DS}R_C$,

Street proposed a general model [33] in which he suggests the effective channel length is reduced by d that accounts for the contact regions and he makes an assumption on a constant mobility, from which the potential along the channel $V(x)$ can be expressed as:

$$V(x) = WC_i\mu[V_G - V_T - V(x)]\frac{dV}{dx}$$

(3-12)

Integrate Eq (3-12) along the channel yields:

$$I_{DS} = C_i\mu\frac{W}{L-d}\{(V_G - V_T)V_{DS} - \frac{V_D^2}{2} - [(V_G - V_T)V_c - \frac{V_c^2}{2}]\}$$

(3-13)

where $V_c = I_{DS}R_C$

If the charge mobility is assumed to be field-independent, with each set of V_G, I_{DS} and V_{DS}, V_T and R_C can be derived and the contact resistance is found to vary with the gate bias.

Another model to independently access the channel resistance and contact resistance is the so called Transfer Line Method (TLM) which originally was used to estimate the contact resistance in amorphous silicon. In the linear regime, the channel resistance is give by Eq (3-14):

$$R = \frac{V_{DS}}{I_{DS}} = \frac{L}{C_i \mu (V_G - V_T) W} + R_C ,$$
(3-14)

R is proportional to the channel length.

The contact resistance can be extracted by plotting the normalized channel resistance versus the channel length. Extrapolating to zero channel length will give the contact resistance, while the mobility and threshold voltage can be estimated from the slop of the plot.

Although TLM is straightforward, there are some shortcomings associated with this method. First of all, this method requires a set of multiple samples with various channel lengths. Chances are that the mobility, threshold voltage and contact resistance might not be strictly identical in all the devices. Next, the assumptions of TLM include ohmic contacts and constant mobility in the linear operation regime, which are both apart from the real OFET characteristics. Lastly, the measured contact resistance should account for both source and drain electrodes, where it is known that charge injection into the channel at the source electrode is the dominant factor of contact resistance.

The contact resistance in OFETs has also been directly investigated by the four-probe method instead of the two-terminal architecture [34, 35]. By introducing two additional electrode in the channel, the measurement of the potential drop and the contact resistance can be decoupled, thus yielding the true value of the channel resistance, and the contact resistance at the source/drain electrode can be analyzed independently, as shown in **Figure 3-23.**
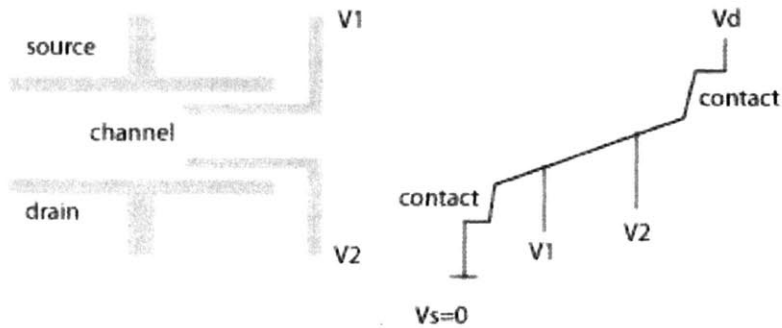
Figure 3-23. Four probe electrodes and corresponding voltage profile

Bürgi et al, systematically studied the contact resistance in a bottom contact polymeric OFET based on scanning probe potentiometry [36]. This powerful approach separates the charge transport properties in the channel and charge injection at the semiconductor/metal contact. Various metals were compared and the results showed that the metal work function is the key factor; both the contact resistance and the charge mobility are gate bias dependent, which was in good agreement with the TLM and four-probe technique.

4.5. Experiment results and discussion

In the previous chapter, MoJet printing arbitrary metal patterns has been demonstrated and here we emphasize again the importance of thermal shielding in determining the final print quality. Using only the metal shielding sheets, a little thermal radiation can still escape and reach the printhead holder, leading to about 5 μm distortion on the printed patterns. To further reduce or even eliminate this distortion, the printhead holder is wrapped with metal foil (In this case aluminum foil was used) to reflect the radiation from reaching the substrate and the printhead holder. **Figure 3-24a** shows schematically the setup of the printer system to achieve almost negligible thermal distortion. Silver stripes with 5 to 10 μm distances can be printed accurately in this way (**Figure 3-24b**). Two different metals can be printed in sequence to form asymmetric

contact pads, as shown in **Figure 3-24c. Figure 3-24d** again shows that less than a 5 µm gap is reproducibly obtained with this system setup.
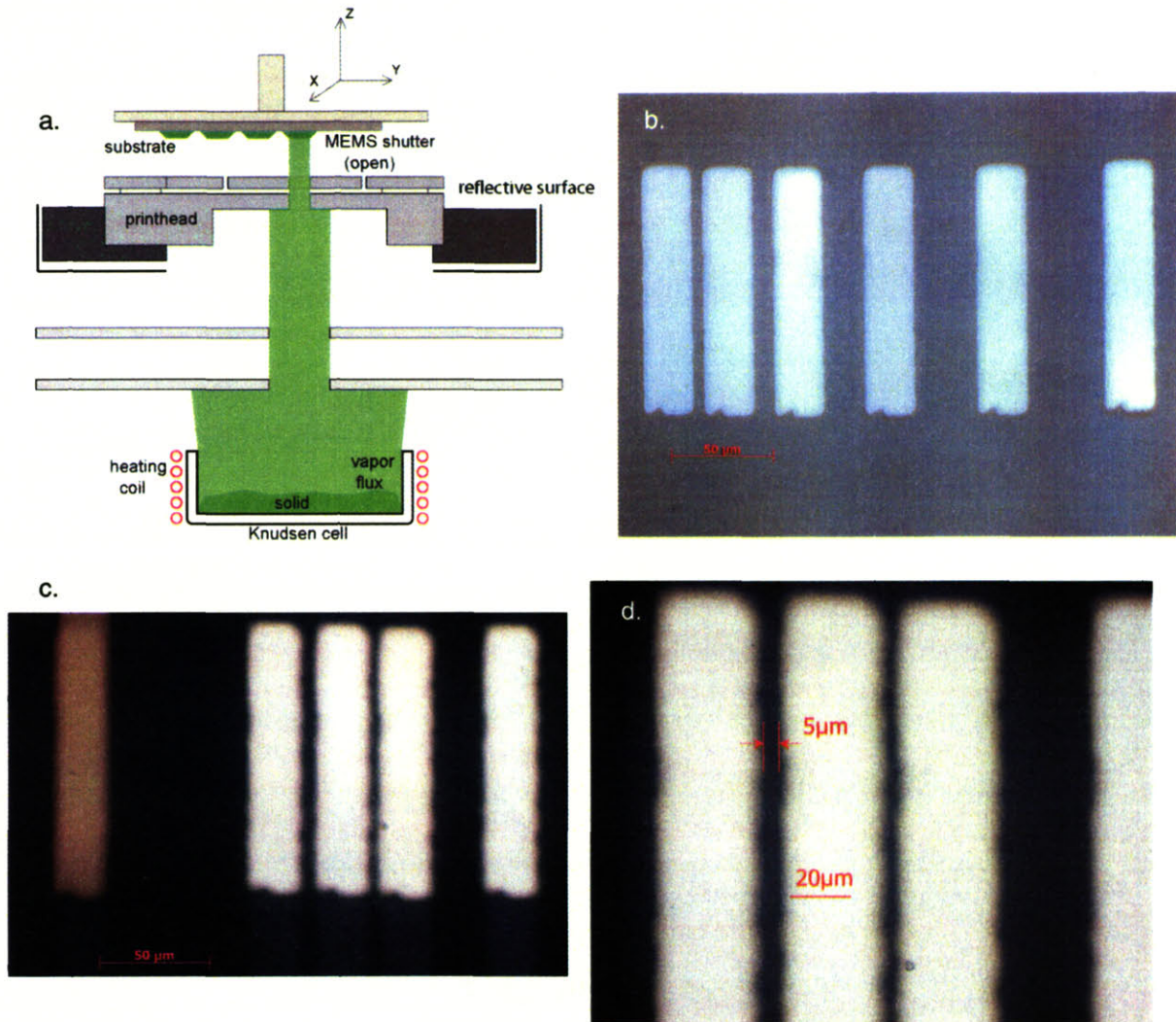
Figure 3-24. Printing OFET metal contacts

Using the MoJet printer, 30 nm thick film of pentacene is printed at 0.2 Å/sec rate as the first layer. The vacuum chamber is then brought to ambient pressure and opened to air. The evaporative source material is replaced with silver pellets and the chamber is pumped down to 10^{-7} Torr. Two strips of silver contacts (30 µm×130 µm in size, 40 nm thick) are printed 15 µm apart to define the source and drain contacts and the channel length. To ensure that two different layers of materials (pentacene and silver) are sequentially printed and correctly aligned, the

105

position of each layer is registered in the computer's memory for reference. **Figure 3-25**

illustrates the structure of an OFET printed on a p-type thermal silicon wafer. 2000 Å thick

thermal oxide grown on top the wafer serves as the gate dielectric layer.
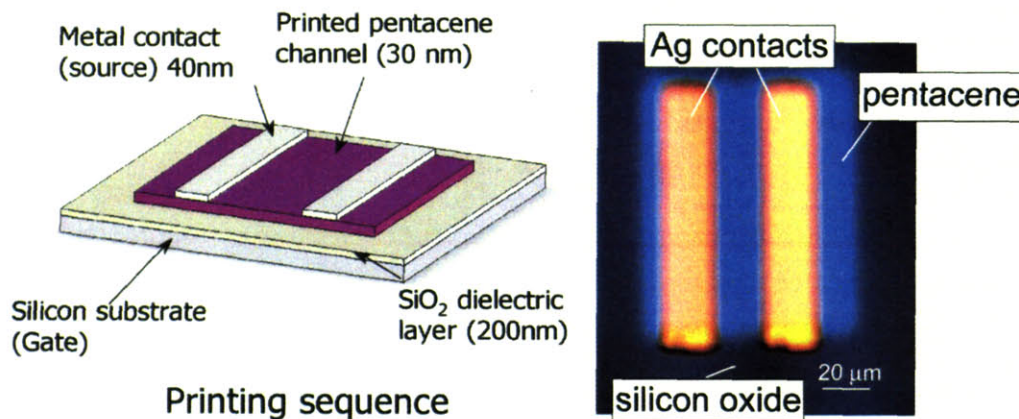
Figure 3-25. Structure and microscope image of MoJet printed OFET. Micrograph of a single MoJet printed OFET on silicon oxide surface of a silicon substrate. Pentacene film (30 nm thick) and silver contacts (60 nm thick) are printed in sequence.

Figure 3-26a shows the typical morphology of MoJet printed pentacene layer on thermal

oxide which matches the dendritic morphology of blanket evaporated films. In **Figure 3-26b**

silver vapor condenses on the pentacene crystal and forms nanometer size particles embedded in

pentacene crystals, heavily doping the contact area for better charge injection. I-V characteristics

of the MoJet printed OFET are shown in **Figure 3-26c**. The effective mobility of this OFET is in

the range of 0.05~0.20 cm^2/(V·s) in the saturation region, similar to other pentacene OFETs

fabricated using shadow masks [37]. We note that the manufacturing application of the MoJet

technique might require high pentacene deposition rates, which could result in growth of small

pentacene grains with the consequence of lower effective OFET mobility. Increase in the

effective mobility has been demonstrated when a selected self-assembly monolayer (SAM) is

coated as gate insulator before pentacene layer deposition, [38] which might similarly benefit the

MoJet-printed pentacene.
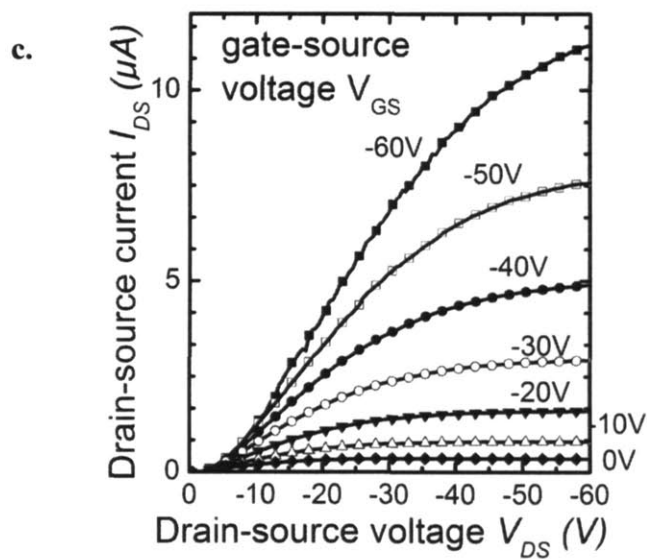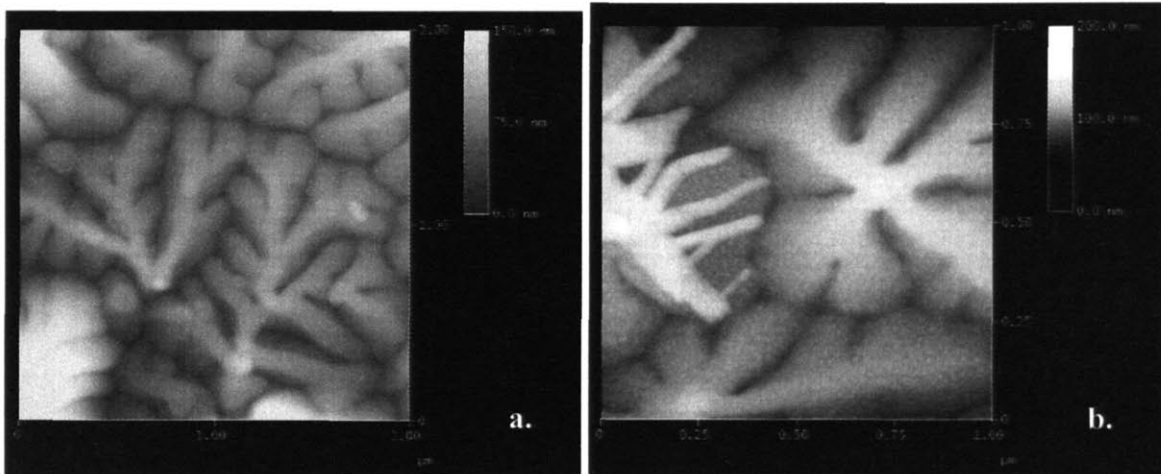
Figure 3-26. (a). Atomic force microscopy (AFM) image of the MoJet printed pentacene channel (30 nm thick). (b). The metal contact region. (c). The I-V characteristics of one of the transistors. The gate voltage Vg is varied from 0 to –60 V in 10 V steps.

The MoJet printing technique can be applied to define different contact metals and to vary the channel lengths to assist in the study of charge injection and transport in OFETs. **Figure 3-27a** depicts that on a same pentacene OFET, depending on whether gold or silver is used as the charge injection contact (source), the behavior of the OFET will change. **Figure 3-27b** shows the I_{DS} vs. the channel length defined by the MoJet printer.
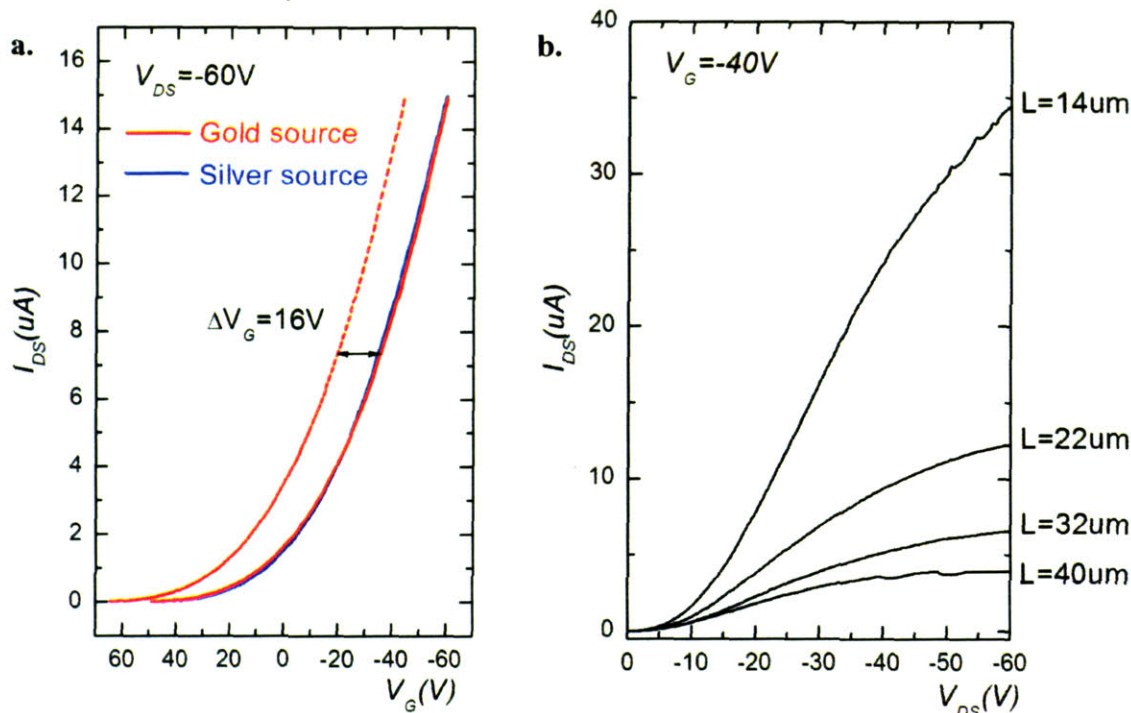
Figure 3-27. (a). Asymmetric behavior of MoJet printed OFET with gold and silver contacts. (b). channel conductance as a function of channel length printed by MoJet.

5. Summary of MoJet I

In summary, by the use of a MEMS printhead with a moving stage, the MoJet printing technique has been developed to directly print active organic electronic devices, in which electro-luminescence layer, semiconducting channel or metal contacts features have been patterned at smaller than 30 micron scale size, equivalent to 800 ppi pattern resolution. The printing technique allows one to digitally fabricate patterns of molecular organic semiconductors and metals and to scale the fabrication to large substrate plates. The size of the printed pattern can be broadened and the broadened region is strongly dependent on the geometry of the printer system. This effect is associated with the trajectory of the traveling molecules in vacuum, analogous to the deposition with shadow masks. It should also be noted that when depositing metals, thermal radiation could induce excess distortion to the printed pattern. Thermal shielding

108

layers have to be applied to minimize the thermal effect. The printing technique described here can be extended to fabricate multilayer structures, as demonstrated in the all MoJet printed OFET devices. We expect that full color displays with different structure subpixels should be possible to print with the MoJet technique, and to speed the printing process, multi-nozzle printhead can be utilized.

Reference

[1]. S. R. Forrest, P. E. Burrows, and M. E. Thompson, IEEE Spectrum, 37, 29 (2000).

[2]. M. Shtein, P. Peumans, J. B. Benziger, and S. R. Forrest, J. Appl. Phys., 93, 4005 (2003).

[3]. C. J. Drury, C. M. J. Mutsaers, C. M. Hart, M. Matters, and D. M. de Leeuw, Appl. Phys. Lett., 73, 108 (1998).

[4]. H. Sirringhaus, T. Kawase, R. H. Friend, T. Shimoda, M. Inbasekaran, W. Wu, and E. P. Woo, Science, 290, 2123 (2000).

[5]. Blanchet, G. B., Loo, Y.-L., Rogers, J. A., Gao, F. & Fincher, C. R. Appl. Phys. Lett., 82, 463 (2003).

[6]. M. Shtein, P. Peumans, J. B. Benziger, and S. R. Forrest, Adv. Mater., 16, 1615 (2004).

[7]. C. Kim, S. R. Forrest, Adv. Mater., 15, 541 (2003).

[8]. D. Albertalli, SID symposium, 36, 1200 (2005).

[9]. R. D. Deegan, Phys. Rev. E,, 61, 475 (2000).

[10]. V. Leblanc, S.H. Kang, J. Chen , P. J. Benning, M. A. Baldo, V. Bulović and M. A. Schmidt, Transducer'05, 2, 1429 (2005).

[11]. V. Leblanc, J. Chen , S.H. Kang, V. Bulović and M. A. Schmidt, J. of Microelectro-mech. Syst., 16, 2 (2007).

[12]. K. Yase, J. Cryst. Growth, 166, 942 (1996).

[13]. J. Chen, et al, Direct Patterning of Molecular Organic Materials and Metals Using a Micromachined Printhead, Mater. Res. Soc. Symp. Proc. 870E, H1.8 (2005).

[14]. M. Shtein, H. F. Gossenberger, J. B. Benziger, and S. R. Forrest, J. Appl. Phys., 89, 1470 (2001).

[15]. I. V. Antonets, L. N. Kotov, S. V. Nekipelov, and Ye. A. Golubev, Nanostructure and Conductivity of Thin Metal Films, Technical Physics, 49, 306 (2004). Translated from Zhurnal Tekhnichesko, Ĭ Fiziki, 74, 24 (2004).

[16]. Jurchescu, Baas, Effect of impurities on the mobility of single crystal pentacene, Appl. Phys. Lett., 84, 3061 (2004).

[17]. G. B. Blanchet, et al., Contact resistance in organic thin film transistors, Appl. Phys. Lett., 84. 296 (2004).

[18]. R. A. Street and A. Salleo, Polymer thin-film transistors with chemically modified dielectric interfaces, Appl. Phys. Lett., 81, 2887 (2002).

[19]. I. Kymissis, D. C. Dimitrakopoulos, and S. Purushothaman, High-performance bottom electrode organic thin-film transistors, IEEE Trans. Electron Devices, 48, 1060 (2001).

[20]. W.H. Mills, M. Mills, J. Chem. Soc., 101, 2194 (1912).

[21]. N Koch, Conjugated organic molecules on metal versus polymer electrodes: Demonstration of a key energy level alignment mechanism, App. Phys. Lett., 82, 1 (2003).

[22].M. C. J. M. Vissenberg, Theory of the field-effect mobility in amorphous organic transistors, PHYSICAL REVIEW B, 57, 20 (1998).

[23]. G. Horowitz, Temperature Dependence of the Field-Effect Mobility of Sexithiophene. Determination of the Density of Traps, J. Phys. III France 5, 355 (1995).

[24]. G. Horowitz, Organic Field-Effect Transistors, Adv. Mat., 10, 5 (1999).

[25]. G. Horowitz, Grain size dependent mobility in polycrystalline organic field-effect transistors, Synth, Metal,, 122, 185 (2001).

[26]. D. Knipp, Pentacene thin film transistors on inorganic dielectrics: Morphology, structural properties, and electronic transport, J. Appl. Phys., 93,1 (2003).

[27]. M. Shtein, Effects of film morphology and gate dielectric surface preparation on the electrical characteristics of organic-vapor-phase-deposited pentacene thin-film transistors, Appl. Phys. Lett., 81, 2 (2002).

[28]. N. Tessler, Y. Roichman, Two-dimensional simulation of polymer field-effect transistor, Appl, Phy Lett., 79, 18 (2001).

[29]. N. J. Watkins, Electronic structure symmetry of interfaces between pentacene and metals, Appl. Phy. Lett,, 80, 23 (2002).

[30]. I. Kymissis, Patterning pentacene organic thin film transistors, J Vac, Sci, Technol. B 20, 956 (2002).

[31]. Hagen Klauk, Organic electronics : materials, manufacturing and applications, Wiley-VCH, Weinheim (2006).

[32]. P. V. Necliudov, M. S. Shur, D. J. Gundlach, T. N. Jackson, Modeling of organic thin film transistors of different designs, J. Appl. Phys., 88, 6594 (2000).

[33]. R. A. Street, A. Salleo, Contact effects in polymer transistors, Appl. Phys. Lett, 81, 2887 (2002).

[34]. P. V. Pesavento, R. J. Chesterfield, C. R. Newman, and C. D. Frisbie, Gated four-probe measurements on pentacene thin-film transistors: Contact resistance as a function of gate voltage and temperature, J. Appl. Phys., 96, 12 (2004).

[35]. I. Yagi, Direct observation of contact and channel resistance in pentacene four-terminal thin-film transistor patterned by laser ablation method, Appl. Phys. Lett., 84, 5 (2004).

[36]. L. Bürgi et al, Close look at charge carrier injection in polymer field-effect transistors, J. Appl. Phys., 94, 9 (2003).

[37]. K Ryu, I. Kymissis, V. Bulović, C.G. Sodini, Elec. Dev. Lett., 26, 716 (2005).

[38]. C.D. Dimitrakopoulos, P.R.L. Malenfant, Adv. Mater., 14, 99 (2002).

Chapter 4. Second generation Molecular Jet printing technique

CONTENTS

1. Overview

2. Proof of concept

3. Numerical simulation by DSMC

4. MEMS based MoJet II printer

5. Experimental results and discussion

6. Conclusion of MoJet II

1. Overview

We introduced in the previous chapter that the first generation MoJet printing system requires the use of a vacuum environment to pattern active organic and metal films. Consequently, a large percentage of the source material is wasted on coating the chamber walls; the surface micromachined moving shutter operates in a close distance to the substrate and it is prone to damage by direct impact; furthermore, clogging of the print nozzles by material accumulation requires special procedure to clean up the printhead. In this chapter, we introduce an improved version of the printhead, which is redesigned to permit simple, reliable patterning of organic materials with high material use efficiency. The most important fact is that the vacuum chamber can now be eliminated from the print system.

In this chapter the MoJet II printing method/theory is developed; Direct Simulation Monte-Carlo (DSMC) is adopted and the simulation result is used to explain the pattern formation mechanism; printing experiments and results are presented; the capability of MoJet II is demonstrated.

2. Proof of concept

micro-pores

nozzle
heater

TIJ Head

TIJ resistor
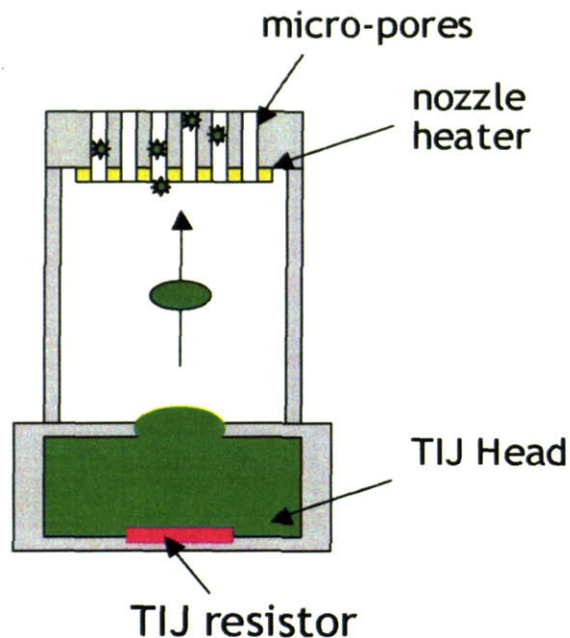
Figure 4-1. Schematic illustration of the MoJet II concept

The MoJet II concept is distinct from Inkjet, as illustrated schematically in **Figure 4-1**. The

inkjet printhead (TIJ) is used only as a "metering" tool to dispense exact quantities of organic ink

into the MoJet II porous printhead. The MoJet printhead then removes the solvent in the ink by

heating and directly prints dry ink materials (organic semiconductor molecules) onto the

substrate. Here the solvent compatibility issue is eliminated because no solvent is involved in the

formation of the deposited organic layers. The MoJet II concept essentially decouples the

delivery of organic materials and the formation of the organic films. Organic molecules are

delivered to a local micro-evaporator in liquid form; the local evaporator will heat up on-demand

to minimize substrate heating, nozzle clogging and to maximize material use efficiency.

There are two key issues that must be considered in determining the validation of this

concept: the first is finding a porous medium and a method to separate the ink into solvent and

organic solutes; the second is transporting organic molecules in ambient environment to a

substrate surface without losing pattern features. Two proof-of-concept experiments are designed and conducted.

Experiment I: Anodized alumina disc as porous inking medium

The key concept of MoJet II is to integrate a porous medium to the printhead, which serves dual purposes. The first is to temporarily store organic materials inside the pores while solvent evaporates; the second is to discharge the organic materials from pores after being heated up. Here an anodized alumina disc is chosen for its properties such as high porosity, rigid mechanical characteristics and high aspect ratio, as shown in **Figure 4-2**.
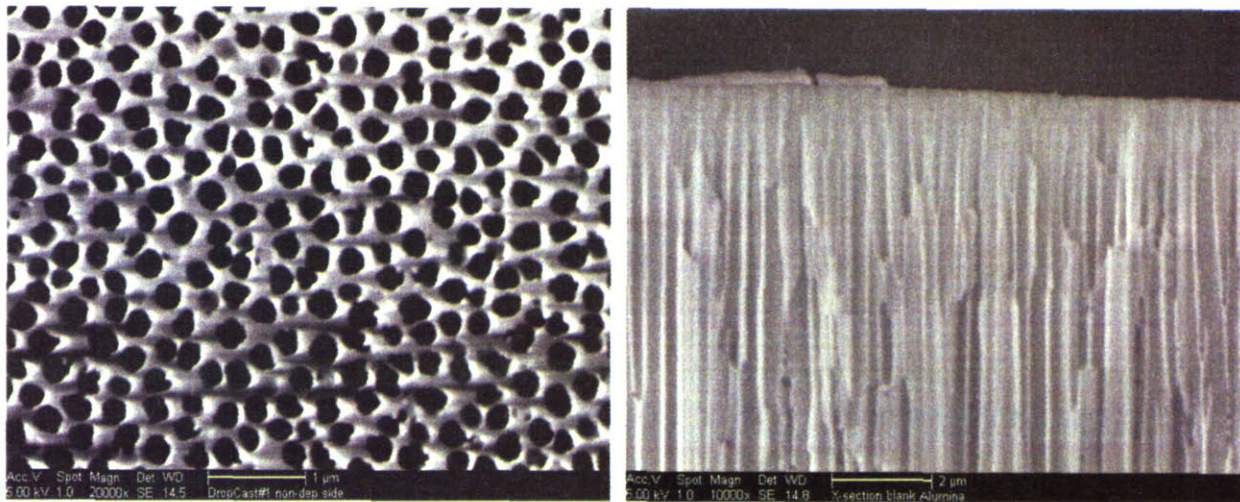
Figure 4-2. SEM images of porous alumina disc (a). surface (b). cross-section morphology. Sample is purchased from Whatman (Anodisc series). Disc thickness is about 60 μm thick, pore size about 0.2 μm in diameter, aspect ratio about 300: 1, and 50% porosity.

Loading of the ink material is done either by drop casting into the pores a testing ink sample (Alq3 dissolved in chloroform at 50mg/mL concentration) or by vacuum thermal deposition of Alq3 onto the disc surface. Both can be verified by looking at the PL image under an optical microscope, as shown in **Figure 4-3**.

a.

Alq3 ink loaded inside anodisc micropores by drop casting

b.

Alq3 ink only deposited on the surface of the anodisc
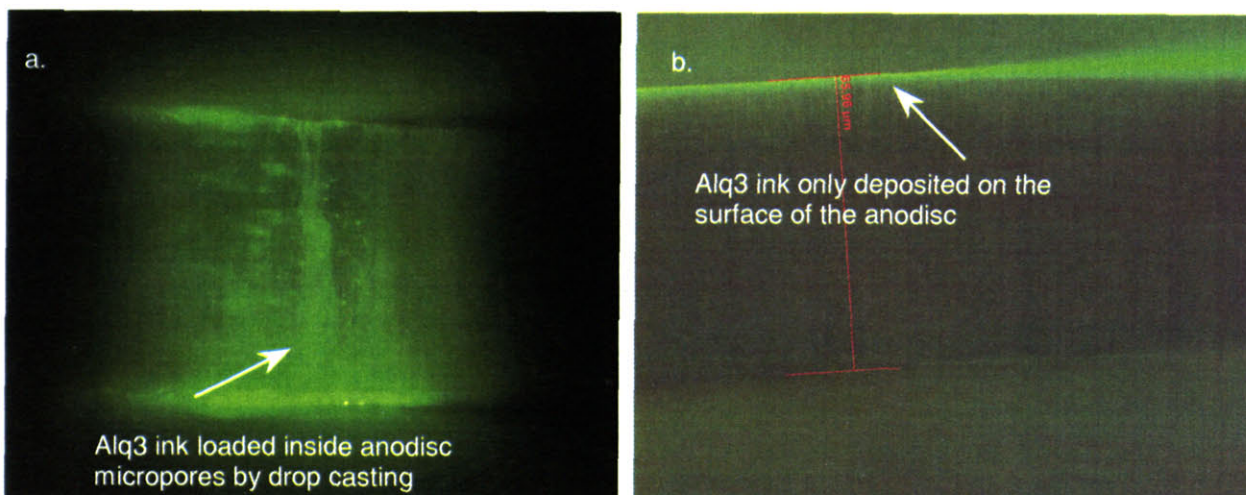
Figure 4-3. PL microscope images of cross-sections of Anodiscs loaded with Alq3 (a). by drop casting and the pores are soaked with Alq3; (b). by thermal evaporation. Only the surface is coated with a layer of Alq3.

Figure 4-4 demonstrates that the porous disc indeed can be used to store and transfer organic material to the designated substrates by heating. The source disc is loaded with Alq3 ink by drop casting and then sandwiched between two blank receiving discs. Upon heating the three discs in vacuum at 230 ºC, Alq3 molecules will diffuse out of the source disc and transfer into the receiving discs, leaving identical patterns in all the three discs afterwards.

Drop cast
source disc

Blank discs

Stacked samples heated to 230 ºC in vacuum

Disc #1   Disc #2   Dics #3
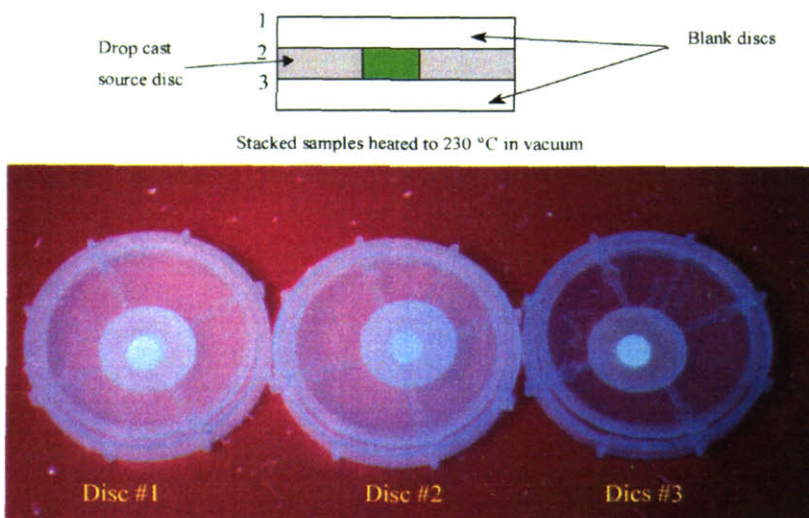
Figure 4-4. Experiment setup of transfer printing Alq3 pattern. PL of drop-cast Alq3 pattern being transferred from disc #2 to disc #1 & #3.

To pattern an Alq3 layer, a metal shadow mask is placed at the front side of the anodisc while the backside is blanket deposited an Alq3 layer of about 1000 Å thick. Another anodisc is placed about 50-100 μm away from the mask to receive the transferred patterns. The whole process is illustrated in **Figure 4-5**. Similarly Alq3 source can be loaded by drop casting method.
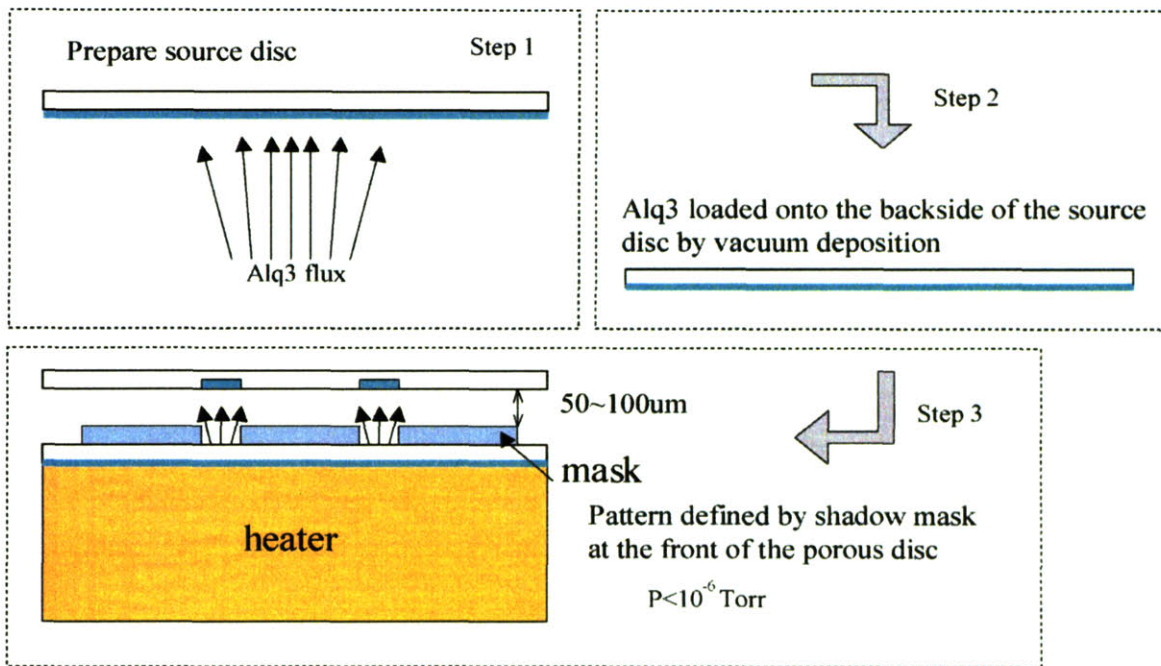
Figure 4-5. Alq3 pattern transferred through the anodisc and a metal shadow mask
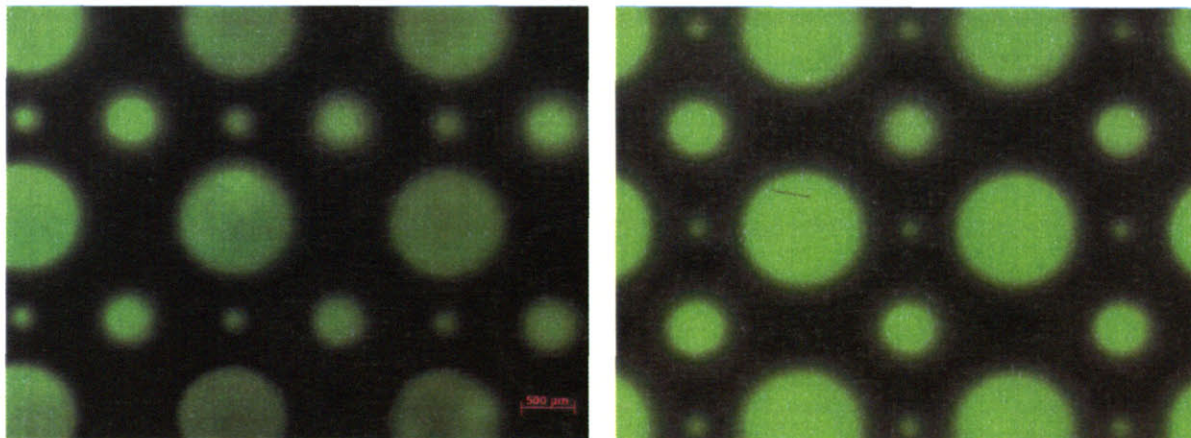
(a). Vacuum deposition loaded Alq3   (b). Solution drop cast loaded Alq3

Figure 4-6. PL microscope images of successful Alq3 pattern transfer through the anodisc and a metal shadow mask. The scale bar is 500 μm.

119

From the experimental results shown in **Figure 4-6** the validity of the key concept can be verified that a porous medium can store Alq3 molecules and then thermally discharge the organics out of the micro pores upon heating.

Experiment II: transport of alq3 in ambient condition

The size of desired organic pattern in the OLED or OFET devices ideally should be less than 100 μm for achieving high definition printing. In a typical vacuum deposition system, this can be done by using a shadow mask with feature size on the order of tens of micrometers; for example, in the application of the first generation MoJet printer, 30 μm pixel can be patterned by using 25 μm nozzle. When the deposition background pressure increases, the mean free path decreases and the inter-molecule collision occurs more frequently. The mean free path (MFP) is defined as the average distance molecules travel between collisions, which is given in equation (4-1).

$$m = \frac{RT}{\sqrt{2}\pi d^2 N_A P} \qquad (4\text{-}1)$$

where R is the gas constant, T is temperature, d is the diameter of molecules, N_A is the Avogadro's constant and P is the pressure.

The consequence of more inter-molecule collision is a broadening effect on the deposited pixels. A simple numerical analysis is done to study the MoJet printed pattern size for different background pressures [1] and the results are shown in **Figure 4-7**. It is concluded that when the MFP is shorter than the printhead-substrate gap (~100 μm), the printed pattern starts to diffuse much wider than the print nozzle size (~50 μm), which shows from the computation results that it starts to occur at pressures higher than 0.01 Torr.

Pattern size Vs. background pressure

aperture opening = 50 um
substrate-MEMS spacing = 100 um

Simulation results

FWHM=50 um   53 um   62 um   123 um
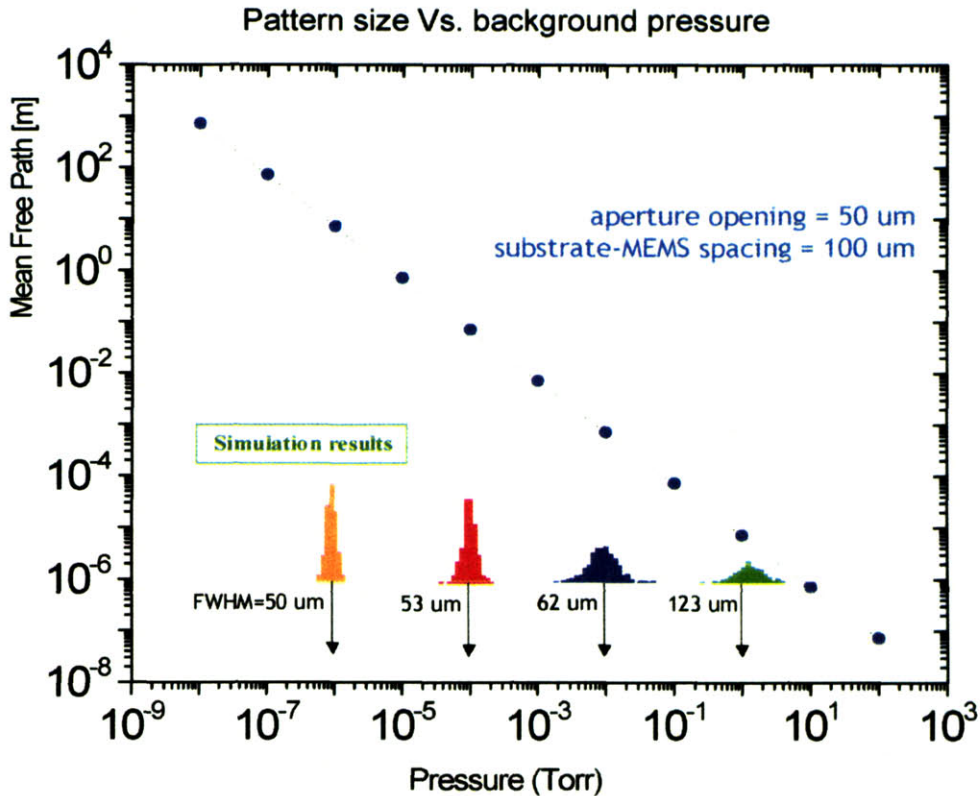
Figure 4-7. Pattern definition at different background pressures

In a similar situation observed in Organic Vapor Jet Printing (OVJP) [2], Shtein et al. demonstrated lateral patterning of organic semiconductor could be done at pressures higher than 1 torr. This occurs because a). organic molecules are heavier than the carrying gas molecules, thus can retain most of the momentum even after a series of collisions with the carrying gas molecules; and b). substrates are placed very close to the nozzle. Before the organic species condense spontaneously, they can impact the substrate surface and deposit on it.

To evaluate the concept of depositing organic materials in ambient condition by carrying gas, a test printhead is designed and fabricated; most of the parts are Teflon plastics that are inert to heat and molecular organic vapor. The structure is illustrated in **Figure 4-8**. A first generation MoJet MEMS chip is attached to the printhead, primarily because its 25 μm nozzle size is ideal for the testing the flow dispersion.

121
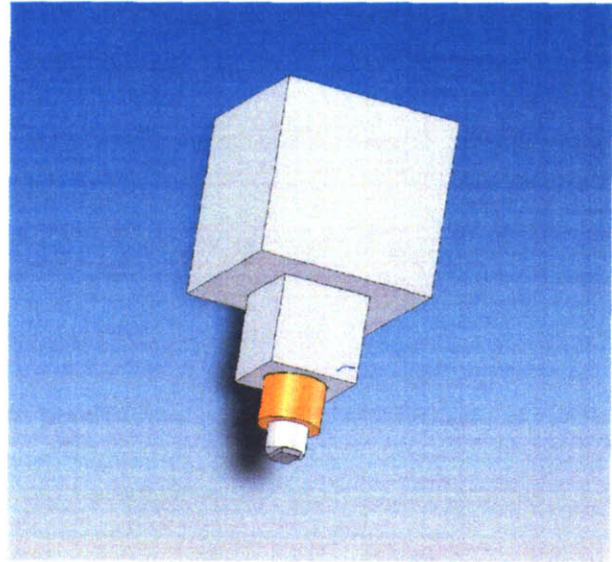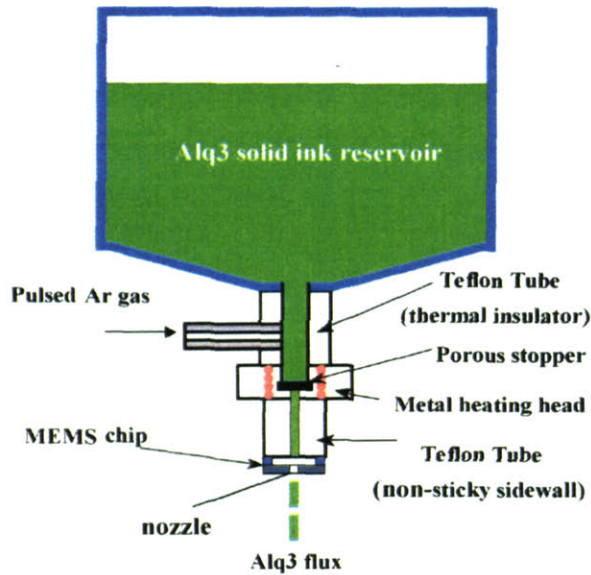
Figure 4-8. Test printing Alq3 in ambient with MoJet I MEMS printhead

In the test setup, argon gas is used as the carrying gas to bring Alq3 vapor out of the heating

chamber (~250 °C). The thermal performance of the heating chamber is shown in **Figure 4-9**.
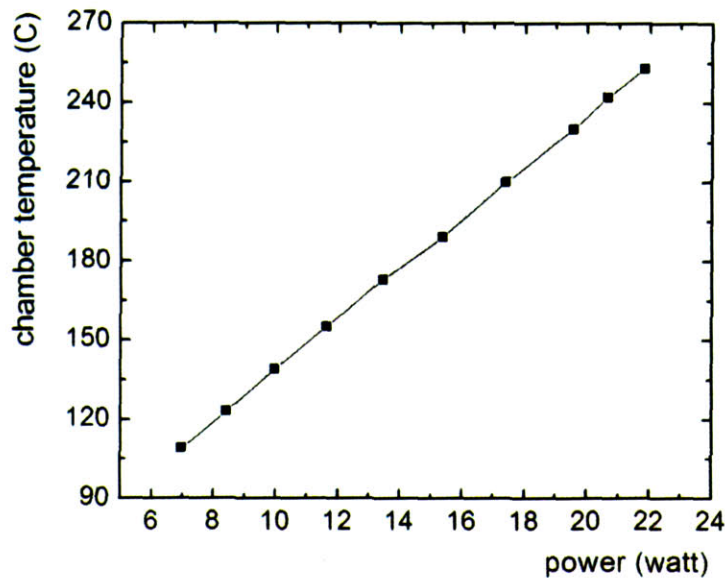
Figure 4-9. Power consumption of Alq3 heating chamber

Parameters affecting the organic pattern size are studied, which include jetting speed, pulse

duration, and printhead to substrate separation. Effects of these parameters are summarized in

Figure 4-10.

122
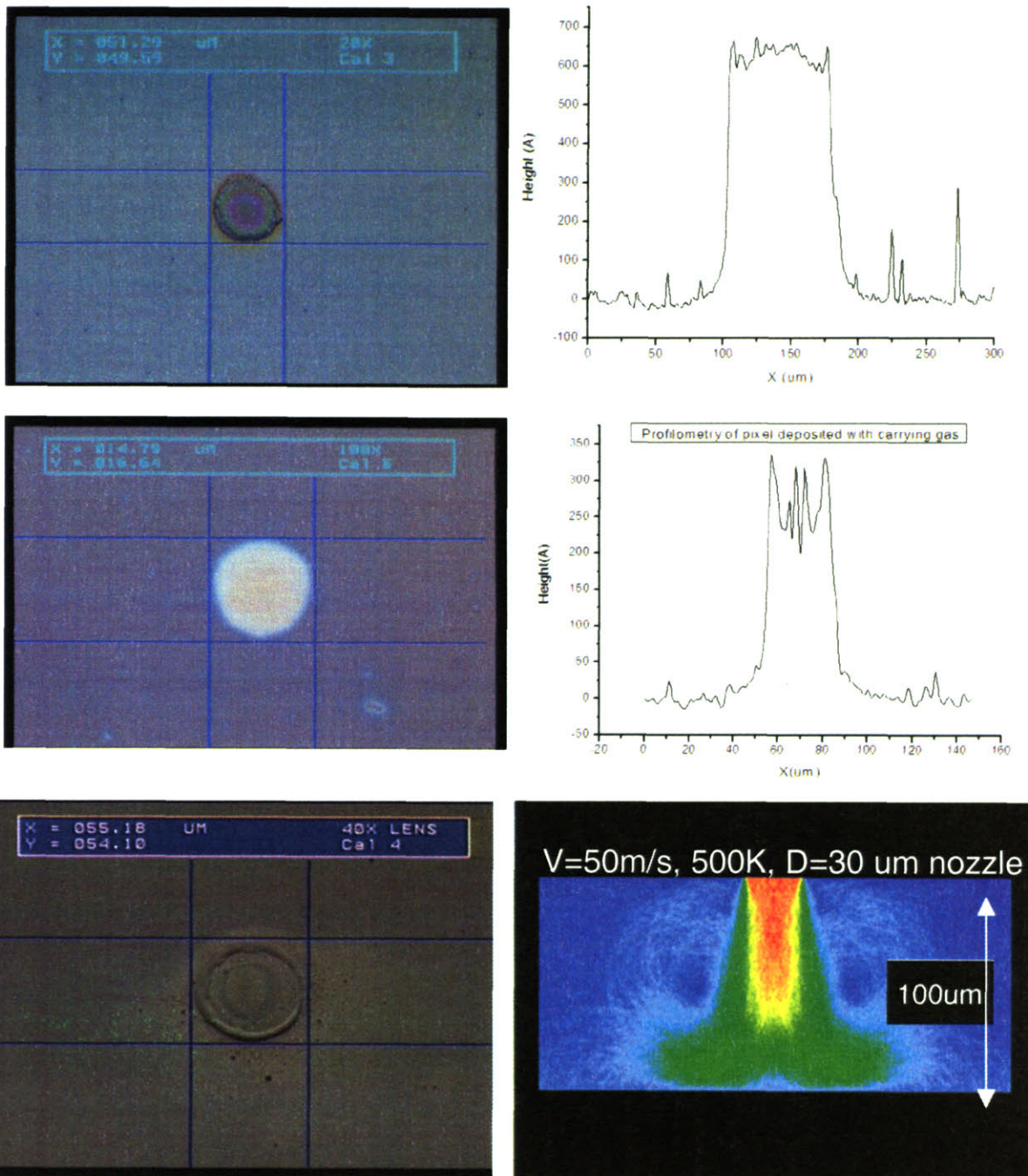
Figure 4-10. Results of printing Alq3 on silicon substrates in ambient conditions. (a). Jetting speed V=85 m/s, separation g=150 μm, duration t= 1 second; (b). V=100 m/s, g= 150 μm, t =0.1 second; (c). Concentric pattern formation caused by organic molecules in-plane flow on the substrate's surface. Gas flow dissipates heat to the film as the outflow vapor cools down along the substrate's surface plane and form a ring structure outside the center pattern.

123

It is not surprising that this concept works well. In the theory of OVJP transport regime analysis developed by Shtein [3], the final printed pattern size is related to the horizontal momentum transferred to the organics by collisions with the carrying gas molecules, and the radial diffusion rate of the organic molecules. The control factors are primarily the nozzle size, nozzle-to-substrate separation, background pressure, and the weights of the molecules. The minimal feature is printed at the lowest possible background pressure. In our experiments, the background pressure is a secondary influence. The pattern formation is largely determined by the nozzle size, jetting speed (V), the printhead-substrate gap (g) and the duration of jetting (t). The minimal feature is attainable at small gap and short jetting duration respectively. The pattern size and the film thickness often times are correlated at a constant gap. If the gap is too small, concentric Alq3 patterns can be observed, due to the local heating from the jetting stream.

3. Numerical simulation by DSMC

At the time of our experiments there is not yet an analytical formula for describing and predictting the pattern formation process. As uncharted territory, we have to rely on the Direct Simulation Monte Carlo (DSMC) method developed by Bird [4] to analyze how the experimental parameters affect the results.

The numerical model is illustrated in **Figure 4-11**, along with some key points that should be incorporated into the simulation. DSMC method can be used to visualize the flow field. Initially random location and velocity values are assigned to each individual particle following the Maxwell velocity distribution. Then the entire flow field is broken down into many discrete sections/cells. Only when particles reside inside the same cell will one particle be allowed to interact with another particle. This greatly reduces the computation size from Order $[N^2]$ down to Order $[N]$, requiring much less computation time. Symmetry geometry is adopted so that it

requires only upper half flow to be simulated (mirror images). All together one to two million particles are simulated in this system. The typically run time is from 2 hours to 2 days on a Pentium 4 PC.
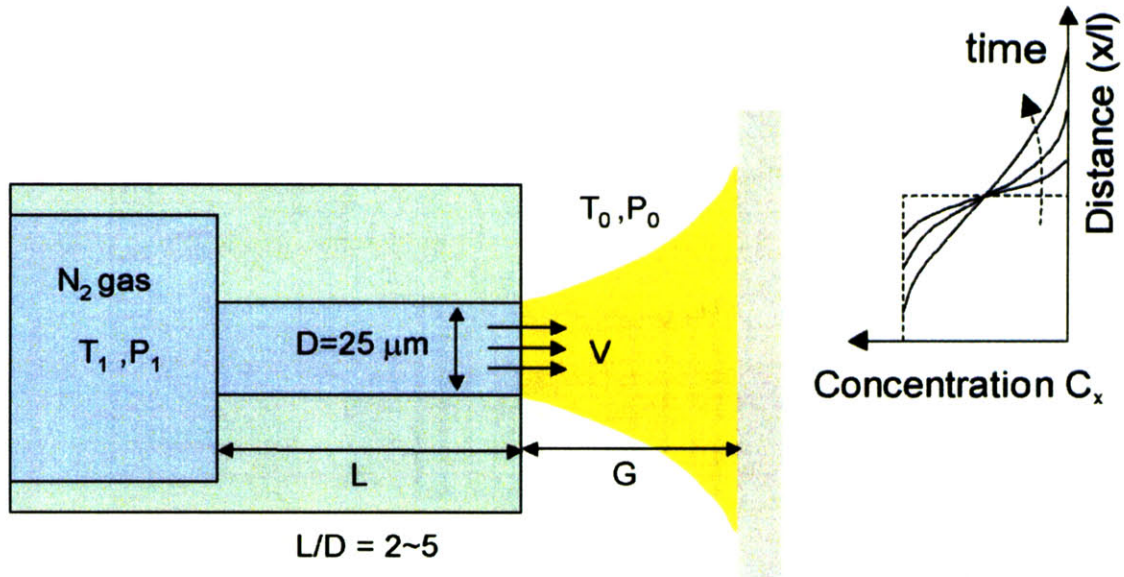
1. Mean free path reduced from meters down to micro-meters ⟹ Jetting trajectory is no longer straight. Organic molecules diffuse into ambient gas over a certain traveling distance.

2. Alq3 molecules collide with carrying gas molecules ⟹ System in equilibrium. Super saturated gas (molecules) may spontaneously condense

3. Additional in-plane velocity component ⟹ Organic molecules transport along the substrate's plane leads to the formation of concentric circles.

Figure 4-11. (a). Simulation system geometry. The nozzle size is 25 μm in diameter, 2~5 times this number in length. And the surface temperature is maintained at 300°C high enough to avoid cold wall condensation. The ambient pressure and temperature are constant at 1 atmosphere and 300K. (b). Schematic illustration of the concentration along the substrate plane to reflect the diffusive motion of the organic molecules. (c). Issues that need to be addressed in the simulation model.

Figure 4-12 summarizes the gas stream trajectories of the simulated flow field. In the simulation model, both the nozzle size and the jetting speed are variable. For nozzle size of 25 µm, the molecular jet initiates at about 60 m/s and the jetting molecules penetrate at least 100 µm throught the nozzle into the ambient environment when the jetting velocity reaches 120 m/s; while for nozzle size of 50 µm, the flow stream can penetrate further at lower jetting velocities. In both cases the ideal jetting speed should be in the range of 60 to 120 m/s. The organics cannot be jetted out of the nozzle when the speed is too low (10 m/s); when it is too high (500 m/s), it will significantly broaden the deposit on the substrate.
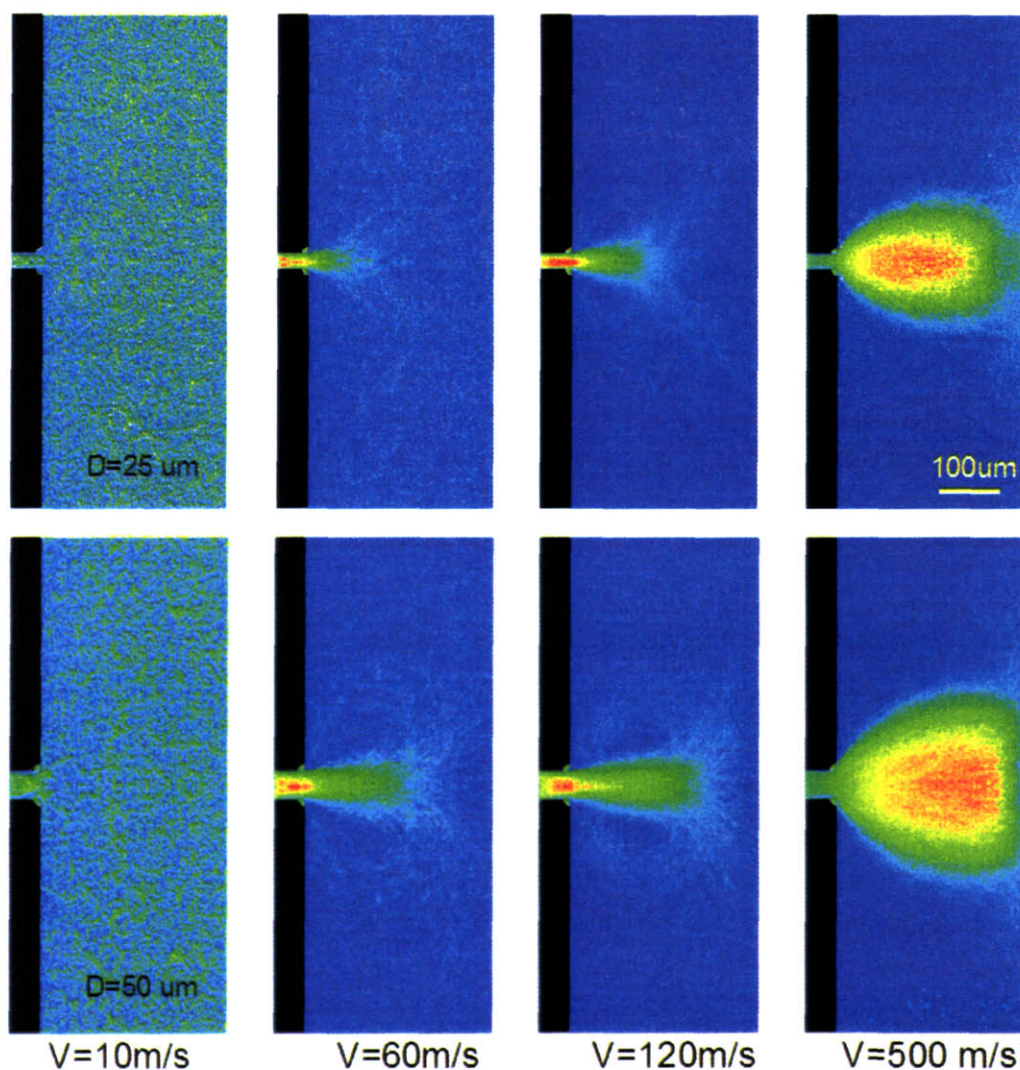
Figure 4-12. DSMC flow fields at different jetting velocities with different size nozzles

4. MEMS based MoJet II printer

Introduction

Organic light emitting device (OLED) technology, considered for use in flat panel display (FPD) applications, would greatly benefit from development of a reliable, repeatable, additive deposition technique for forming patterned organic thin films, as needed in OLED applications. Today's full-color OLED displays primarily utilize white emitting OLEDs filtered by color filters to generate light emission of red-green-blue (RGB) pixels. Although this display scheme bypasses the challenge of RGB pixel patterning, it is a power inefficient approach to forming full-color display technology. The most efficient OLED displays would utilize patterned electroluminescent (EL) RGB layers, one color for each pixel, removing the need for color filters. Several approaches have been adopted to pattern the EL layers; among them the predominant methods include shadow masking for molecular organics and InkJet printing for polymeric materials [5].

Although the method of patterning molecular EL thin films through metal stencil masks has been around for a long time in the commercial fabrication of molecular OLED displays, there are still shortcomings. The deposition usually requires a vacuum environment. The shadow mask accumulates the evaporated material that did not reach the substrate and consequently serves as an inadvertent source of dust particles as the deposited material flakes off of the shadow mask. In the present OLED fabrication schemes, cleaning the shadow mask and the vacuum chamber contributes to significant down time of the fabrication line. Shadow masks have also been hard to scale beyond Gen3 size substrates. All these shortcomings of the shadow mask-patterning step identify it as the bottleneck for advancement of the OLED display technology. Alternatively, InkJet technology was shown to be able to print arbitrary patterns drop-on-demand on substrates

as large as Gen 8 size glass [6]. However, the pinning of the contact line of the ink drops on the substrate surface typically leads to the formation of "coffee ring stain" patterns [7], which correspond to non-uniformity in the layer thickness and are generally considered incompatible with OLED structures, as shown in **Figure 4-13**. For OLEDs, which are current driven devices, uniform thickness across the device is needed for uniform distribution of current density and light intensity, and consequently uniform device aging.
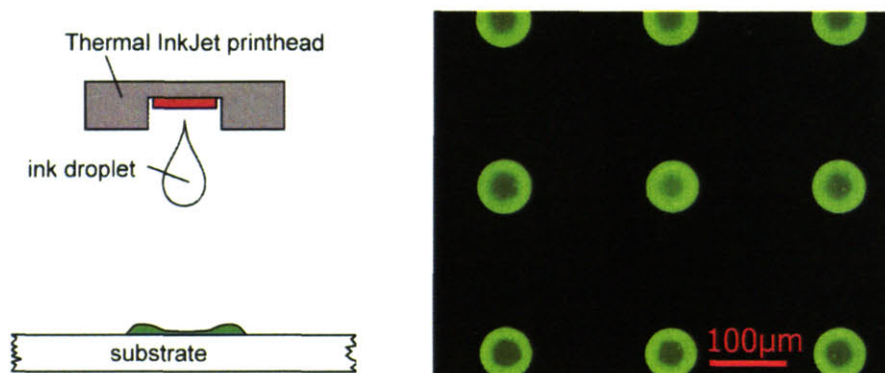
Figure 4-13. Inkjet printing Alq3 and coffee ring effects
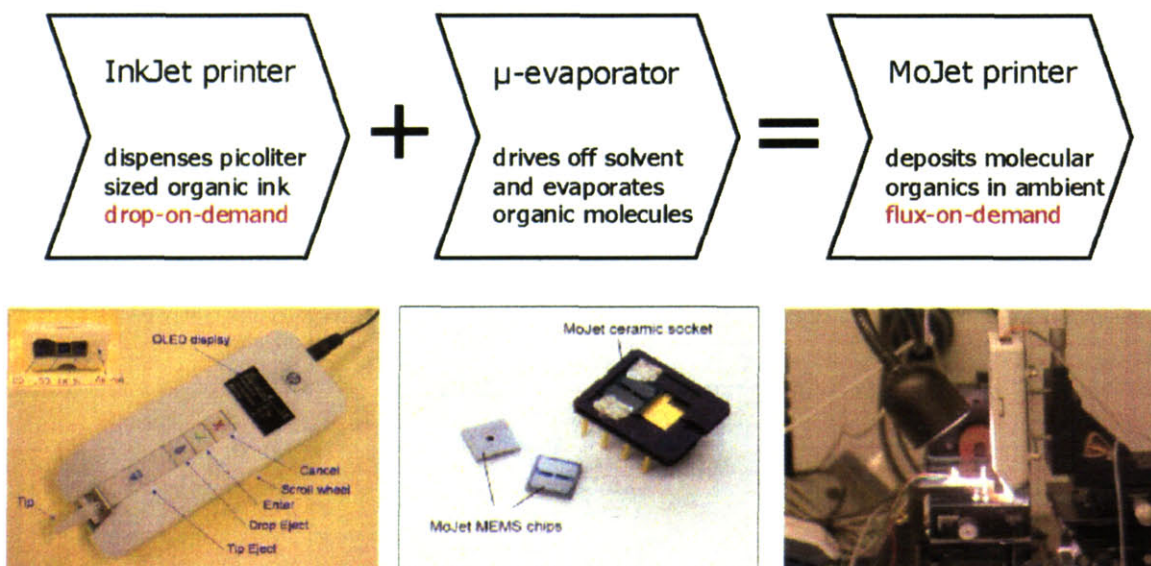
Figure 4-14. Concept of MoJet II flux on demand

By combining the strengths and eliminating the weaknesses of these previous methods, we developed a new printing technique that can combine the high quality of uniform thin films

128

provided by thermal evaporation and the reconfigurability and scalability enabled by InkJet printing, as illustrated in **Figure 4-14**.

Previously we demonstrated that the first generation MoJet printhead based on MEMS technology was successfully applied to pattern a vacuum deposited active molecular OLED [8-10]. In this section we present an improved version of this MEMS printhead and the concept of MoJet printing in ambient conditions.

Working principle
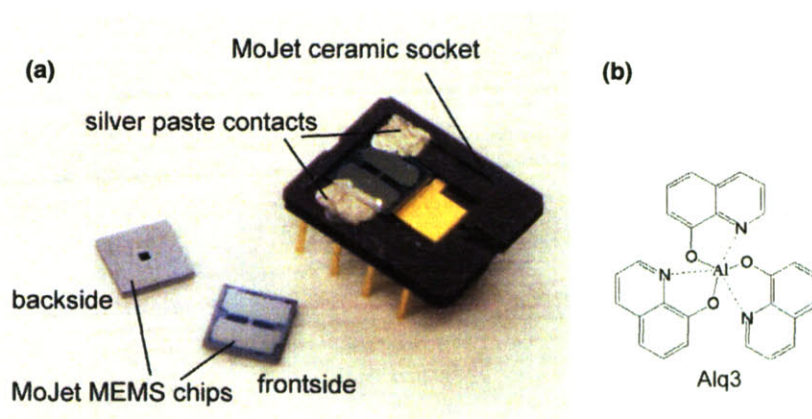
Figure 4-15. (a). MoJet printhead chips and package. The chip dimension is 4mm by 4mm. (b). Chemical structure of ink material.

The structure and process flow of the new MoJet printhead are described in detail in another article [11]. In essence, this new MoJet II chip acts as a single-nozzle micro evaporator that consists of an array of 8×8 two-micron pores and a platinum heater. As shown in **Figure 4-15**, the MoJet II chip is mounted onto a ceramic socket and connected to the socket terminals with a thin layer of silver paste.

We applied the MoJet technique to the deposition of thin films of a molecular organic material Alq3 (tris(8-hydroxyquinoline) aluminum), which is often used as the green light emitter. 0.1M Alq3 solution was prepared and filtered through a 5μm filter into an HP thermal InkJet printhead to serve as the ink. The InkJet printhead was installed on top of the MoJet II

printhead. A clean glass slide was attached to a moving stage to digitally translate the to-be-printed pattern image to the motion of the substrate. The glass substrate was suspended between the MoJet printhead and a video camera. The InkJet nozzle and the MoJet nozzle were aligned using this video camera viewing from underneath. The loading of ink material was controlled by the ink concentration, the volume of the InkJeted drop and the number of droplets ejected from the InkJet printer.
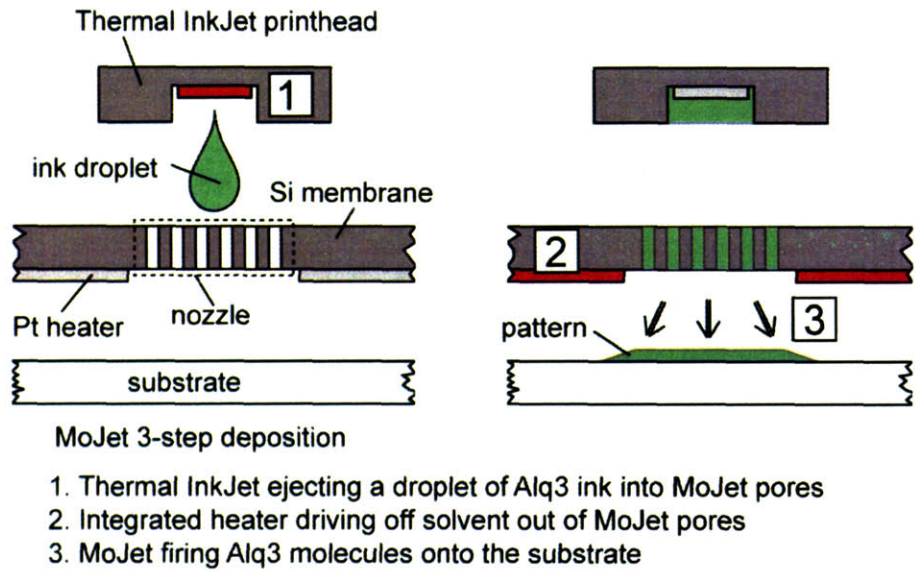
Figure 4-16. Schematic of the MoJet II working principle

Figure 4-16 illustrates the working principle of the MoJet printer. The printing process starts with the ejection of an ink drop from the InkJet printhead above the MoJet chip. The ink drop impinges the backside of the MoJet chip and fills the inside of the MoJet nozzle pores. A small current is passed through the integrated Pt heater to gently drive off solvent from the ink, and then a larger pulsed current is applied to heat up the nozzles to reach above the sublimation temperature of the molecular source/ejector within milliseconds [11], forming a stream of molecular flux. The molecular flux discharged out of the MoJet nozzle condenses on a near-by substrate and forms a deposited pattern. The entire process is completed within a few

milliseconds. This short thermal time constant is achieved by the MoJet chip design that reduces the thermal mass of the printhead.

Printer system setup

Figure 4-17 is the MoJet II system, consisting of several functional components such as Inkjet, Mojet controller, moving stage and a video camera. The Inkjet printhead is mounted right on top of the MoJet MEMS printhead and the two MoJet and InkJet nozzles are well aligned.
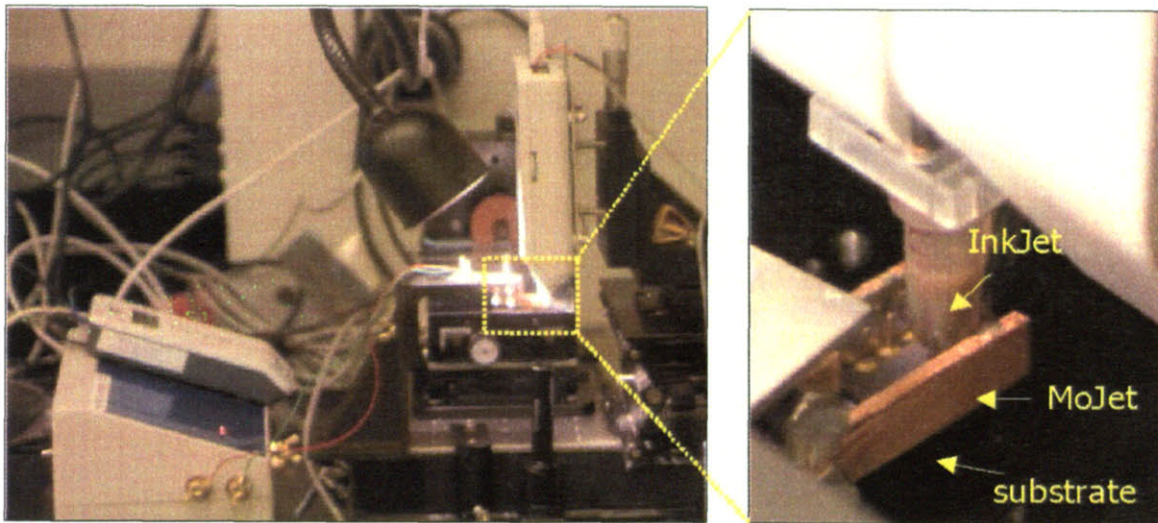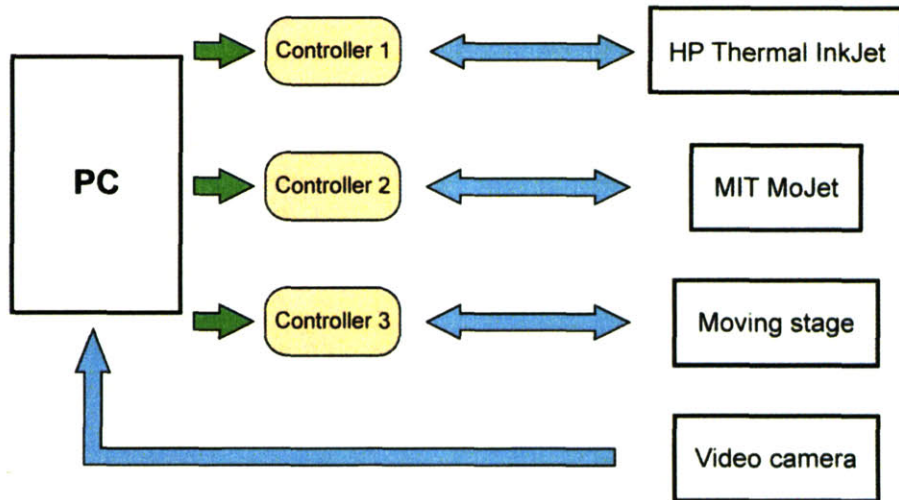
Figure 4-17. MoJet II printer functional blocks and system setup

The MoJet II printhead consists of a microporous membrane and a platinum heater. To characterize the heater performance, the testing circuit is shown in **Figure 4-18a**. The heater operates with a pulse-train signal that is generated by a MoJet controller. The pulse frequency and magnitude can be varied independently to determine the jetting energy of the MoJet printhead. The MoJet firing signal is recorded by a Tektronix TDS 210 digital oscilloscope (**Figure 4-18b**). As the heater's temperature goes up its resistivity increases and the voltage drop on the serial resistor decreases, as shown in **Figure 4-18c**, which can be used to determine the thermal time constant of the printhead (**Figure 4-18d**).
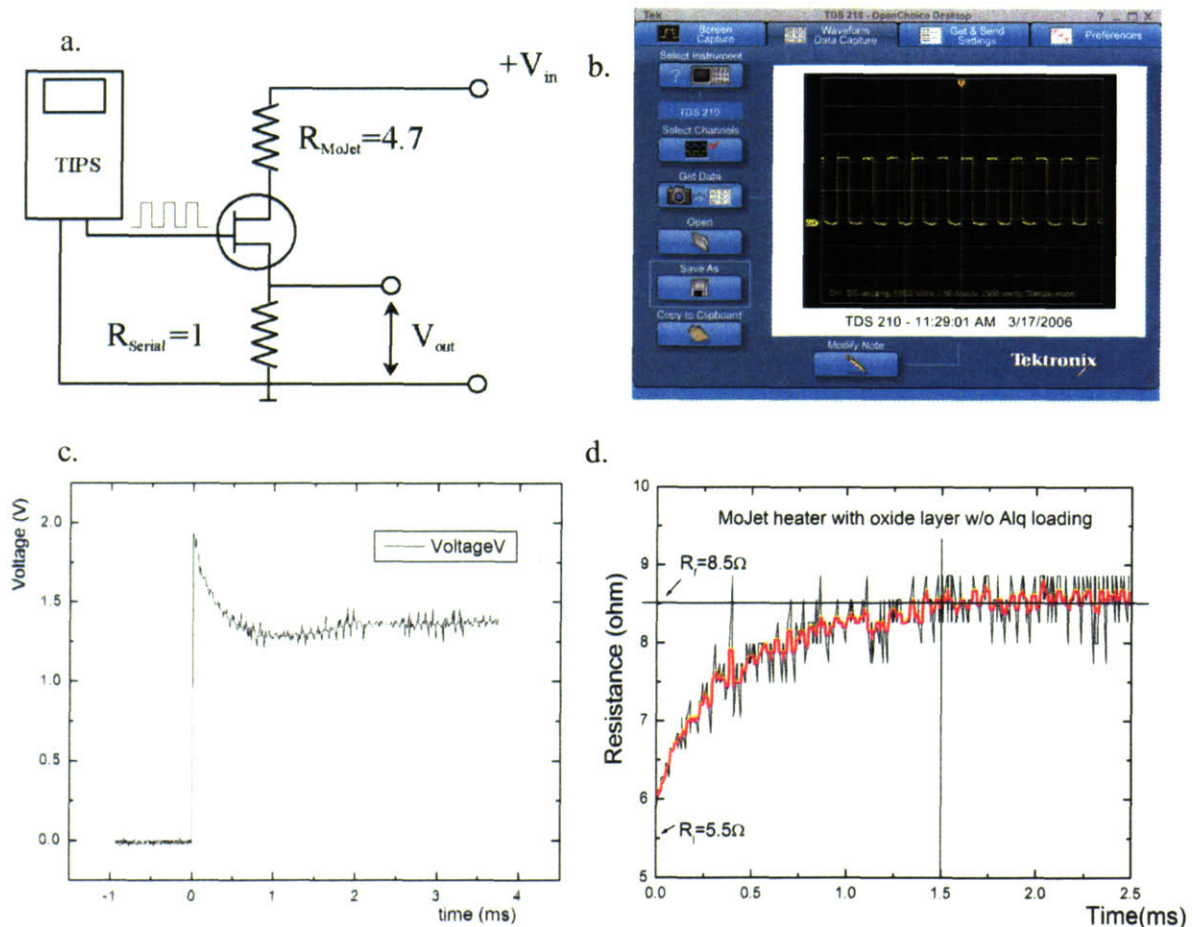
Figure 4-18. Characterization of MoJet II MEMS heater

The detailed performance of the MoJet heater under constant DC voltage is presented in another reference [11,12]. Essentially the MoJet heater behaves as a resistive heating element that converts electric energy to joule heat at the nozzle. The MoJet jetting energy is modulated with a computer controlled pulsed DC power supply. The temperature that the nozzle can reach is directly related to the jetting energy. A pulse train is generated in phase with the motion of the substrate. The jetting energy is adjustable by the DC voltage, the number of pulses in a pulse train and the length of each pulse. For typical deposition the pulse length is in the range from 1 µs to 10 ms, and the number of pulses also varies between 80 and 400.

5. Experiment results and discussion
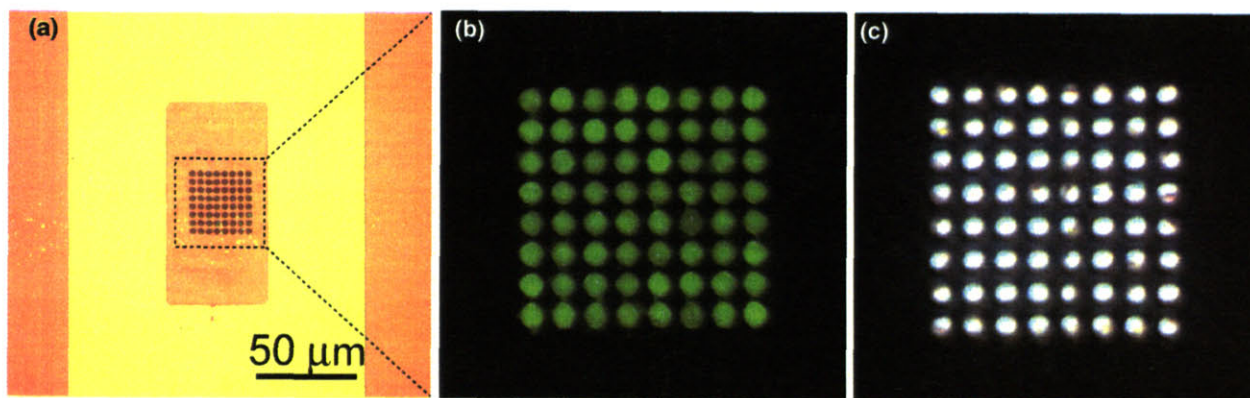
Figure 4-19. Optical microscope image of the MoJet printhead. (a). Before ink loading; (b). Photoluminescent image of MoJet nozzles filled with Alq3 solids; (c). Empty pores after MoJet heater firing and complete evaporation of Alq3 in pores

Prior to the loading of ink drops in the MoJet printhead, all of the MoJet pores are empty, as seen in **Figure 19a**. The photo-luminescent (PL) image of MoJet nozzle after loading of ink and driving off of solvent is shown in **Figure 19b**. Green PL emission is the signature of Alq3 solids presented inside the pores. The nozzles become empty again, by the intensive firing of Pt heater. This is confirmed by white light that can pass through the pores as shown in **Figure 19c**, which

133

indicates that the MoJet printhead is ready to receive another drop of ink to repeat the same printing cycle.

During the MoJet printing process, the final pattern size is strongly influenced by the background pressure. Previously we demonstrated that a pattern size of ~30µm can be defined in a vacuum chamber of 10^{-6} Torr by using a 25µm silicon membrane stencil mask [8,10]. However in an ambient environment (N_2 atmosphere), frequent collisions between Alq3 molecules and nitrogen molecules will lead to the broadening of the deposited pattern. **Figure 4-20a** reveals the result of MoJet printing conducted at 1 atmosphere. With a 30µm pore-array nozzle, the size of Alq3 pattern is ~60µm. This is a broadening factor of about two for the MoJet printhead suspended 100µm above the glass substrate surface. To define smaller feature size, it may be necessary to scale down the nozzle size, or alternatively to use micro pores of larger aspect ratio to direct the molecular flux.
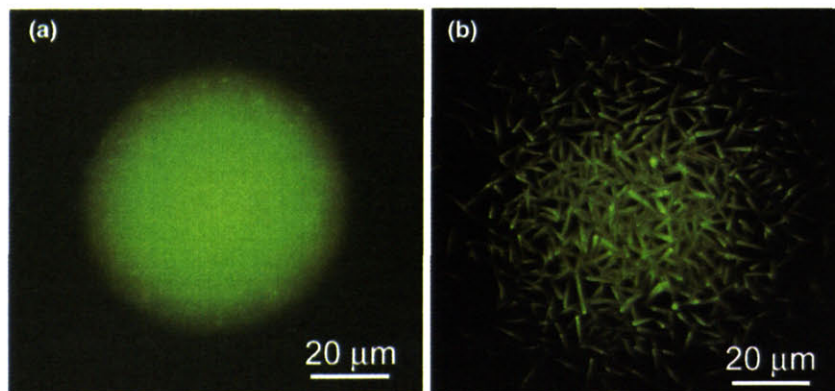
Figure 4-20. PL images of MoJet printed Alq3 patters in different conditions (a) solvent was completely driven off from the pores before the evaporation of Alq3 (b) Excessive solvent still exists while doing the Alq3 deposition

The solvent residual in the pores also affects the geometry and topography of the printed pattern. When a spongy stopper was placed on the backside of the membrane to prevent the solvent from drying up, the deposited Alq3 patterns were found to re-crystallize from the

134

amorphous phase in excessive solvent flux. Small Alq3 needle-shape crystals obtained by solvent vapor annealing [13] can be observed in **Figure 4-20b.**
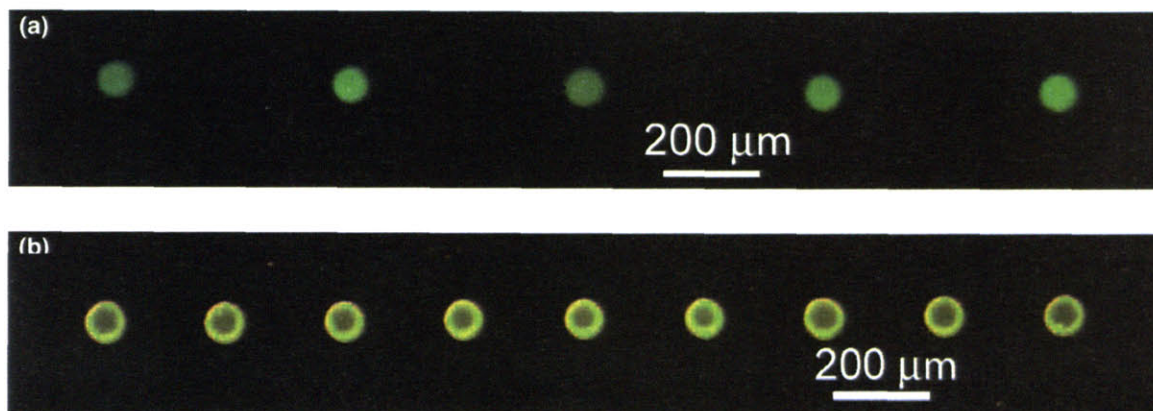
Figure 4-21. Comparison of results of (a)MoJet printing and (b)Inkjet printing

Figure 4-21a shows the PL image of an array of Alq3 thin film patterns of ~ 60μm diameter that were deposited 500μm apart on a glass substrate with the MoJet printer. The same ink solution was also printed by thermal InkJet on a glass substrate and the patterns were compared with the MoJet patterns. Ejected ink drops of ~150pL volume impacted the substrate surface, spreaded to ~60μm diameter. A PL image of typical "coffee ring" patterns is shown in **Figure 4-21b**, indicating a non-uniformity in the film thickness of InkJet printed films.

6. Summary of MoJet II

We printed patterned organic semiconducting thin films of Alq3 by direct evaporative deposition. The printing results were compared to those prepared by InkJet printing the same ink solution on similar substrates, showing more uniform patterns for the MoJet-printed films. The MoJet printing demonstrates the possibility of using flux-on-demand methods for patterning organic semiconductors in an ambient environment to simplify the fabrication of large-area organic electronics with high pattern precision.

Reference

[1]. S. H. Kang, Master thesis, MIT 2004.

[2]. M. Shtein, Ph.D. Thesis, Princeton 2003.

[3]. M. Shtein, H. F. Gossenberger, J. B. Benziger, and S. R. Forrest, Material transport regimes and mechanisms for growth of molecular organic thin films using low-pressure organic vapor phase deposition, J. Appl. Phys. 89, 1470 (2001).

[4]. G. A. Bird, Molecular gas dynamics and the direct simulation of gas flows, Oxford University Press, London 1994.

[5]. S. R. Forrest, "The path to ubiquitous and low-cost organic electronic appliances on plastic", Nature, 428, 911 (2004).

[6]. http://www.litrex.com

[7]. R. Deegan, O. Bakajin, T. F. Dupont, G. Huber, S. R. Nagel, and T. A. Witten, "Capillary flow as the cause of ring stains from dried liquid drops", Nature, 389, 827 (1997).

[8]. J. Chen, V. Leblanc, S.-H. Kang, M. A. Baldo, P. J. Benning, V. Bulović and M. A. Schmidt, "Direct Patterning of Organics and Metals Using a Micromachined Printhead", Proc. MRS Spring, H1.8. (2005).

[9]. V. Leblanc, S.H. Kang, J. Chen , P. J. Benning, M. A. Baldo, V. Bulović and M. A. Schmidt, "Micromachined Printheads for the Patterning of Organic Materials and Metals", Proc. of Transducers (Seoul 2005), pg. 1429.

[10]. V. Leblanc, J. Chen , S.H. Kang, V. Bulović and M. A. Schmidt, "Micromachined Printheads for the Evaporative Patterning of Organic Materials and Metals", J. of Microelectromech. Syst., In Press.

[11]. V. Leblanc, J. Chen, P. Mardilovich, , V. Bulovic, M. A. Schmidt, "A Micromachined Printhead for the Direct Evaporative Patterning of Organic Materials", DF2006 Session: Printhead technologies

[12]. V. Leblanc, Ph.D. thesis, MIT 2007.

[13]. D. J. Mascaro, M. E. Thompson, H. I. Smith, and V. Bulovic, "Forming oriented organic crystals from amorphous thin films on patterned substrates via solvent-vapor annealing", Org. Electron., 6, 211(2005).

CHAPTER 5: Inkjet printing nanocrystal inks

CONTENTS

1. State of the arts nanocrystals

Introduction

Nanocrystals with interesting size and shape dependent properties have become an attractive research topic as this new class of structures offer many unique optical and electrical properties that are otherwise not obtainable in bulk semiconductors. Nanocrystals are a new form of synthetic materials, with dimensions spanning from several to hundreds of nanometers (1-100 nm). In particular, for nanocrystals of a few nanometers in size, in which carriers are confined in a scale smaller than the De Broglie wavelength, their energy becomes quantized. This quantum confinement effect occurred previously only in the case of single atoms or point imperfections (i.e., impurities). In that sense, this type of nanocrystals, often times in sphere or rod shapes, are referred to as quantum dots (QDs), quantum rods (QRs), or "artificial atoms". Nanocrystals also have a high surface to bulk ratio. As a result surface properties play an important role in determining the properties and applications of nanocrystals. Materials most commonly used for creating nanocrystals include II-VI group or III-V group semiconductors, metal oxides, or single elements such as silicon, silver or gold, etc.
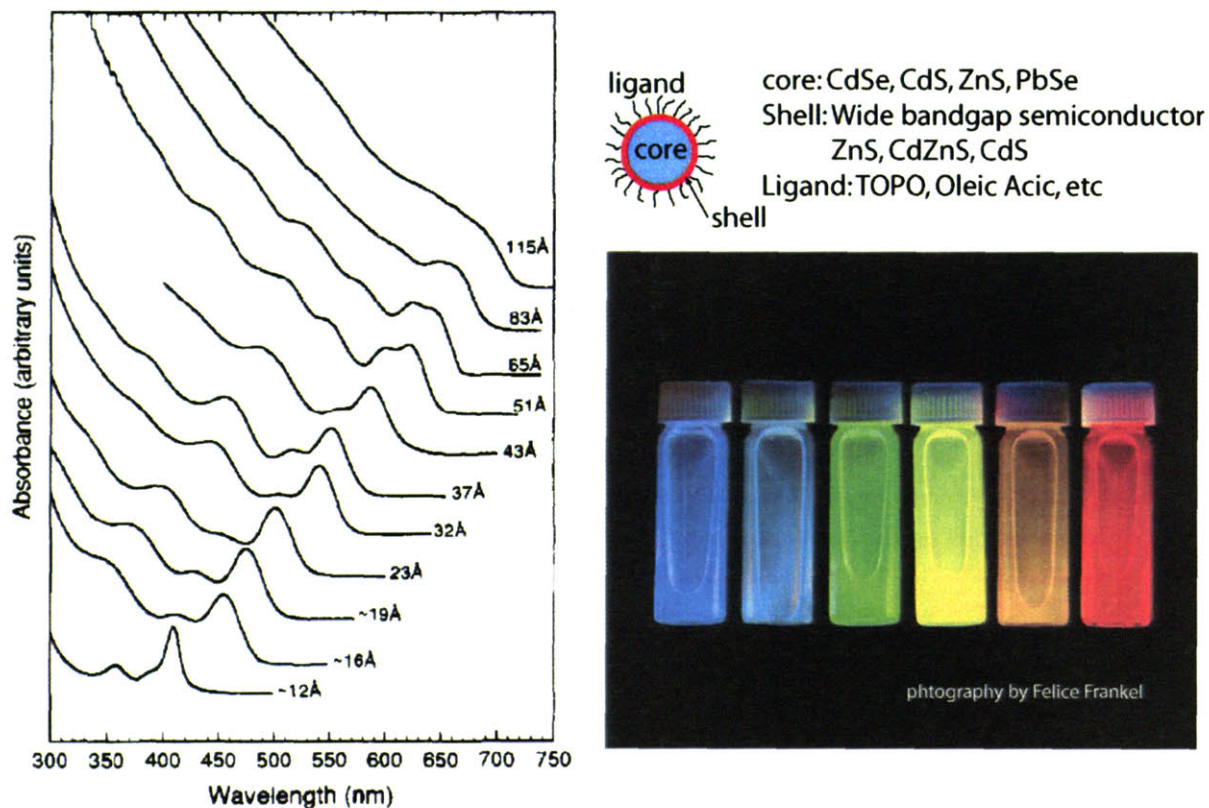
Figure 5-1. Size dependent absorption spectra of quantum dots

Semiconductor quantum dots (QDs) are zero dimensional matter. The size, shape, the number of confined electrons and the energy level structures of quantum dots can be tailored. This makes it possible to create a model to study the characteristics of QD system and compare the theoretical results to the experimental data, for example, the radiative recombination process in a few-particle system. The size tunability and the discrete energy level of quantum dots offer flexibilities in the design and application of many QD's opto-electronic properties, the most significant ones being the linear discrete absorption spectra and photo/electro-luminescence over a large range of wavelengths even with the same material sets [1,2], as seen in **Figure 5-1**. The surface to bulk atom ratio is substantially higher in quantum dots than the bulk material. Large surface area can have some drawbacks such as surface states that act as traps or annihilation centers leading to significant reduction of luminescent yield. However, this can be solved by

140

carefully pacifying the quantum dot surface. Surface passivation can also be used to modify quantum dot's surface properties, making it soluble in some organic solvents (vehicle) or selectively bond to certain specimens. There is a growing interest in using surface functionized quantum dots in life-science application (bio-imaging, bio-labeling, etc). But we will focus more on the applications where quantum dot solutions are used as printable electronic inks. Last, but not least, quantum dots can be easily incorporated into organic or inorganic systems to behave like super-molecules, which presents almost infinite possibilities to the selection of "pseudo-atoms" beyond the periodic table of the elements.

The unusual properties of nanocrystals have enabled promising applications in electronics and opto-electronics, which in turn have stimulated extensive research efforts and a rapid development of production technologies.
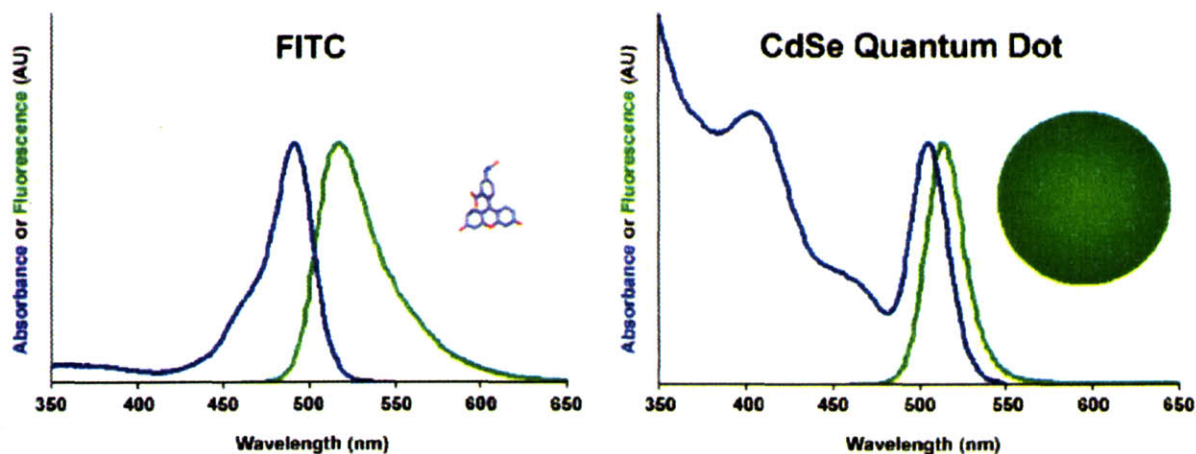
Figure 5-2. Comparison between fluorescent dye and quantum dot spectra

Quantum dots have many advantages over bulk semiconductors and organic dyes when it comes to the absorption spectra. Bulk semiconductors tend to have a flat absorption curve

141

beyond the band gap, the absorption cut-off frequency is correlated to the optical band energy levels and thus is difficult to alter. A possible solution is to dope the semiconductor with ionized impurities to form so called "color center". Unfortunately the choice of such dopants is limited. Meanwhile, organic dye molecules have large absorption cross-sections at a distinct band of resonant frequency with a narrow absorption peak. This results in a situation where each kind of dye molecule will require a matching excitation wavelength, which might limit the option of selecting efficient excitation light source (**Figure 5-2**). Also, organic dye molecules can be photo-bleached, a degradation process caused by the changes of molecular structures or photochemical reactions in the dye molecule. Combining the advantages of both the bulk semiconductor's broad absorption curve and the narrow absorption peak of a molecule dye, with low photodegradation rate, a.k.a. a long fluorescent stability, quantum dots are superior light absorbents. Together with the size-tunable, sharp light emission properties in any of the visible or infrared frequency, there is a huge potential for quantum dot applications.

Applications of Quantum Dots

To reveal details inside a biological system, traditionally organic dye molecules are designed to selectively bind to the target sites. However, organic dyes suffer from short fluorescent lifetime, when the fluorescent brightness gradually decreases by photobleaching. Another drawback of using an organic dye as a bio-labeling reagent, is the limited excitation light source that has to match the dye molecule's absorption peak wavelength, posing difficulties to visualize multiple color image [3]. All these problems can be overcome by substituting organic dyes with quantum dots. Stable, color coded bio-images can be distinguished and captured. Although this application seems very compelling, quantum dot bio-labeling reagents might not completely

replace organic dyes, primarily due to economic issue: QDs are relatively expensive at the current stage in comparison with organic dyes, but the market is growing rapidly.

Authenticating products, such as legal documents, securities, currencies, identification paper, etc, often involves using unique substances as the authentic characteristics or features, such as absorption or emission of certain colors under specific circumstances. Special inks, for instance, those used to print currencies, need to be extremely durable yet with superior color. QD inks are natural fit in such anti-counterfeit applications [4].

Current LED or OLED technology is based on electroluminescence from a p-n junction or junction like interface. Electrons and holes are recombined at this interface to produce an exciton, whose energy is restricted by the energy level of the semiconductors (i.e. bandgap) and so is the corresponding emission wavelength. Each semiconductor material gives a certain wavelength but the methods currently used to tune the exciton energy is doping to either shift the Fermi level or create energy transfer site or change the solid-state solvation effect. The LED structure can also affect the emission color, for example, using a micro-cavity to selectively enhance output of a certain wavelength [5]. Lack of versatility is the one challenge that is often encountered in the design of LED, to select different material set for each output wavelength further complicates this issue. The size dependent bandgap alternation in quantum dots can provide a versatile research platform for developing LEDs with any photon wavelength emitted in the range from visible to infrared, which is nearly impossible in the traditional semiconductor LEDs [6-10]. Discussion of QD quantum confinement can be referred to the references [11,12] and Appendix A.

2. Surface science behind inkjet printing

In this section we will discuss basic behaviors of pattern formation by inkjet printing. Ink composition may include organic semiconductor solutions or quantum dot solutions.

The dynamics of droplet wetting and drying, following the inkjet process can be very complicated. Here, a few examples will help to illustrate the need to understand the phenomena of ink droplet wetting and drying. Physical and chemical properties of the substrate surface, as well as the ink composition all play an important role in the formation of the final pattern on the substrate.

Wetting
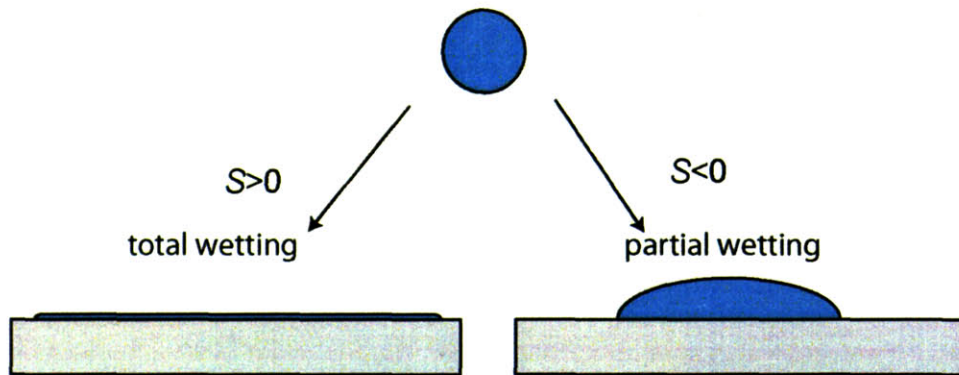
Figure 5-3. Two wetting regimes depending on the spreading parameter S

When an ink drop lands on the substrate, there are two regimes of wetting depicted in **Figure 5-3**. The parameter that describes them is the spreading parameter, defined as the difference between the surface energy per unit area of the substrate before and after wetting:

$$S = \gamma_{sg} - (\gamma_{sl} + \gamma_{lg}),$$
(5.1)

where the three coefficients γ are the surface tension at the solid/air, solid/liquid and liquid/air interfaces (**Figure 5-4**).
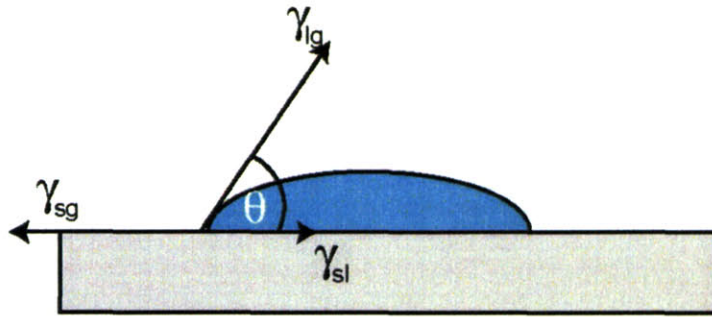
Figure 5-4. A contact angle of a liquid sample

$S > 0$: total wetting. The drop spreads completely to minimize its surface energy, where the contact angle is much less then $10°$.

$S < 0$: partial wetting. The drop forms a spherical cap on the substrate with a contact angel θ (neglecting gravity).

Young-Dupré equation

The theoretical description of surface wettability is attained from thermodynamic equilibrium between the substrate surface (S), liquid droplet (L) and the ambient (G) known as the Young-Dupré equation:

$$\gamma_{sg} - \gamma_{sl} - \gamma_{lg} \cos\theta = 0 \qquad (5.2)$$

where θ is the experimental contact angle. Thus the contact angle can be used to determine an interfacial energy. If the contact angle is less than $90°$, the liquid is said to mostly wet the substrate, and not to wet the substrate if the contact angle is greater than $90°$.

Substituting equation (5.1) into (5.2), we obtain:

$$S = \gamma_{lg} (\cos\theta - 1) \qquad (5.3)$$

Zisman's Rule: wetting criteria

The surface energy of the solid itself is not sufficient to predict wettability. When the surface interaction is purely the van der Waals type, the spreading parameter S can be related to the electric polarizabilities of solid and liquid [13,14].

The van der Waals energy Vss per unit area is related to polarizability of the solid α_s through the relation $Vss = \kappa \cdot \alpha_s^2$, where κ is a constant. When bringing two semi-infinite solid surfaces in contact, the total surface energy of the resultant solid is zero, giving:

$$2\gamma_{sg} - V_{ss} = 0 \qquad (5.4)$$

When solid and liquid are in contact, the interactions yield:

$$\gamma_{sl} = \gamma_{lg} + \gamma_{sg} - V_{sl} = \gamma_{lg} + \gamma_{sg} - \kappa\alpha_s\alpha_l \qquad (5.5)$$

For liquid-liquid interactions:

$$2\gamma_{lg} - V_{ll} = 0 \qquad (5.6)$$

Combining equations (5.4-5.6), the spreading parameter S can be estimated as:

$$S = V_{sl} - V_{ll} = \kappa(\alpha_s - \alpha_l)\alpha_l \qquad (5.7)$$

Equation (5.19) leads to the wetting criteria that a liquid spreads completely on the solid if it is less polarized than the solid; for a non-polar liquid, the wetting is only dependent on the surface properties of the solid. High-energy surfaces that are made of ionic, covalent or metallic materials with high chemical binding energy (>1eV) can be wetted by almost any liquid; while low- energy surfaces (binding energy $\sim kT$) including molecular materials and plastics are hardly wettable.

## Contact angle hysteresis and pinning of the triple line

The previous discussion can predict the contact angle that is entirely based on the chemical properties of the surface, assuming it is clean, planar, solid, smooth and free of defects. However,

146

often time the physical properties of surface are not always ideal, in some cases the contact angle is not constant, but depends on the surface preparation conditions. The so-called contact angle hysteresis can occur when the triple line is pinned on the substrate surface as the drop volume and the contact angle vary.

Two types of triple line pinning might occur during the droplet drying [15-17]. This first type of pinning is usually caused by the irregularities or defects of the substrate where the defects are more wettable than the rest of the substrate surface, additional energy will be needed to displace the triple line as a result of "stretching" the triple line. The contact line will be pinned if the stretching force is not enough to break off the line and bypass the defects; the second type of pinning is called self-pinning, which takes place when the internal friction of the solution is so high that the contact line loses its mobility. This can also be explained as the effect of solute precipitation near the contact edge (self-pinning).

Coffee ring effect explained

a. contact line no pinning; b. contact line pinning
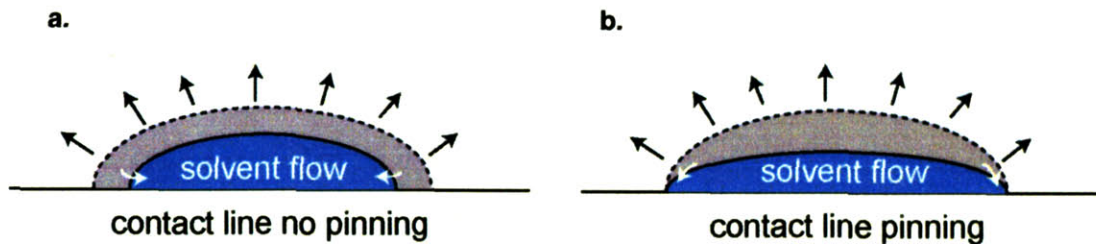
Figure 5-5. Illustration of solvent advection

(a) no contact line pinning drop; (b) contact line pinning drop

The origin of the coffee ring non-uniformity effect can be explained as the outflow of ink to the contact line, as illustrated in **Figure 5-5** [18]. The schematics show that if the contact line is not pinned, the interface can move freely, the drop shape as well as the contact angle will maintain unchanged. As the solvent evaporates, all the solutes will move inwards, leaving no deposit at the contact line. When the contact line is pinned due to the substrate roughness or

147

thermodynamically more wettable defects, the base of drop can't shrink and the ink will replenish the liquid removed from the edge [19, 20]. The ink advection accumulates solutes at the contact line, which condense on the substrate and strengthen the self-pinning, eventually deplete the solutes inside the ink, leaving a ring like pattern on the surface.

Because the moving speed of solutes is diffusion limited, the ring pattern formation will compete will the evaporation rate of the solvent. For very fast solvent evaporation, solutes might not diffuse far enough to reach the edge before the ink becomes too viscous or the solvent completely dries out, it can leave a more uniform deposit at the center. Intuitively to reduce the coffee ring effect, either more volatile solvent or heated substrate should be adopted, minimizing the necessities to modify the surface properties.

Dewetting

Dewetting refers to the withdrawal of a liquid film from a hostile surface [15], an essential step related to the restoration of a dry pattern. Dewetting can be observed when a large drop is placed on a non-wetting surface. The drop will contract into a spherical cap or break up into smaller drops due to the instability of the liquid. The breaking up of liquid thin film can be interpreted as the nucleation and growth of the dry zone, which leads to minimization of surface contact between the liquid and the substrate. Three stages are involved in dewetting: first, random appearance of holes break up thin films on partially wettable surface; then the holes grow and the rims head of the holes merge forming cellular structures; third, the resulting unstable ribbons reshape into smaller droplets [21]. The whole process is controlled by a competition between interfacial capillary forces and viscous flow [22]. Dewetting is one of the main phenomena that cause thickness non-uniformity of inkjet printed patterns.

3. Inkjet printing II/VI group QDs for energy down conversion

EL devices

Electroluminescent (EL) devices that emit light by exciting thin film or powder form of phosphors in strong AC electrical field have emerged long before other flat panel display techniques such as TFT-LCD or OLED. To date rugged EL displays embedded in portable, impact resistant electronic instruments can resist harsh environments; on the other end, low cost ACEL signages can be made on flexible substrates simply by screen-printing processes, where other display technologies are inadequate for such applications [23]. A comparison between thin film EL display and other key display technologies is listed in **Table 5-1** by Planar [24]

Table 5-1. Compare thin-film EL display with other display technologies

|	TFEL	OLED	AMLCD	PLCD	VFD*	LED
Visual Performance	1 = Excellent		2 = Very Good		3 = Good	4 = Poor
Brightness	1	1	1	3	1	2
Response Time	1	1	2	4	2	1
Contrast	1	1	1	2	3	3
Viewing Angle	1	1	2	3	1	1
Color Gamut	3	1	1	3	2	2
Gray Scale	3	1	1	2	3	2
Sunlight Readability	2	1	2	1	1	3
Graphics-friendly	1	1	1	3	2	2
Environment	1 = Excellent		2 = Very Good		3 = Good	4 = Poor
Temperature Range	1	1	3	2	1	1
Humidity	1	1	3	2	1	2
Shock & Vibration	1	1	3	2	2	1
EMI	2	1	1	2	1	1
Power Consumption	2	2	2	1	3	3
Cost of Ownership	1 = Excellent		2 = Very Good		3 = Good	4 = Poor
MTBF	1	1	3	2	2	1
Operating Life	1	3 or 4	2	2	2	2

*Vacuum Florescent Display

Despite early commercialization of EL devices, the realization of achieving full-color capability, especially obtaining saturated red emission from EL devices still remains one of the largest challenges to be met. The three basic structures of implementing individual addressable red-emission EL pixels include: directly patterning red emission phosphors [25], filtering of a broad spectrum by a passband filter (red by filtering) [26-28] and wavelength downconversion of blue to red emission (color by blue) that will be described here.

Device structure

ACEL devices are capacitor type structures where the luminescent materials (phosphors) are sandwiched between two electrodes, and at least one side of the electrode contains an insulating layer to couple AC charges into the phosphors layer, the structure of powder ACEL is shown in **Figure 5-6** and the cross section in **Figure 5-7**.
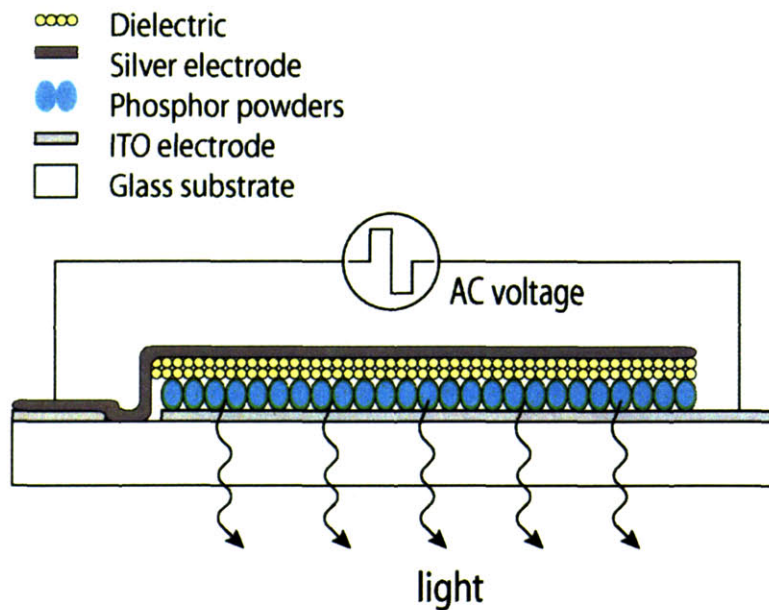
Figure 5-6. Structure of ACEL with phosphor powders

The phosphor materials are essentially wide bandgap semiconductors doped intentionally with impurities into the semiconductor lattice and thermally activated to produce acceptor levels or color centers for a particular wavelength emission inside the wide bandgap matrix/host. A co-

dopant that might have no effect on the emission wavelength, but can largely increase the concentration of activators inside the phosphors, is often referred to as the co-activator. Alternatively, co-activators in the matrix can create donor levels to capture electrons and facilitate electron-hole combination probabilities, leading to stronger EL emission.
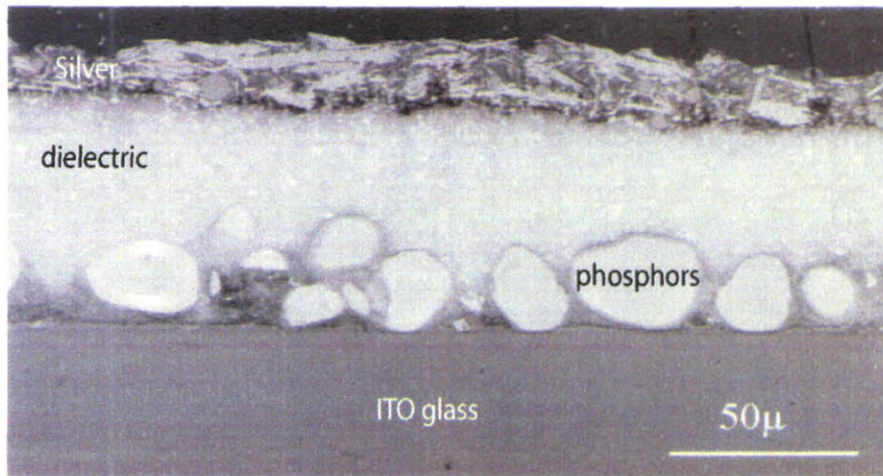
Figure 5-7 Cross section of powder ACEL device [29]

The host material usually is a wide bandgap material that doesn't absorb visible wavelengths while each activator creates distinct energy level, corresponding to different emission colors of the EL phosphors. ZnS with an energy gap of 3.7 eV is a common host material for these phosphors, and is commercially available in powder forms from DuPunt or Osram Sylvania. Other wide band gap semiconductors such as GaN has also attracted considerable attention [30].

Working mechanism

The working mechanism of an ACEL device is different from inorganic LED or OLED. An ACEL device is driven by alternating voltages. Light is emitted when the voltage is above a certain threshold voltage; below it the device is purely capacitive; and luminescence is generated by the effects of impact ionization and avalanche multiplication due to high kinetic energy electrons exciting electron-hole pairs and their sequential recombination at the luminescent

centers, while in LED or OLED structures, light is generated when free electrons and holes are

recombined (donor-acceptor pair recombination) at the junction interface/shallow traps. .
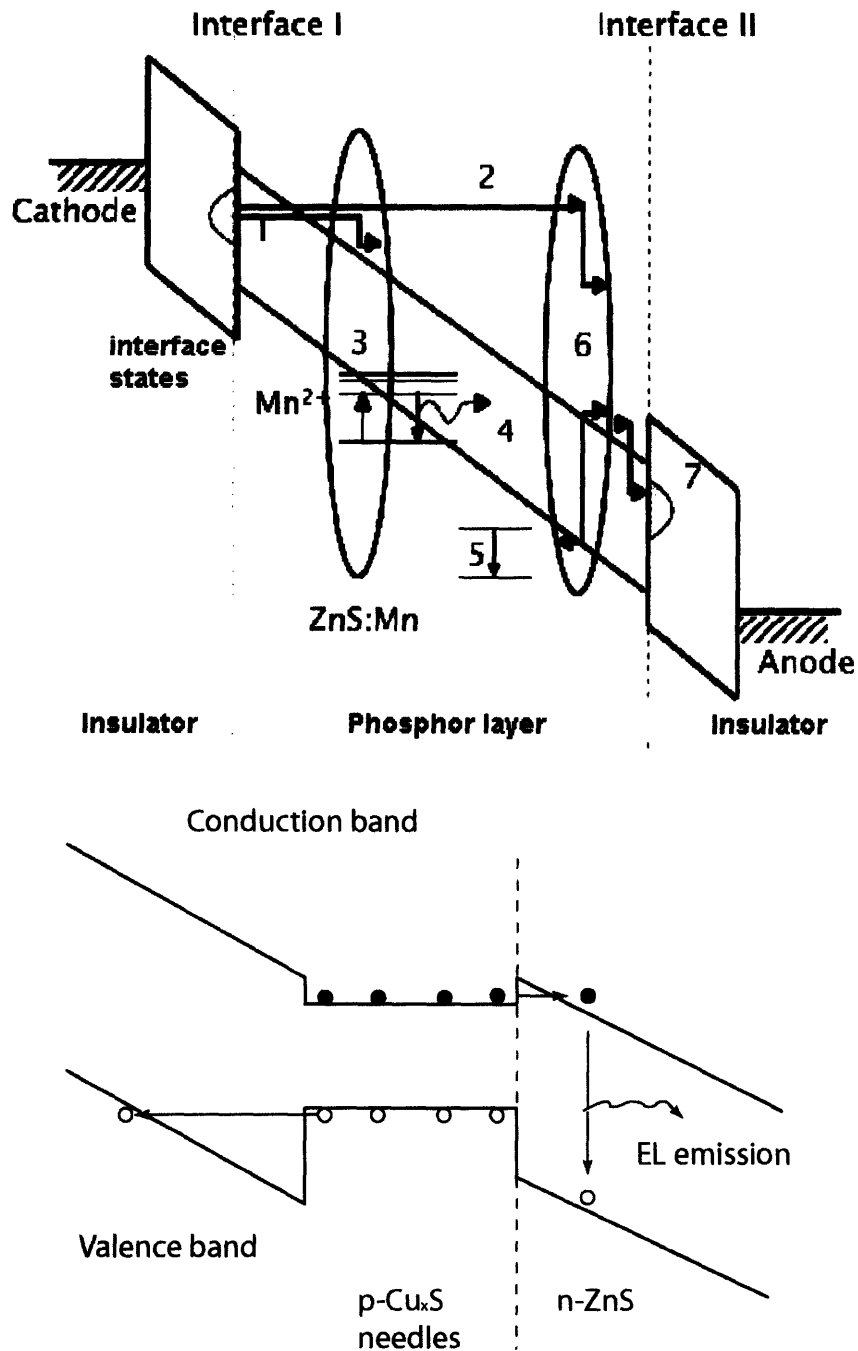
Figure 5-8. Energy band diagram of (a). thin film ACEL and (b). powder ACEL.

Although there are many publications about the ACEL devices, a single unified theory still

does not exist to explain the luminescence in EL devices. The generally accepted agreements are

in the most studied materials for ACEL: ZnS:Mn (thin film) and ZnS:Cu (powder). Simple models to describe the working mechanism of luminescent center in ACEL devices are shown in **Figure 5-8**. In ACTFEL (ZnS:Mn thin film), electrons are tunnel-injected from the surface states into the host material from the dielectric/host interface., Then these electrons are accelerated in the conduction band of the host material above the threshold voltage. While traveling inside the host material, these electrons acquire kinetic energy sufficiently larger than the bandgap of the host material before the impact-excitation occurs. H igh energy electrons, now described as hot electrons, can directly excite the luminescent centers through kinetic impact. When the exited electrons at the luminescent centers return to ground state, EL light is emitted. Some excited electrons may decay non-radiatively, and some hot electrons can generate more than one excited electron as it travels. Finally electrons are trapped at the other side of the electrode;. When the polarity of the ac voltage wave forms is reversed, same process in the opposite direction will take place again [31].

For EL emission from powder phosphors (ZnS:Cu powder), the working mechanism is different. Copper additives in ZnS play two roles, other than forming the luminescent centers (Cu [Ar] $3d^{10}$ $4s^1$, Zn [Ar] $3d^{10}$ $4s^2$), excess copper sulfide (Cu_xS) crystallizes in needle shape that can induce hole injection (field emission) into the host material at high field and trapped at the Cu recombination cites; when the field is reversed, trapped holes will recombine with electrons to produce light at the Cu_xS/ZnS hetero-junction regions. However, these tiny spikes are easily worn out in high humidity environments, the result is a slowly decreasing EL brightness [32].

The luminescence of these ACEL devices uses mostly the transitions of inner shell electrons, which are unlike the free electrons that contribute to the current (moving charges). The inner shell electron configuration of Mn is [Ar] $3d^5$ $4s^2$: two s electrons to form bonds, five electrons

in the *3d* shell that when one of the electrons is impacted by any of the high kinetic-energy electrons, it will be excited (within the same ionized atom). If the quantum number remains unchanged, the relaxation of this excitation is prohibited and thus the excited state is long-lived. The theory of only inner shell transition of electrons contributing to the electroluminescence process limits the selection of activators to transition metals such as Mn with unfilled 3d shells and noble metals such as Cu and Ag with unfilled 4d shells or alternatively rare earth metals showing 4f-4f transitions that are also dipole forbidden and long-lived [33,34].

In the next section we will focus on powder EL phosphors and their applications. Typically ACEL powder luminescence is used in making the "fixed pattern" panels and signages. Commercially available ZnS:Cu, Cl powder was purchased from Osram Sylvania Co.

Experiment: Printing QD down conversion layer

Ink formulation

QD as highly efficient fluorophores have found potential applications in solid-state lighting devices, flexible LEDs, color filters, etc. In the fabrication of these devices, QD layers have to be patterned either as close packed monolayer thin films or multiple stacking layer thick films. For thick film composites for down conversion application, highly luminescent QDs need an effective surface passivation method, i.e. an overcoating layer of the dots with a wide bandgap shell and a transparent insulator polymer matrix that quantum dots can be embedded inside. The literature have shown that polymers such as PLMA or PMMA can fulfill this requirement [35, 36], they are both transparent in the whole visible spectral range; the short wavelength (blue) excitation light and the green or red emission from the CdSe QDs can pass through the polymer matrix, plus they are chemically compatible with quantum dot solutions, making least likely energy transfer (light re-absorption) among QDs.

Here we use an alternative polymer poly isobutylene (PIB -(-CH_2-$C(CH_3)_2$-)$_n$). PIB is a synthetic elastomer (rubber) and is gas impermeable. There are two reasons why PIB is blended into the ink. First, PIB is optically transparent polymer matrix that can be used as host for QDs; secondly, blending a small amount of PIB into CdSe QD/hexane can increase the solution's visco-elasticity. For inkjet printing quantum dots, the ink needs to be specifically designed. QDs are readily dissolved in hexane, which makes it relatively difficult when it comes to the situation when more than one layer of QD thin film is printed at the same spot: after the first layer is printed, the coffee ring effect will leave most of the quantum dots to accumulate near the edge, while the second layer is put on top of the first layer, hexane will likely redissolve the previous layer and cause a pronounced coffee ring effect; the more layers that are put down, the more severe this phenomenon will be. Eventually, a very non-uniform thickness distribution will appear. PIB will form a protection coating on the previously printed layer to prevent it from being attacked again by hexane before hexane evaporates, leading to better uniformity.

Printing QD layer
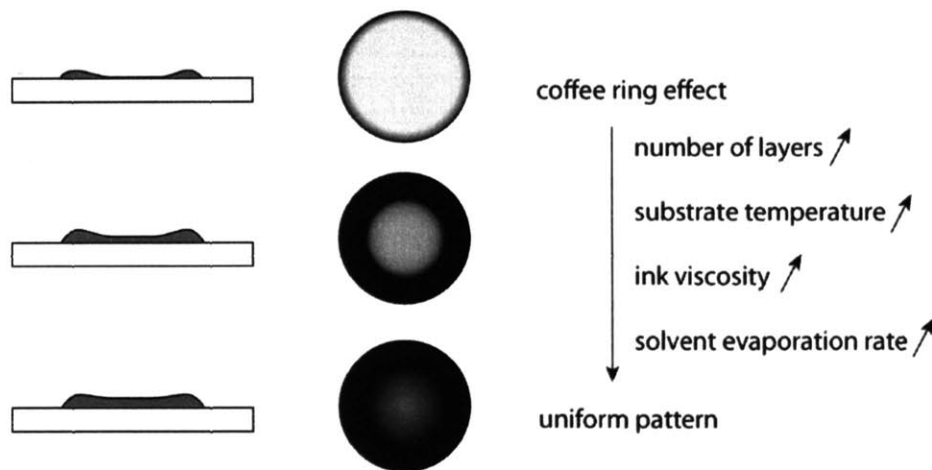
Figure 5-9. Uniformity of printed pattern and the printing conditions. In general more uniform pattern will form when the printing conditions are towards high end of those parameters

A PbS QD in Hexane:Octane (9:1 volume ratio) dispersion solution is initially used as the ink for the experiment. The ink solution is compatible with the HP thermal inkjet system, such as TIPS. However, the surface chemistry of the substrate surface is extremely critical. Under normal printing conditions, the ink vehicle wets the substrate surface really well, forming significant coffee ring patterns as shown in **Figure 5-9**.

The first layer printed on a glass substrate is highly non-uniform, as most of the QDs accumulate towards the pattern edge, not allowing a uniform down conversion output. To minimize the coffee ring effect, three special alterations are adopted. First, about 1% volume ratio of PIB is added into the ink solution to raise the ink viscosity, making it more frictional for the QDs to diffuse to the edge, therefore reducing the spreading of the ring. PIB also serves as a polymer matrix to isolate QDs from directly contacting each other. Optical loss due to energy transfer from luminescent (good) dots to non-luminescent (bad) dots is greatly lessened. The second approach is to heat up the substrate as it prints. Higher substrate temperatures will enhance solvent evaporation. Because the diffusive aggregation of the dots at the edge needs to compete with the drying of the solvents, shorter drying time allows less diffusion of dots. The final alteration is to print more than one pass of ink on the same spot. As the previous pattern air-dries, the second drop will fall into the center spot and fill the well formed in the previous step, spreading of QDs to the edge is thus lowered. The result is an improved smoothness of the final pattern, as shown in the microscope image of **Figure 5-10**.
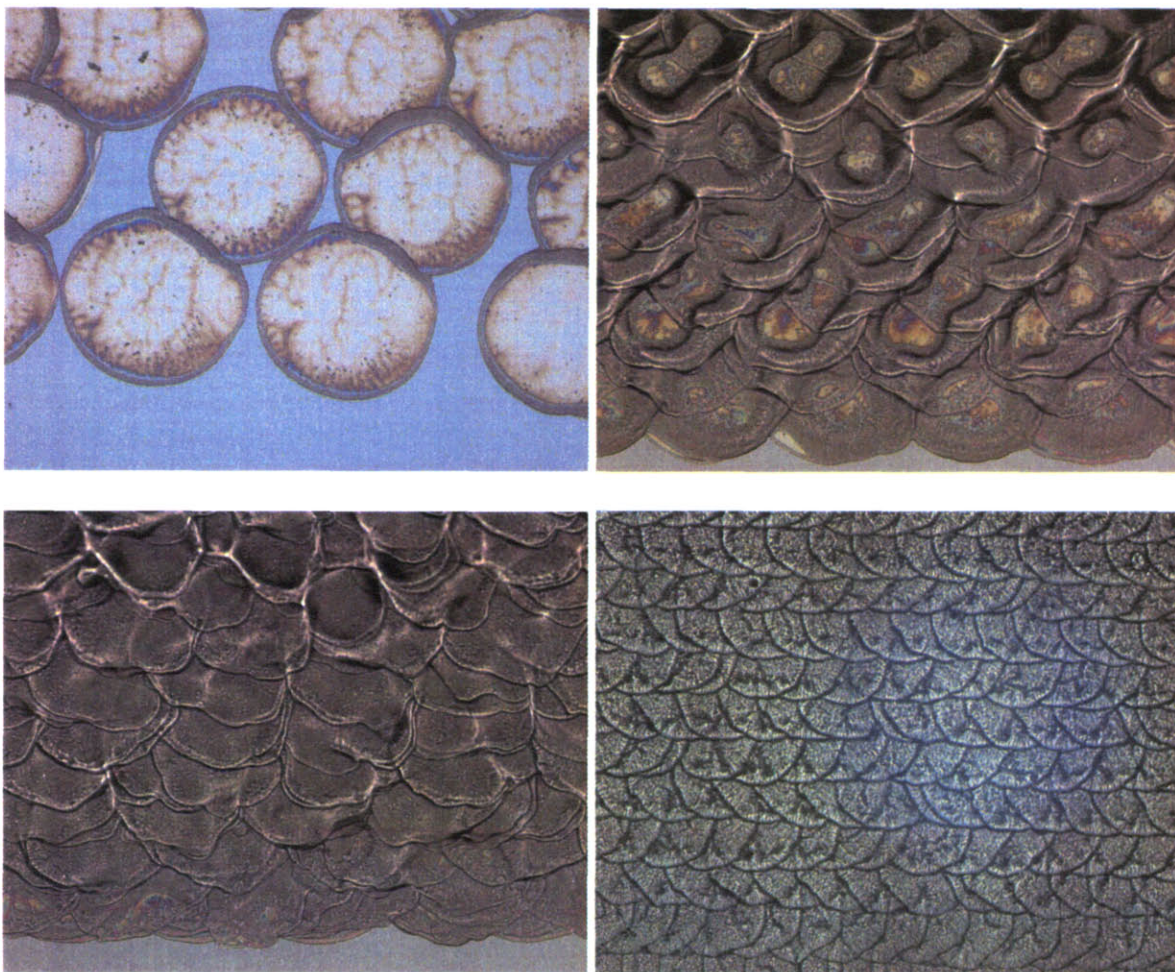
Figure 5-10. 1mg/mL PbS QD in hexane: Octane (9:1) solution printed on clean ITO glass by HP TIPS printer. Pitch size is 150 μm. All images are taken at the same magnification, viewing from the top of the QD patterns. (a). Single layer pattern. Darker edge indicates aggregation of PbS dots. (b). 4 layers of such patterns printed (c). 6 layers printed at substrate kept at RT. (d). 8 layers of PbS dots printed on a substrate heated to 60 ºC. The pattern is smoother than (a)-(c).

To illustrate the feasibility of incorporating printed QD layers into the ACEL device, red CdSe QDs in Hexane:Octane dispersion solution is printed in designated checkboard patterns onto an ITO glass substrate. The ITO glass is degreased with ethanol prior to the printing. A 5mm by 5mm chessboard pattern is printed directly on top of the ITO layer. Here ITO is a transparent electrode from which side the light will emit. Same printing conditions are adopted as those in printing PbS QD ink. The printing results are shown in **Figure 5-11**, which is a

photographic image of the printed QD pattern under the UV lamp excitation that shows a nearly pure red color emission peaked at around 620nm. And the spectra of the QD-ACEL device is shown in Figure 5-12.
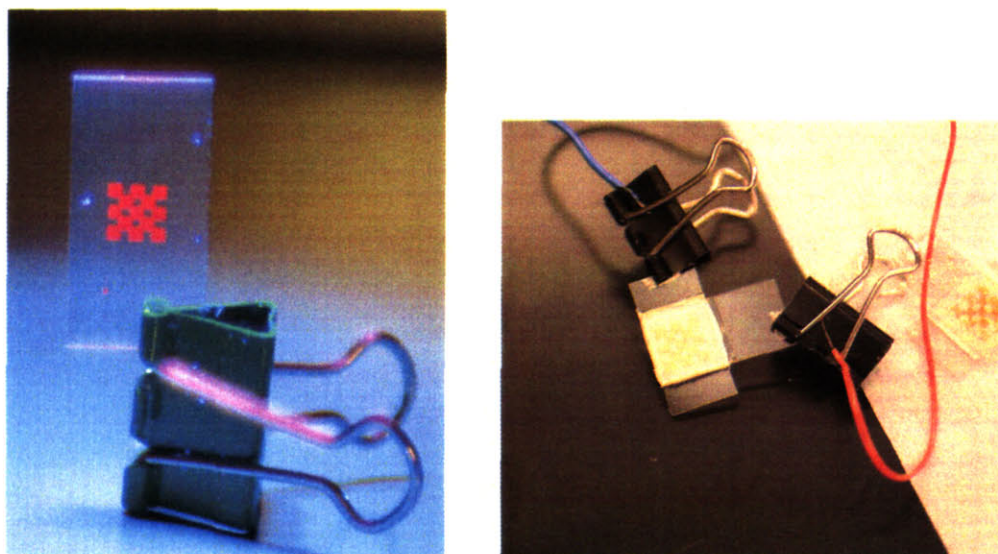
Figure 5-11. 1mg/mL CdSe QD in hexane: Octane (9:1) checkboard pattern printed on clean ITO glass by TIPS. Each square is 2mm by 2mm. Image is taken under a UV excitation.
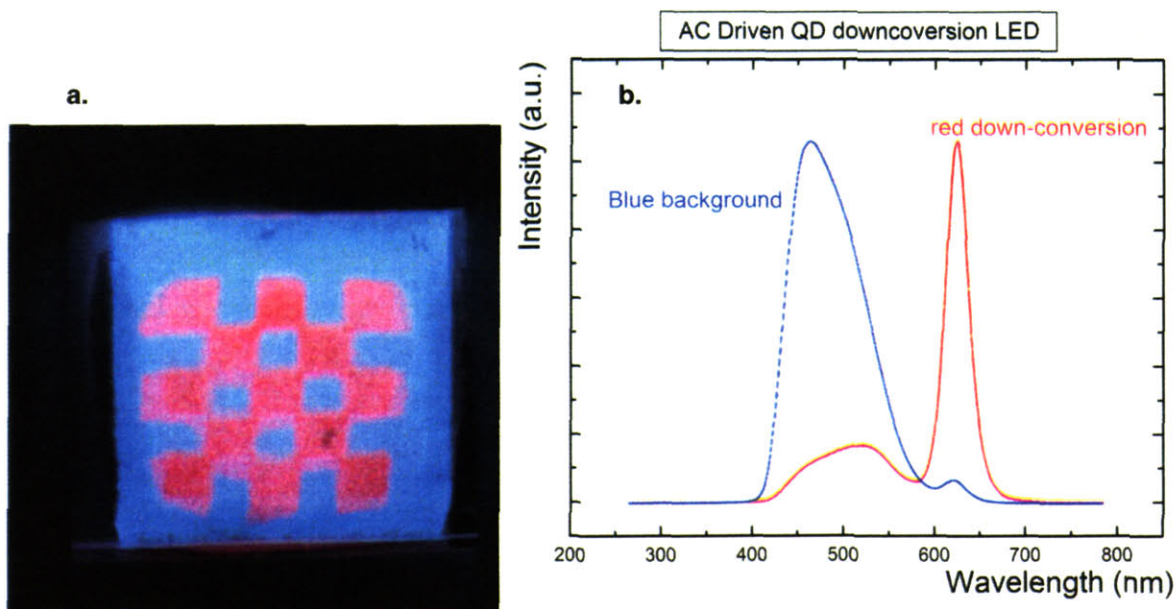
Figure 5-12. QD down conversion ACEL devices with a printed checkboard pattern. The blue background is emitting from the ZnS:Cu phosphors, brightness is 280 Cd/m^2; the red emission is from the wavelength down conversion QD layer, brightness is 200 Cd/m^2.

4. Inkjet printing metal nanocrystals

Background

Inkjet printing is one of the key successes behind the digital fabrication revolution, spanning an ever-increasing number of applications. Modern inkjet printing technology allows functional components of a variety of materials be accurately deposited with this additive approach. During recent years inkjet printer has turned into a viable industrial printing tool to replace traditional high-cost, subtractive photolithographic process and enable manufacturing of low cost electronics, possibly on flexible substrates. The aim of the section is to demonstrate the feasibility of printing metal lines using inkjet technology to achieve electrical and mechanical functionality. As part of the project, we have investigated two metal nanoparticles, silver and gold. The results are expected to show that Inkjet printing offers more versatility as it removes the need for etching to produce patterned features.

Advantages of Inkjet printing metal lines

In conventional processing methods, metal lines are deposited using vacuum thermal deposition and patterning by photolithography. While photolithography is suitable for patterning very fine feature size, creating a patterned layer is a time-consuming and costly multi-step process, requiring coating photoresist and etching the away of undesired materials with more than 90% of the evaporated materials being wasted. In contrast, the cost benefits of using inkjet printing nanoparticles ink are obvious: fewer processing steps are required; material utilization can be highly efficient; and large format inkjet printers are already well established to accommodate large size substrate, as revealed in **Figure 5-13 [37]**.

Today's photolithography wastes > 90% of material and takes 5+ pieces of equipment

OR

Replace with IJ or other hi-speed printing

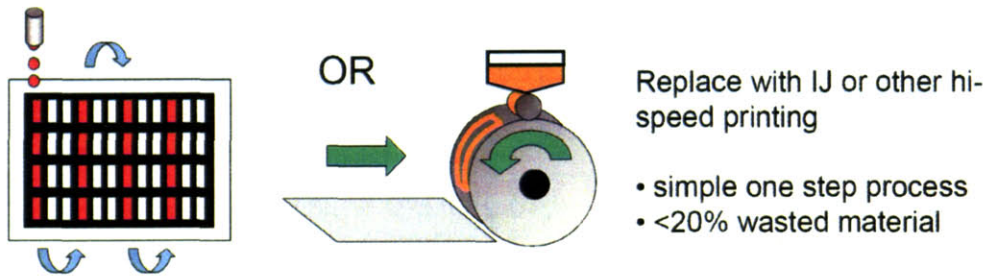• simple one step process
• <20% wasted material

Figure 5-13. Advantages of inkjet printing over photolithographic process

Printable silver ink

Liquid based silver conductor nanoparticles ink can be purchased from Cabot Printable Electronics and Displays (Cabot PED), a company that is specialized in producing metal conductor nanoparticles ink. Specifications and properties of the Cabot ink are summarized in **Table 5-2 [38].**

Table 5-2. Key properties of Cabot silver ink

Composition	Function	Properties
Silver nanoparticles	Solid contents20 wt%	30-50nm
Ethylene glycol	Ink vehicle	Viscosity: 14.4cP Density: 1.24 gcm^{-3} Surface tension: 31 dyn/cm
ethanol,1-propanol, ethylene glycol, 1,3-dihydroxy-2-propanone,glycerol, etc	Cosolvent, surfactant, buffer, viscosity modifier	
Proprietary polymer	Polymer shell	
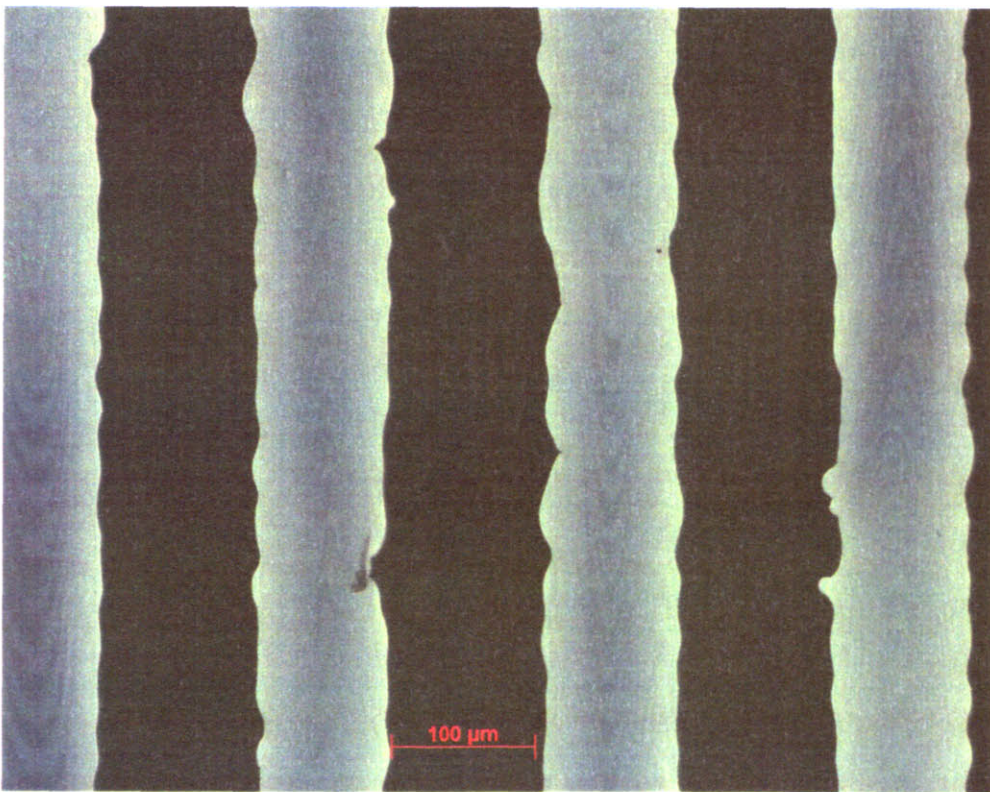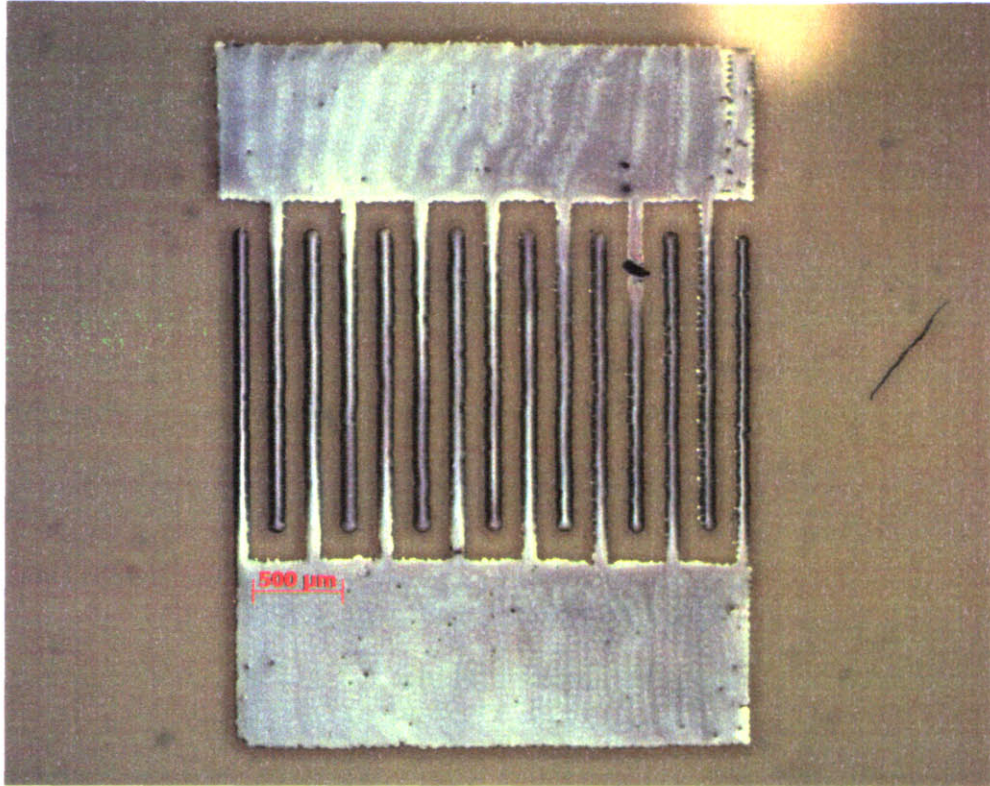
Figure 5-14. Inkjet printed silver nanoparticles on glass

Inkjet Printing Process for silver nanoparticles conductors

Technological details of the Inkjet printing process has been discussed in the previous sections, whilefor printing silver nanoparticles ink, additional factors may come into play. When inkjet depositions of nanoparticle silver are made, the particle packing and drying of the films is crucial to achieve high performance.

Experiment and discussion

Silver nanoparticle ink purchased from Cabot contains about 20% wt loading of solid contents. The ink solution is diluted with ethanol in 1:1volume ratio, giving the final ~10% wt loading solution (ink). The mixture is stirred for 1 hour before being transfer by pipette to the inkjet printhead. About 100 μL volume of ink is loaded each time. The printhead nozzle is 10 pL. Each pass will print 1 drop at 40 μm pitch size to form the 4 mm by 4 mm interdigital pattern. Only one pass is printed on a clean glass substrate kept at room temperature (25 °C). Each pass prints the contact pads only once and the finger twice (back and forth) at 1 kHz firing rate. The final printed pattern is shown in **Figure 5-14**. Note that this pattern is still wet until annealing in air at 100 °C for 30 minutes, a standard procedure to dry the film.

Since the ink composition has been optimized by Cabot to generate the best printing quality on hydrophilic substrates, it is not surprising to see a very well defined pattern as the final result. This is also in good agreement with the results printed using Piezo inkjet printer by researchers at Cabot and Dimatix [39].

However, real challenges occur when one attempts to print the same ink on hydrophobic surfaces. A practical difficulty associated with standard drying procedures is the dewetting of ink

and formation of cracks. In **Figure 5-15**, huge cracks are observed to exist in the printed pattern on spun coated, untreated poly vinyl acetate (PVAc) after drying at 100 ºC.
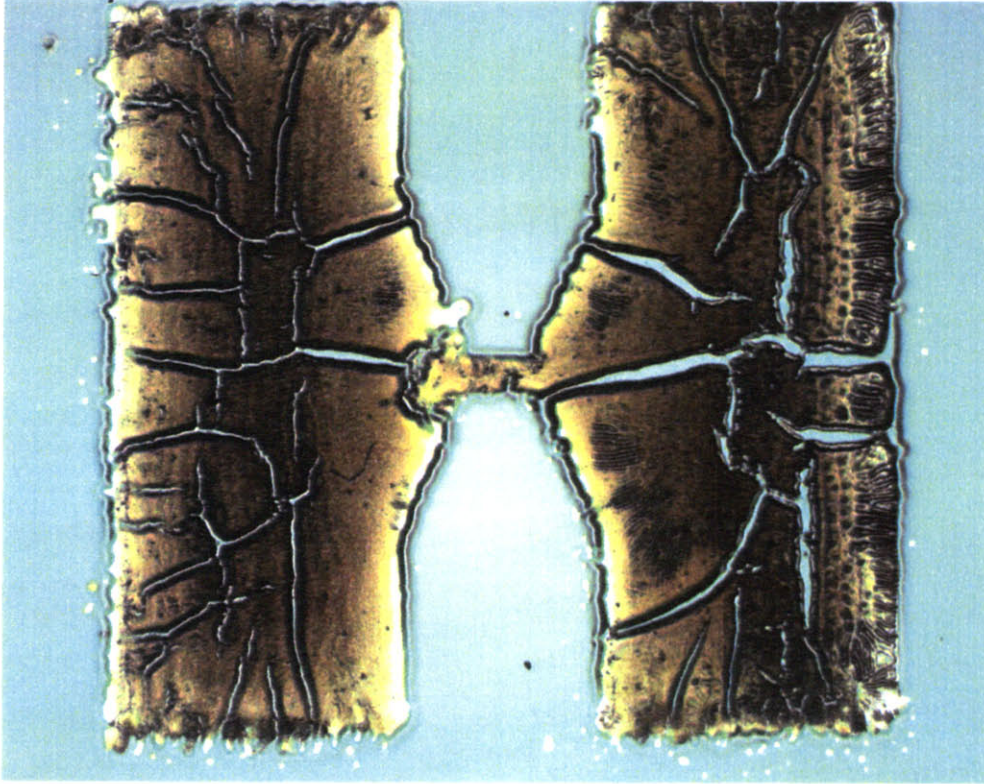
Figure 5-15. Cracks in printed silver pattern on hydrophobic PVA surface
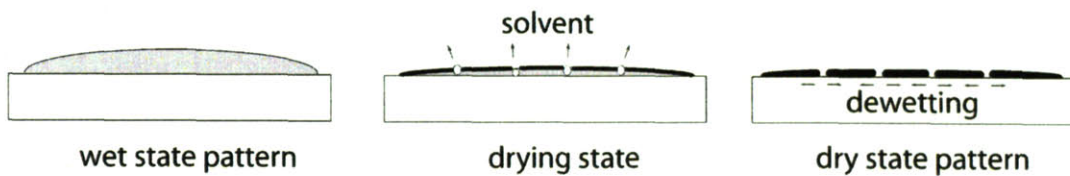
Figure 5-16. Cracks forming during thin film drying

The crack formation is probably due to the combination of two effects: uneven drying and dewetting of the ink. At the basic level, cracks are caused by stress buildup in the silver nanocrystal film that exceeds the film strength upon drying. Non-uniform drying can result from several underlying problems. Too rapid drying might be the first obvious reason. Films that

experiences more rapid (forced) drying can experience higher stresses and are more likely to crack; another cause of un-even drying is the non-uniform thickness of the film. During rapid heating, it is possible to trap vapor bubbles between the solidified hard shell and the base. In areas close to the edge solvent vapor can diffuse through a relatively thinner layer without leaving any cracks behind. While in the thicker regions, vapor bubbles can induce stress concentration at a weak point and initiate a crack; Sharp corner stress concentration effect is less likely a reason here as almost all the cracks form inside the pattern but not at the corners. **Figure 5- 16** depicts the process of crack forming. After the initial cracks formed, cracks will propagate as the silver thin films start to dewet from the hydrophobic substrate surface.
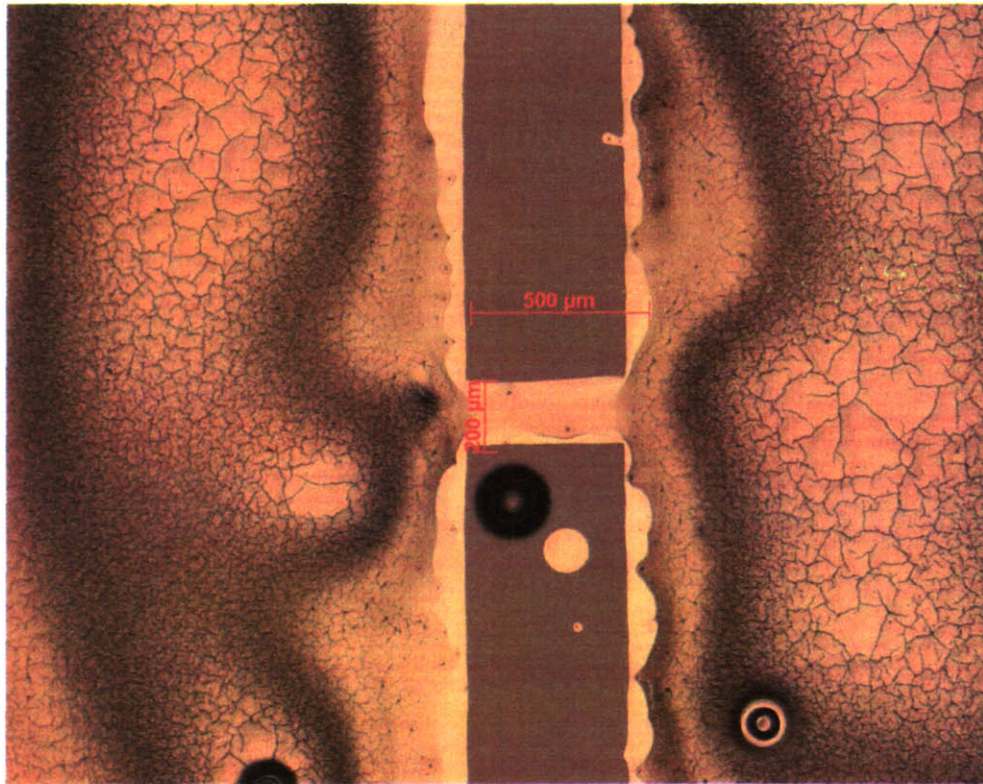

Figure 5-17. Cracks in printed silver pattern on oxygen plasma treated PVA surface

The solution to this problem must focus on one of two things, either to minimize stress build up or increase the strength of the Ag film. Chemical modifications of the ink formula are important and most suitably performed by Cabot researchers, while we explore some possibilities of modification of the substrate surface properties.

An oxygen plasma cleaner is used to treat the hydrophobic substrate. Polyvinyl acetate (in acetone: ethanol) solution is deposited on a glass substrate by spin coating, left for air dry at 80 °C, and then treated with oxygen plasma for 1 minute (3mTorr oxygen flow). Without this step the ink will not wet the substrate properly, and very severe cracks will appear after a regular drying procedure. Although the oxygen plasma treatment can increase the substrate wettability, smaller cracks still form during the drying stage. **Figure 5-17** shows smaller cracks form in the pattern on oxygen plasma treated PVA surface. This indicates that the drying conditions are not optimal. Therefore in-situ substrate heating is introduced by placing the substrate on a heating pad that can heat up to 200 °C at 20V. A heated substrate can force solvent evaporation and solidify the ink in shorter time, resulting in a crackles film as shown in **Figure 5-18**.

The process of oxygen plasma treatment as well as the in-situ substrate heating essentially provides a method of freezing the ink droplets on the surface, so that the patterned structure and the particle packing is preserved. On a hydrophobic PVAc substrate it is found that 1 minute oxygen plasma treatment (or so called surface activation) plus keeping the substrate at 60 °C during printing can achieve optimal deposition. In additional to the surface treatment, the ink-drying rate greatly affects the nanoparticle packing.
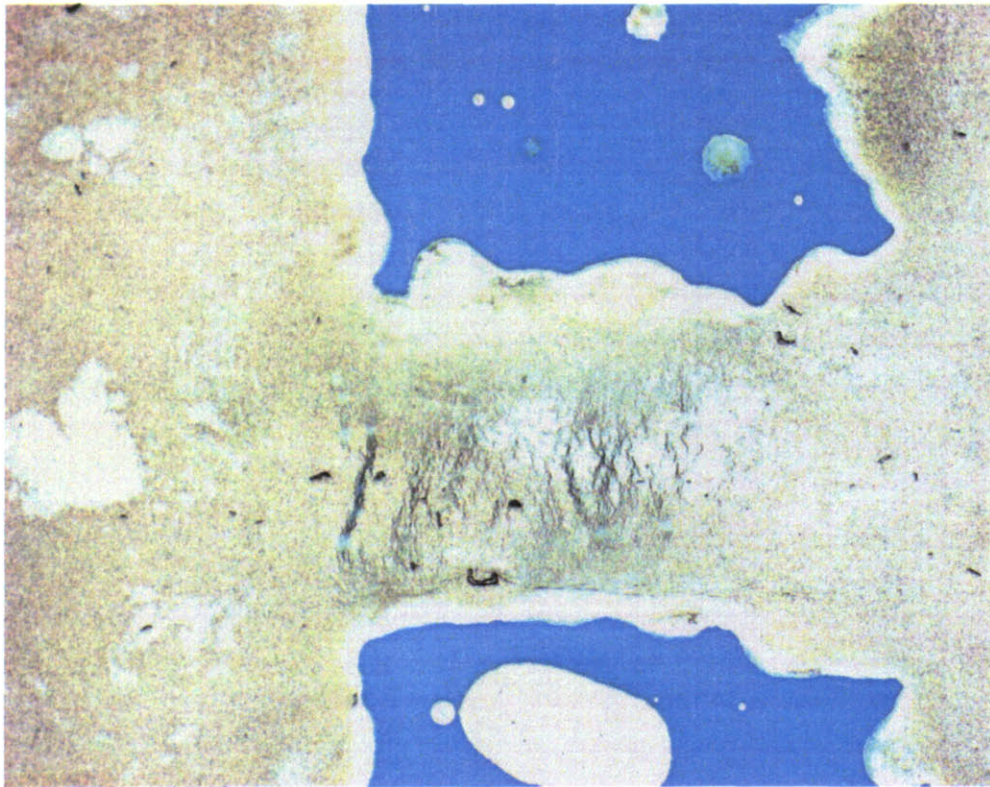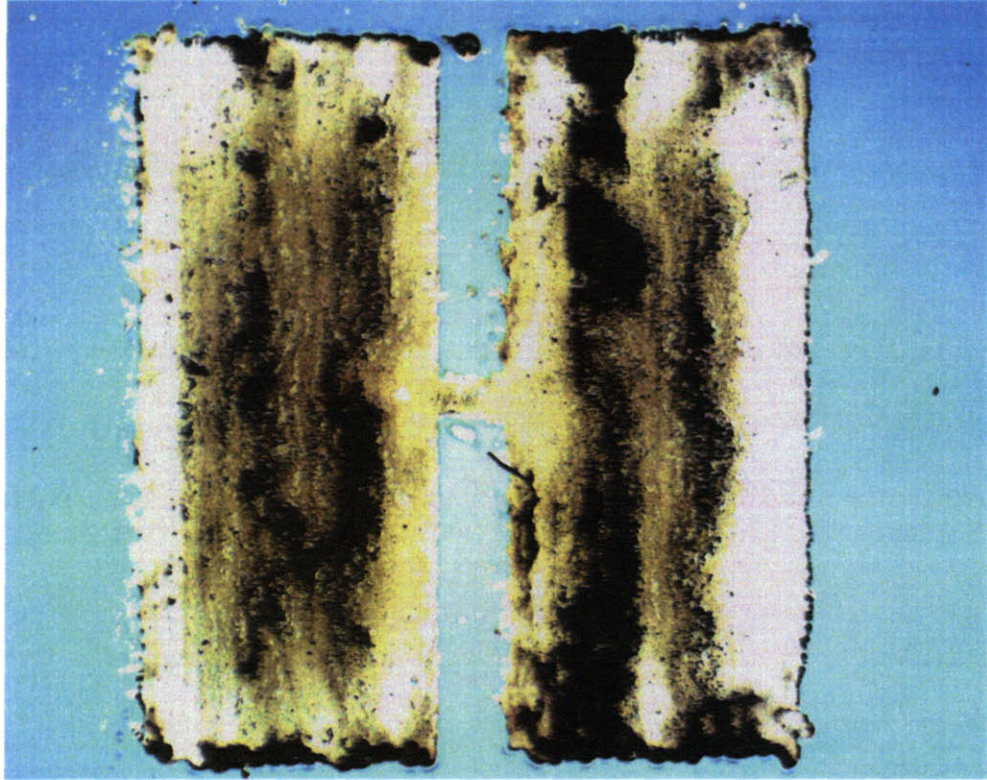
Figure 5-18. Silver pattern printed on oxygen plasma treated, in-situ heated substrate at 60 ºC

Inkjet Printing Process for gold nanoparticle dispersion

The second ink in our study is composed of gold nanoparticles dispersed in toluene at 1mg/mL concentration prepared by our colleagues at the Bawendi lab. This ink is very dilute compared with the Cabot silver ink. The ink vehicle toluene dries much faster, making it easier to quickly evaporate solvent without heating the substrate and results in less spreading of the ink. The final result of a double layer of printed Au nanoparticles on glass is shown in **Figure 5-19**. A printed line width of about 40 μm can be achieved by using 10 pL nozzle and 3 drops / burst print conditions. Preliminary results of printing dilute Au dots confirm the system compatibility with the TIPS printer. As gold nanoparticles are more stable in air, less likely to oxidize and have a higher work function than silver, we might find some interesting applications that require high performance conductive gold nanoparticles.
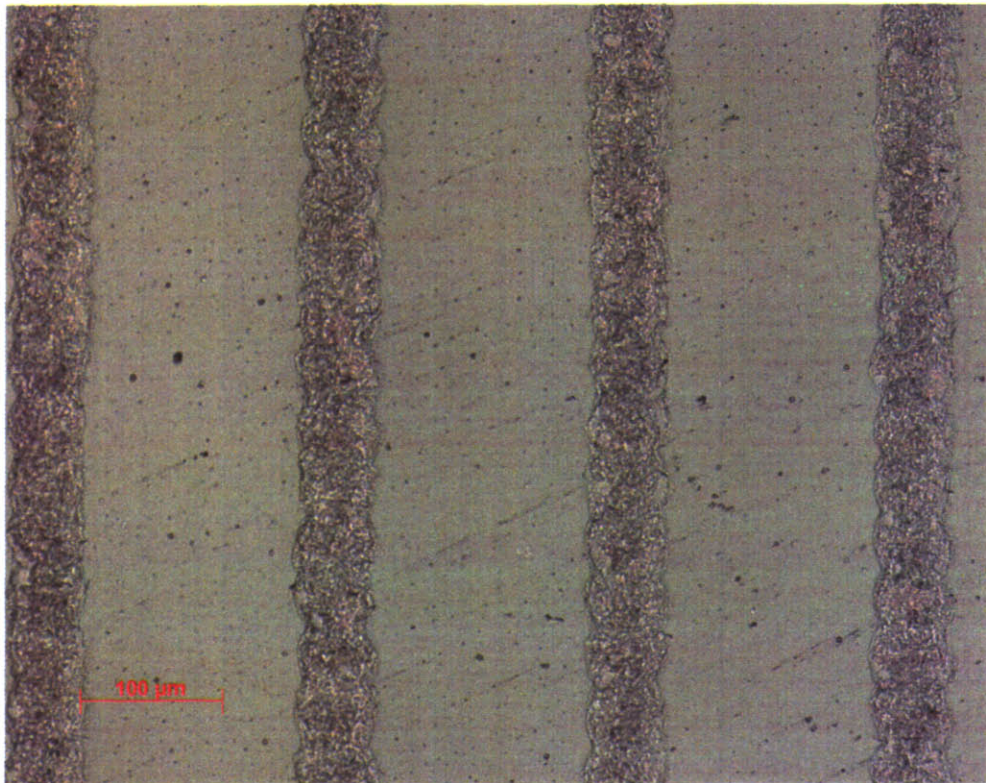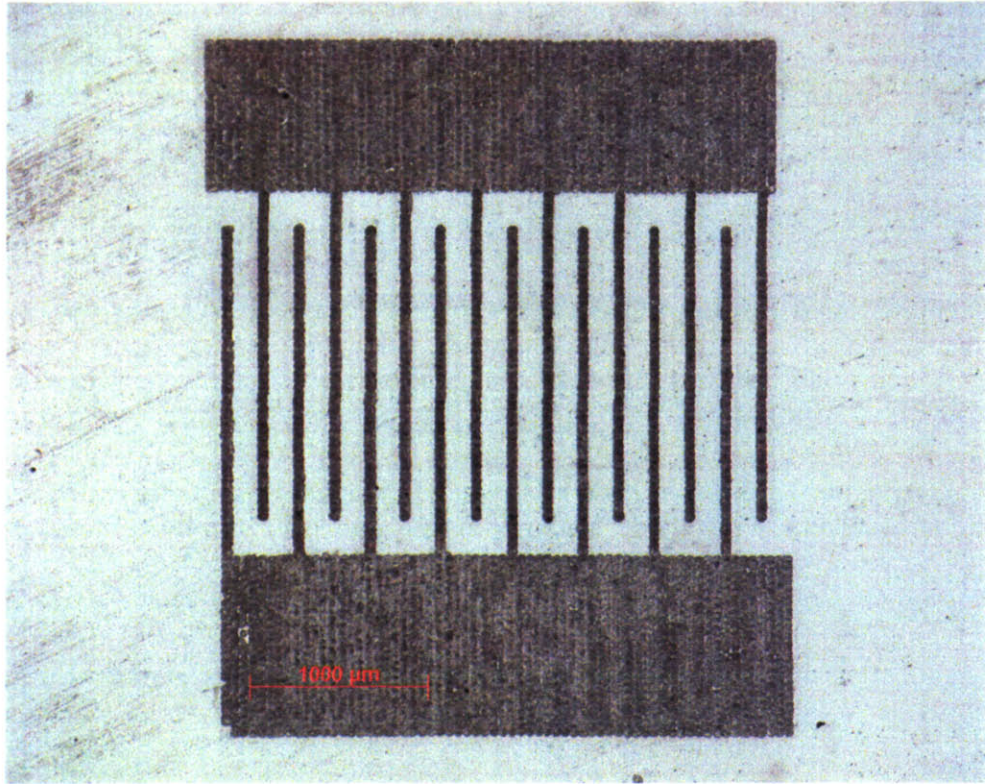
Figure 5-19. Printed Au nanoparticles prior to annealing

168

Reference

[1]. C. B. Murray et al., Synthesis and characterization of nearly monodisperse CdE (E = sulfur, selenium, tellurium) semiconductor nanocrystallites, J. Am. Chem. Soc., **115**, 8706 (1993).

[2]. S. Coe-Sullivan, J. S. Steckel, W. K. Woo, M. G. Bawendi, and V. Bulovic, Large-Area Ordered Quantum-Dot Monolayers via Phase Separation During Spin-Casting, Adv. Funct. Mater., **15**, 1117 (2005).

[3]. R. E. Bailey, A. M. Smith, and S. Nie, Quantum dots in biology and medicine, Physica E, 25, 1 (2004).

[4]. http://www.evidenttech.com/applications/quantum-dot-ink.php

[5]. P. E. Burrows, G. Gu, V. Bulovi'c, Z. Shen, S. R. Forrest, and M. E. Thompson, Achieving Full-Color Organic Light-Emitting Devices for Lightweight, Flat-Panel Displays, IEEE TRANS. ELEC. DEVS., 44, 8 (1997).

[6]. S. Coe, W. K. Woo, M. Bawendi, and V. Bulovic, Electroluminescence from single monolayers of nanocrystals in molecular organic devices. *Nature* **420**, 800 (2002).

[7]. http://lighting.sandia.gov/Xlightinginit.htm#snlngli

[8]. M. Achermann, M. A. Petruska, S. Kos, D. L. Smith, D. D. Koleske, and V. I. Ekimov, Energy-transfer pumping of semiconductor nanocrystals using an epitaxial quantum well, Nature, 429, 642 (2004).

[9]. http://www.evidenttech.com/business-units/led-displays.php

[10]. M. J. Bowers II, J. R. McBride and S. J. Rosenthal, White-Light Emission from Magic-Sized Cadmium Selenide Nanocrystals, *J. Am. Chem. Soc.*, **127**, 15378 (2005).

[11]. A. S. Davydov, Biology and Quantum Mechanics, Pergamon, Oxford 1982.

[12]. U.Woggon, *Optical Properties of Semiconductor Quantum Dots*, Springer, Berlin 1996.

[13]. W. Zisman, Contact angle wettability and adhesion, American Chemical Society, Washington, D.C., 1964.

[14]. P.G. de Gennes, Wetting: statics and dynamics, Rev. Mod. Phys., 57, 827 (1985).

[15] P. G. de Gennes, F. B. Wyart, and D. Quere, Capillarity and Wetting Phenomena, Springer, New York 2004.

[16] A. Oron, S. H. Davis, and S. G. Bankoff, Long-scale evolution of thin liquid films, Rev. Mod. Phys., 69, 931 (1997).

[17]. Tadashi Kajiya, et al, "Piling-to-buckling transition in the drying process of polymer solution drop on substrate having a large contact angle", Phys. Rev., E 73, 011601 (2006).

[18]. R.D. Deegan, et al, Contact line deposits in an evaporating drop, Phys. Rev. E, 62, 756 (2000).

[19]. C. Bourges-Monnier and M.E.R. Shanahan, Influence of Evaporation on Contact Angle, Langmuir, 11, 2820 (1995).

[20]. M.E.R. Shanahan, Simple Theory of" Stick-Slip" Wetting Hysteresis, Langmuir, 11, 1041 (1995).

[21]. G Reiter, Dewetting of thin polymer films, Phy. Rev. Lett., 68, 75 (1992).

[22]. C. Redon, F. Brochard-Wyart and F. Rondelez, Dynamics of Dewetting, Phy. Rev. Lett., 66, 715 (1991).

[23]. http://www.e-lite.com/index.htm

[24]. http://www.planarembedded.com/el_advantage/

[25]. K. Hirabayashi, H. Kozawaguchi, and B. Tsujiyama, Color Electroluminescent Devices Prepared by Metal Organic Chemical Vapor Deposition, Jpn. J. Appl. Phys., 26, 1472 (1987).

[26]. U.S. patent 4954747.

[27]. R.T. Tuenge and J. Kane, Bright Red EL Using a Thin-Film Filter, Digest of SID

International Symposium, p. 279, 1991.

[28]. T. Yosioka, Y. Sano, K. Nakamura, C. Tani, Characteristics of Red Electroluminescence

Devices Using $CaS1-xSex:Eu$ Phosphor Layers, Digest of SID International Symposium, p.

313, 1989.

[29]. http://www.nhn.ou.edu/~bumm/NanoLab/ppt/ACTFEL.ppt

[30]. J. Heikenfeld and A. J. Steckl, Electroluminescent Devices Using a High-Temperature

Stable GaN-Based Phosphor and Thick-Film Dielectric Layer, IEEE TRANS. ELEC. DEV.,

49, 4 (2002).

[31]. Y. A. Ono, Process in Information Display Technology, World Scientific, Singapore (1995).

[32]. A.G. Fischer, Electroluminescent Lines in ZnS Powder Particles, J. Electrochem. Soc., 110,

773 (1963).

[33]. W. Busse, H. E. Gumlich, B. Meissner and D. Theis, J. Lumin., **12/13**, 693 (1976).

[34]. W. Busse, H.-E. Gumlich, W. Knaak and J. Schulze, J. Phys. Soc. Jpn. Suppl. A, 49, 581

(1980).

[35]. J. Lee, V. C. Sundar, J. R. Heine, M. G. Bawendi, and K. F. Jensen, Full Color Emission

from II-VI Semiconductor Quantum Dot-Polymer Composites, Adv. Mater., 12, 15 (2000).

[36]. L. Pang, Y. Shen, K. Tetz and Y. Fainman, PMMA quantum dots composites fabricated via

use of pre-polymerization, OPTICS EXPRESS, 13, 1 (2005).

[37]. K. Vanheusden, Inks for flexible electronics manufacturing: comparing printable

electronics to conventional processes, presentation at the 5th annual conference on flexible

displays and microelectronics, Phoenix, AZ. 2006.

[38]. Cabot ink application notes

171

[39]. Http://www.dimatix.com/markets/electronics.asp

CHAPTER 6. Inkjet assisted stamping quantum dot OLED

CONTENTS

1. Concept and motivation

2. System design

3. Results and discussion

4. Summary

1. Concept and motivation

The organic light emitting device (OLED), incorporated with nanoscale functional materials (e.g. inorganic semiconductor nanocrystals or quantum dots, QDs) as efficient, emission wavelength tunable lumophores, is an interesting study subject, as it creates a new set of test platforms to investigate properties of the functional materials at the quantum mechanical level. Possible structures of QD-OLEDs are summarized in **Figure 6-1** and **Table 6-1** [1].
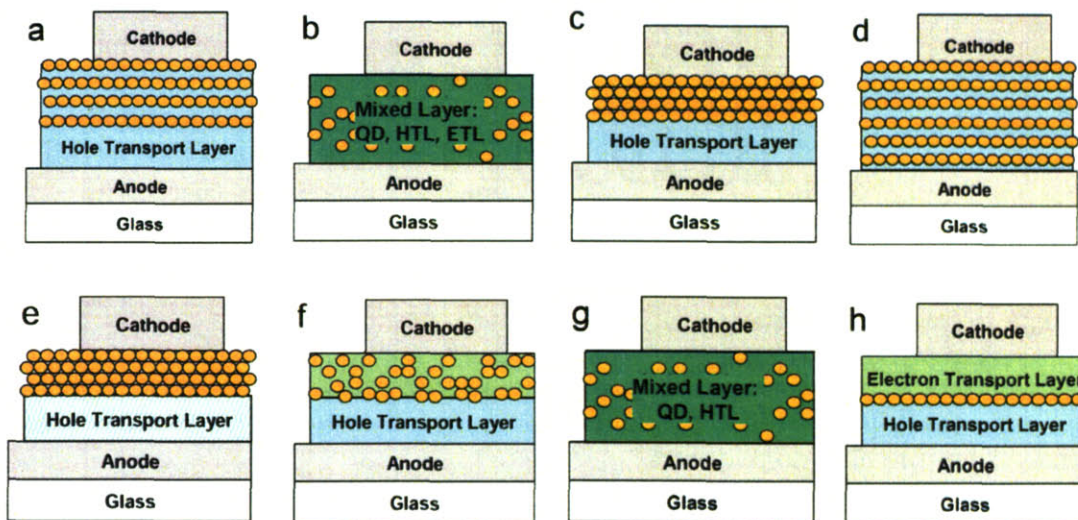
Figure 6-1. Structures of QD-OLED presented in literatures

An efficient QD-OLED structure includes at least an electroluminescent (EL) layer sandwiched between two thin organic charge transport layers and two electrodes, each layer serves different functions. The EL layer ideally contains monolayered quantum dots, or in some

173

Table 6-1. List of QD-OLED presented in literatures

	Structure & Fabrication	Characteristics	η_{EQE} %
a	100nm PPV spun-cast and polymerized at 250°C as HTL; 5 monolayers of 3-5nm colloidal CdSe QDs (w/ hexane dithiol in toluene) as ETL by layer-by-layer approach	Poor electron transport from QD to QD; Impurities cause charge trapping or operate as a quenching site for QD excitons.	<0.01*
b	Span coating mixed CdSe QDs (5-10% by volume), PVK, t-Bu-PBD) as efficient transporters of holes and electrons thin film	QDs interfere with both electron and hole conduction, resulting in charged QDs which are likely to be less efficient emitters due to the Auger process	~0.0005
c	Thermal polymerized PPV thin film as hole transport layer on top which span coat a core-shell QD multilayer	Significant improvement in qefficiency, however the device response time was long, attributed to the presence of trap states within the QD multilayer film.	0.22
d	Layer-by-layer growth of alternating bilayers of CdSe QDs and polymers such as PPV, poly (allylamine) and poly(styrenesulfonic acid)	Fabrication in the presence of water possibly lowed the device performance	NA
e	Layer-by-layer deposited PPV as hole transport layer and cured, QDs of CdSe or (CdSe)ZnS then spun-cast on top of the converted PPV multilayers	In overcoated (CdSe)ZnS QDs, an increase in PL and a decrease in EL quantum efficiency relative to core only CdSe QDs was observed, attributed to a decrease in charge injection into the QDs due to the increased tunnel barrier thickness.	0.1~0.2
f	Similar to e, but neat QD film replaced with a QD/block co-polymer composite film, also deposited by spin coating	Similar to e	0.01~0.05
g	Blended films of QDs and polymers (MEH-PPV) or (F6BT)) were spin-cast between electrodes	(InAs)ZnSe QDs used to generate efficient EL in the near infrared	0.5
h	Phase separation or micro contact printing monolayer of II-VI group QDs in a molecular organic structure	Performance (fast response time and higher ηEL) of these devices matches that of fluorescent OLEDs.	0.5~2

area multiple layered, or dispersed dots. Methods to process QDs solution and incorporate single layer QDs into OLED heterostructures have been described. [2-4].

However both the phase-separation and micron contact printing processes rely upon dispensing nanocrystal solutions with a low material use efficiency method, i.e. spin casting, the amount of wasted QDs accounts for over 99% of the starting solution. High quality colloidal QDs are costly to synthesize, therefore using an alternative dispensing and patterning techniques will be a feasible application to improve the QD usage efficiency.

The method of inkjet assisted stamp (micro-contact) patterning combines the advantages of both dry and wet processes. This method involves three steps: (1). A certain volume of QD ink solution, which is in an amount of picoliter to hundreds of picoliters, is first delivered, for example, by an Inkjet printer, onto the surface of a stamp, the amount of solute can be precisely controlled by the concentration of ink, drop volume and the inkjetting energy. The solvent is then allowed to evaporate from the stamp surface so that only solute (inorganic QDs) is left. The stamp surface can be plain or pre-patterned with fine feature size on the order of micrometers. (2). In the next step, the stamp is placed on top of an adjacent substrate to an intimate contact and the printed patterns are facing the substratePressure is applied between the stamp and the substrate; the solute (QD layer) is then transferred completely or partially from the stamp onto the substrate to form a layer. Compared with the direct inkjet printing, this stamping method can deposit QDs without excess solvent. (3). The stamp is then released from the substrate. The stamp surface might or might not require a following cleaning procedure to restore its clean condition and be reused in step (1) repeatedly. The concept is illustrated in **Figure 6-2**.
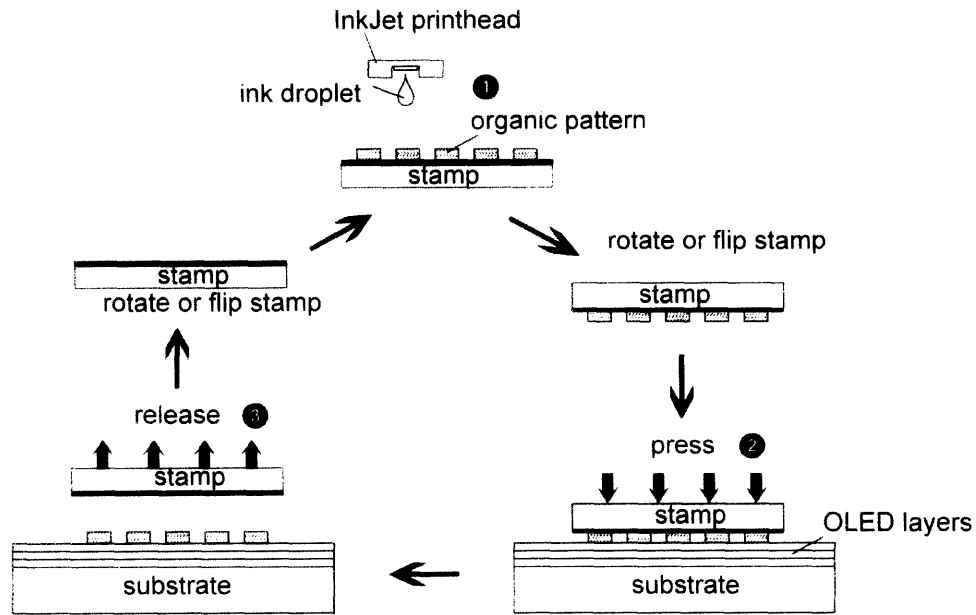
Figure 6-2. Illustration of the 3-step Inkjet assisted stamping process
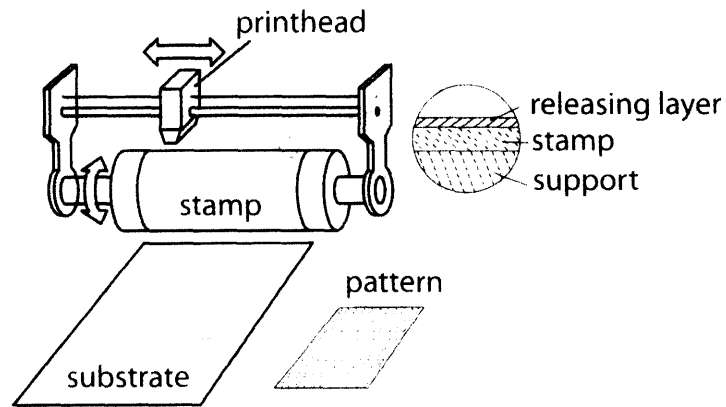
2. System design

Figure 6-3. Illustration of stamp press apparatus

The stamp press includes an Inkjet printer, a stamp (or roller) and a substrate moving machinery, as shown in **Figure 6-3**.

Stamp materials and surface treatment

Many elastic materials that have low elastic modulus may be used as the stamp, in particular such as polyurethanes, polymides [5] polydimethyl-siloxane (PDMS), block polymers, or hydrogels, with a topographically plain or patterned surface. PDMS is most often chosen for its low surface energy, which translates to easy releasing behavior and chemical inertness to inking solvents. The low surface energy of PDMS is a direct result of methyl groups as the surface terminal groups in which the intermolecular forces are almost as weak as possible, only aliphatic fluorocarbon groups (e.g. Teflon) are lower. The soft siloxane backbone also allows the methyl group to rearrange. The consequence is that not many solvents will have enough affinity to PDMS surface, which could be a problem for picking up ink fluids [6].

PDMS Kit is purchased from Dow Corning (commercial name Sylgard 184). The kit containsliquid silicon rubber base, vinyl-terminated PDMS, and the curing agent (a mixture of platinum complex, copolymers of methylhydrosiloxane and dimethylsiloxane). The base and the curing agent are mixed together as the precursor, then the mixture is poured on top of a polished silicon wafer, degassed and cured at ~60 °C overnight to form a cross-linked, blank elastomer stamp.

An optimal stamp surface condition should balance both successful wetting and releasing processes. High surface free energy gives a poor partial releasing transfer of QD films, while ink fluid won't wet well if the surface free energy is too low.

The theoretical description of surface wettability is attained from thermodynamic equilibrium between the substrate surface (S), liquid droplet (L) and the ambient (G) known as the Young-Dupré equation:

$$\gamma_{SG} - \gamma_{SL} - \gamma_{LG}\cos\theta = 0 \qquad\qquad (6\text{-}1)$$
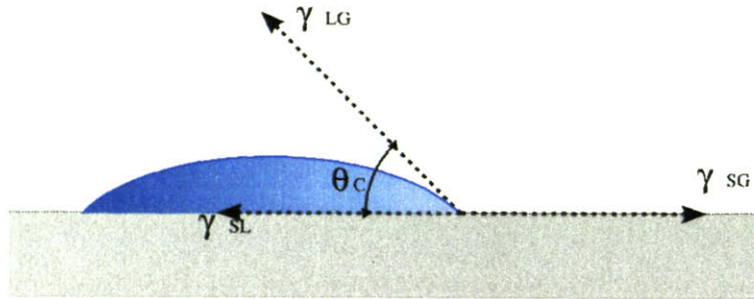
Figure 6-4. A contact angle of a liquid sample

where θ is the experimental contact angle (**Figure 6-4**). Thus the contact angle can be used to determine an interfacial energy. If the contact angle is anywhere from 0°to 90°, the liquid is said to wet the substrate, and not to wet the substrate if the contact angle is between 90° and 180°. If we assume the ambient condition remains the same, there are only two ways left to improve the surface wettability. The first is to change the substrate surface properties, either by substitution of another material (coating another material with higher surface energy) or surface treatment by oxygen plasma or UV ozone to break off surface bonds and increase the density of dangling bonds to improve adhesion. However, surface treatment in oxygen plasma or UV ozone has been observed to change the PDMS surface to a brittle, silica-like layer and increase surface roughness/crack density after the treatment. The second way is to find another solvent with lower surface tension that can spread better on the same surface. This is constraint by the limited number of solvents that are miscible with organic semiconductors or QDs. A better way is therefore to apply an adhesion-promoting surface coating layer.

Parylene denotes a family of poly-para-xylene polymers that can be deposited by vapor deposition, resulting in a conformal, dense and soft coating. In parylene C (the most common form of parylene), a chlorine atom is substituted for one of the hydrogen atoms on the benzene

ring of each phenyl group and therefore it is a slightly more polar variant than PDMS, which possibly leads to an increasing solid-liquid attraction and thus better wetting. 2000 Å of parylene C is the standard coating layer with respect to bare PDMS stamps.
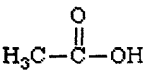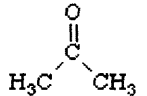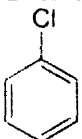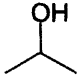
Ink composition

As both dye based and pigment based inks can be directly inkjet printed, molecular organics and quantum dots can be incorporated into the ink design and dispensed using an inkjet printer. The inkjet print quality can be largely affected by the ink composition, and the interaction between the ink and the substrate surface. The primary pattern formation processes are wetting of ink on the substrate, drying of ink vehicle and bonding between the inking substances. By modifying the composition of ink, it is possible to improve the thickness uniformity. The goal is to determine if by just changing the ink, the printing results can be optimized. And the main challenge is to find a substitute solvent to replace chloroform as it is not compatible with the printer system at all – the printhead will be severely attacked by chloroform and fail within a short period of time (less than one hour).

To be able to print molecular organics, it is necessary that the organic molecules are dispensed in solution form, by using an organic solvent which provides a solubility of the organic compounds to a certain extent, and the solvent should be compatible with the liquid delivery system, for example, an inkjet printer. However, choice of organic solvents, which satisfy the above requirements, is limited. For example, aluminum tris-8-hydroxyquinolinate (Alq3) as a molecular organic may be used as the light-emitting material in an organic light-emitting device (OLED). Chloroform as an organic solvent in which Alq3 is soluble is known. However, pure chloroform has high volatility and low viscosity, and is potentially corrosive to

inkjet printhead. As a hydrochlorocarbon, chloroform also has high ozone depletion potential. Consequently, it is desired to develop a solvent system to minimize the use of chloroform as the delivery vehicle of Alq3 or to replace chloroform with a more benign organic solvent while still maintain excellent solubility to Alq3 and compatibility to the printhead. It was found that these criteria were met with a solvent composition, which can be a mixture of a hydrochlorocarbon and partially fluorinated alcohol containing two to six carbon atoms. For example, a fluorinated alcohol (2,2,3,3 – tetrafluoropropanol, or TFP) can serve as a good substitute for chloroform [7].

Table 6-2. Properties of various common solvents at room temperature

Solvent	Structure	Surface Tension (dynes/cm)	Boiling point (°C)	Dipole moment
Acetic Acid	$H_3C-\overset{O}{\overset{\|}{C}}-OH$	28	118	1.74
Acetone	$H_3C-\overset{O}{\overset{\|}{C}}-CH_3$	24	56	2.91
Benzene	(benzene ring)	29	80	0
Chloroform	CH₃-Cl	27	61	1.08
Chlorobenzene	(Cl on benzene ring)	33	132	1.54
Ethyl alcohol	C₂H₅-OH	24	78	1.69
Ether	O	17	35	1.15
Hexane	(hexane chain)	18	69	0
Iso-propanol	(isopropanol OH)	22	82	1.68
Toluene	(toluene ring)	29	111	0.36
Water	H-OH	73	100	1.85

180

QDs depending on the overcoating ligands can be readily dispersed in chloroform, hexane, toluene, alcohol or even DI water. Hexane and ethyl alcohol are selected to substitute for chloroform for their similar surface properties with chloroform, as listed in **Table 6-2** [8,9]. Hexane QD ink is mixed 9:1 volume ratio with octane as co-solvent, which has a higher boiling point for better pattern forming characteristics.

3. Experimental results and discussion

Print OLED Materials

Dynamic contact angle measurement (DCAM): the contact angle is useful in determining the relative surface energy of the print substrate. It is useful in assessing the wetting interactions between the ink and the substrate. Briefly described, a liquid drop of a certain volume is introduced and touched down onto the substrate. A video camera system captures the time-dependent behavior of the contact liquid on the substrates. In practice, for static contact angle measurements, data is recorded 5 seconds after drop touchdown. For dynamic contact angles measured in this analysis, data was captured from time zero to 200 sec (and up to 1200 sec when possible). The angle formed at contact between the fluid drop and the substrate is measured directly; the drop volume is calculated from the height/contour of the drop and its diameter at the interface, and is recorded in μL (microliter). The greater the contact angle, the higher the hydrophobicity of the underlying surface. A variation of 10% for contact angle measurements is acceptable. Since these runs are performed on the same specimen but at different sites, the observed variation is mostly due to differences between the target sites on the substrate. Another source of variation is that, in some cases, it is not easy to accurately determine the baseline since the exact contact points are not well defined.

181
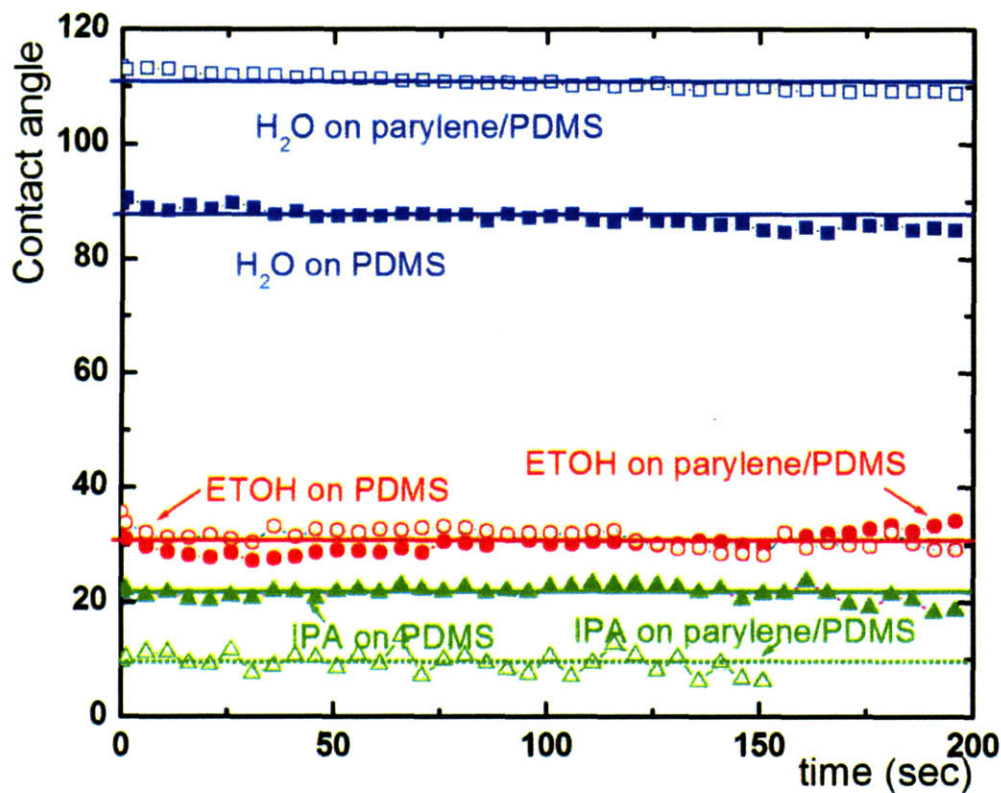
Figure 6-5. Result of DCAM on PDMS and parylene coated PDMS

Although it is also considered a hydrophobic, low surface energy material, the stamp surface becomes less hydrophobic after applying a 2000Å thick parylene C coating, as confirmed in **Figure 6-5**, where contact angle between water and stamp drops from 110° on PDMS to 90° on parylene; meanwhile wetting of polar solvents is improved between parylene and iso-propanol (IPA). Note that visually there is no any sign of changes on the PDMS stamps after the conformal parylene coating.
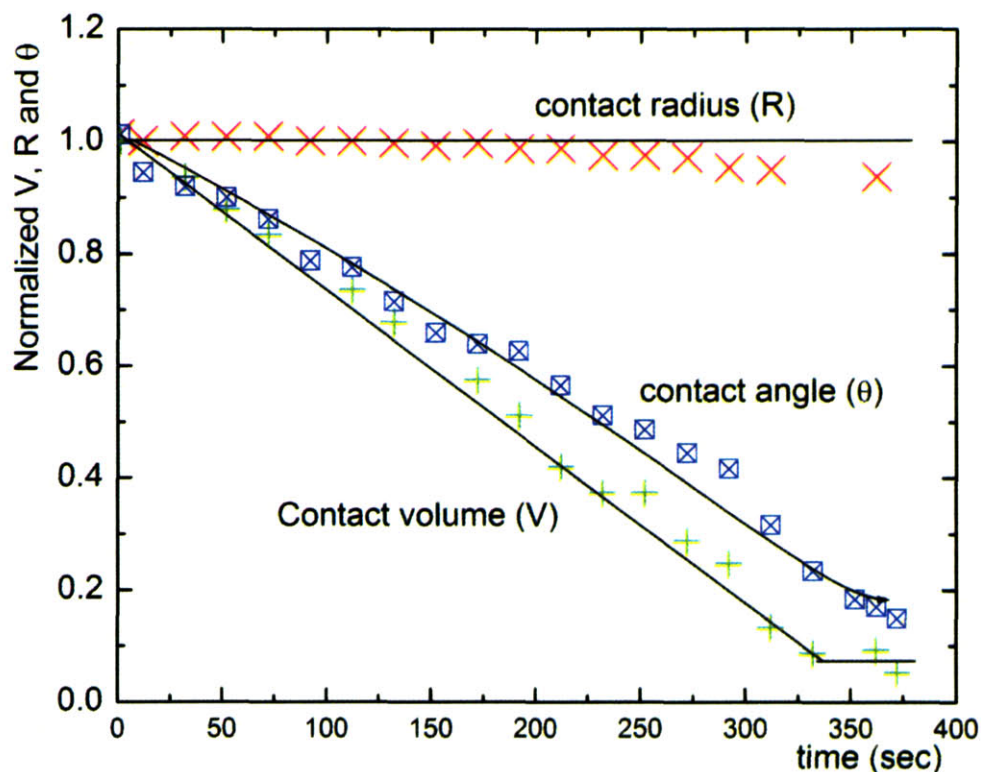
Figure 6-6. Dynamic contact angle measurement of alq3 ink on parylene coated PDMS surface

It is preferable to obtain a uniform organic pattern deposited rather than the ring shape pattern (as discussed in the previous chapter). Substrates with large contact angle with the droplet are prone to form such flat and uniform deposit. In the experiment, the ink solution is Alq3 dissolved in TFP (0.1M). The substrate is a PDMS stamp with no pattern, coated with 2000 Å parylene. The dynamic contact angle measurement shows that both the contact angle and the droplet volume decrease while the contact area (base) remains almost unchanged, which indicates that the droplet contact lines (solid, liquid and gas interface) is pinned once the droplet touches down onto the substrate. **Figure 6-6** shows the time dependency of the TFP droplet volume V, radius R and the contact angle θ. All the numbers are normalized against the initial (t=0) values. The droplet radius remains constant, which is also known as the contact line

pinning, probably the same as the usual pinning of fluid droplets on the substrate caused by the irregularities or defects of the substrates. [10,11]. While the contact area remains constant, the contact angle and droplet volume keep decreasing, until they reach the receding angle and volume and stay unchanged. Although this plot only shows the behavior of the pure solvent, we will proceed as the ink solution has the same behavior.

The final shape of the ink deposit doesn't show any sign of the "coffee stain" effect, as illustrated in **Figure 6-7**, attributable to the concentration of the ink and its viscosity. The deposit becomes almost flat as can be seen in the uniform PL emission in the microscope images.
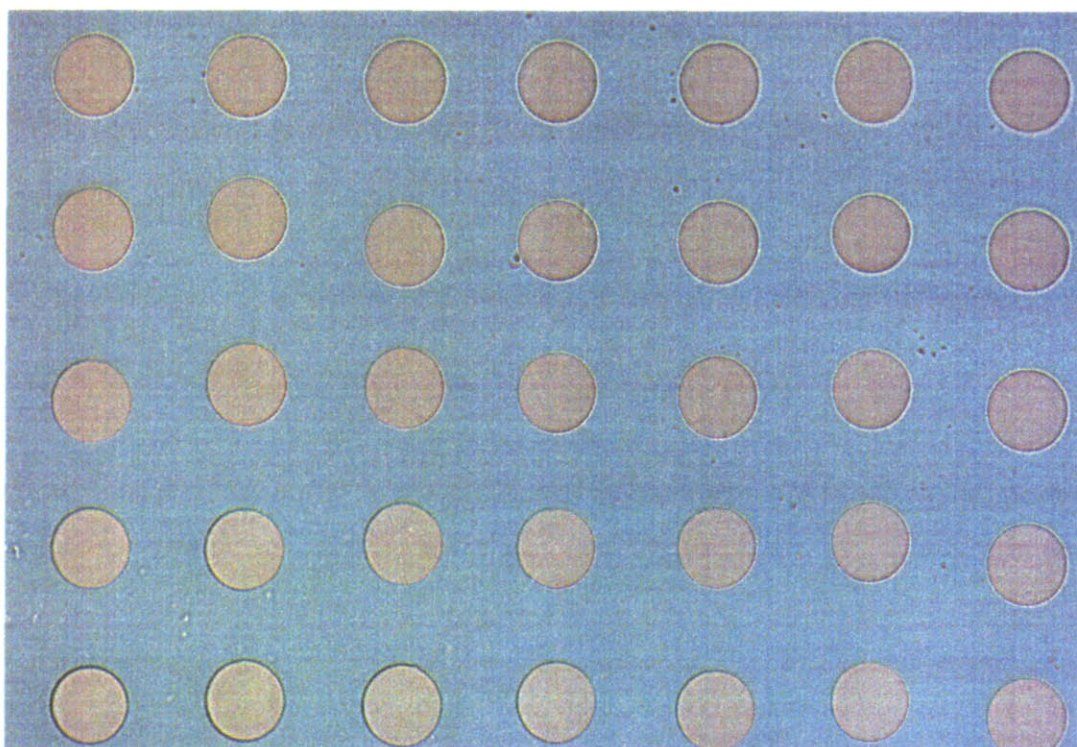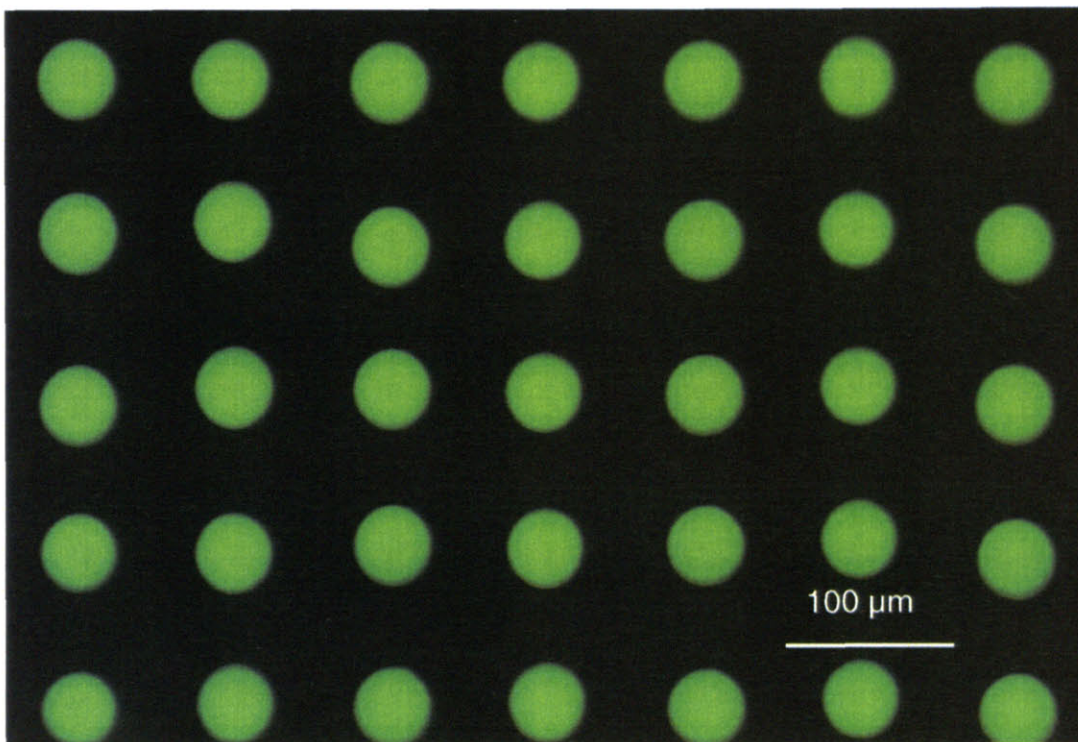
Figure 6-7. Microscope graphics of alq3 ink printed on parylene coated PDMS stamps

Printing alcohol-based QD inks

One of the major goals of inkjet assisted stamping technique is to develop a capability to print QD solutions on blanket PDMS stamp. Successful stamping transfer relies on ink chemistry (solvent type, concentration, etc) and stamp surface treatment. Results of some initial attempts are summarized here.

Table 6-3. Experimental conditions of alcohol based QD inks

Sample	Stamp	Solution (volume)	Concentration (%)*
1	PDMS	EtOH	0.14
2	PDMS	EtOH	0.014
3	Parylene coated PDMS	EtOH	0.14
4	PDMS	EtOH:TFP (1:1)	0.01
5	Parylene coated PDMS	EtOH:TFP (1:1)	0.01
6	Parylene coated PDMS	EtOH:MeOH (1:1)	0.14

* 100% is defined as the initial concentration (~100 mg/mL) of QD solution before dilution
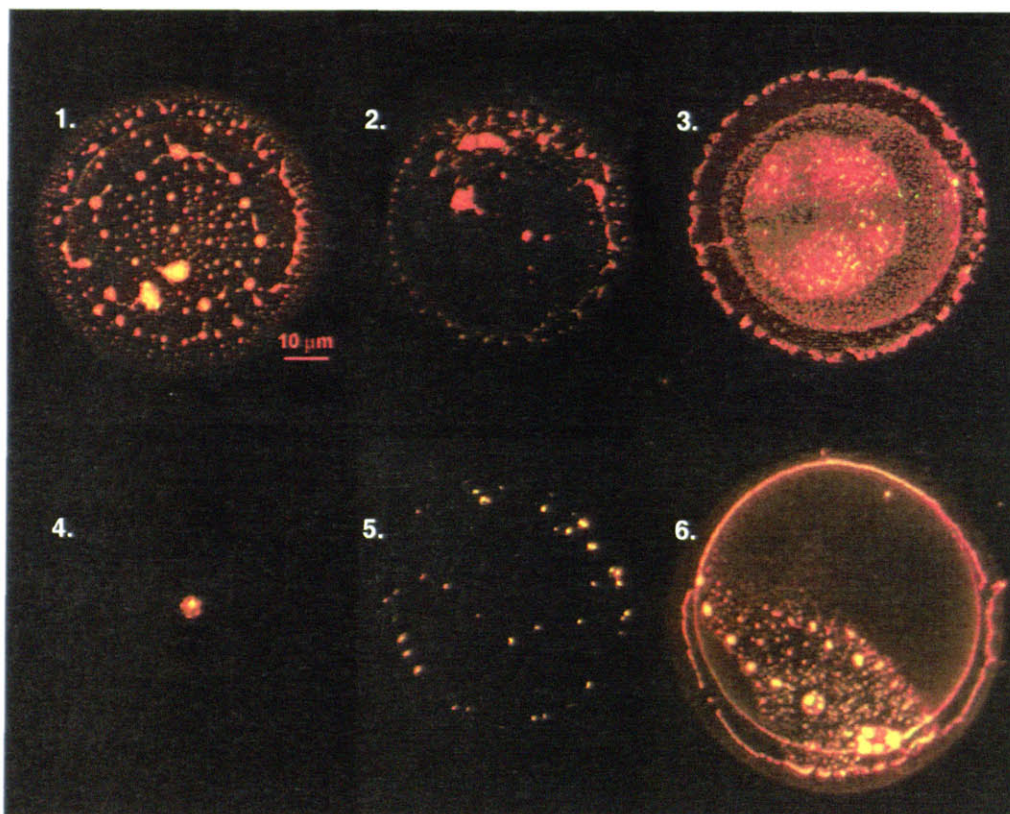
Figure 6-8. Alcohol based QD ink printed patterns

Printing QD inks on PDMS is very different than on a porous medium such as paper. Given that PDMS surface is dense, non-polar and low surface energy, better wettability is expected with also non-polar (or low dipole moment) solvents. Previous contact angle measurement data show a poor wettability by alcohol solvents, as confirmed again in **Table 6-3** and **Figure 6-8.** All the alcohol based QD solutions show a certain degree of dewetting after printing. An extreme case is when TFP is mixed into the QD solution (sample 4), all the QDs dewet from the stamp surface and concentrate to the center of the print or aggregate locally (sample 5), resulting in a discontinuous pattern. Choice of solvent apparently plays a key role in the formation of the final pattern.

186

Printing hexane-based QD inks

A good wettability condition results in a larger diameter QD pattern by making hexane as the ink vehicle. The importance of wettability in the production of uniform QD patterns has been recognized and shown in **Figure 6-9.** The key factor relies again on the choice of solvent that is compatible with the substrate surface characteristics. The secondary factor is the ink concentration and drop size. It is clear from the printing results that for monolayer pattern formation a non-polar solvent, i.e. haxene is a better choice; and low ink concentration as well as small drop volume are preferred. As the drop volume increases, more solvent is delivered and the solvent evaporation time rises, allowing the formation of non-uniform coffee ring patterns (sample d in **Table 6-4**).
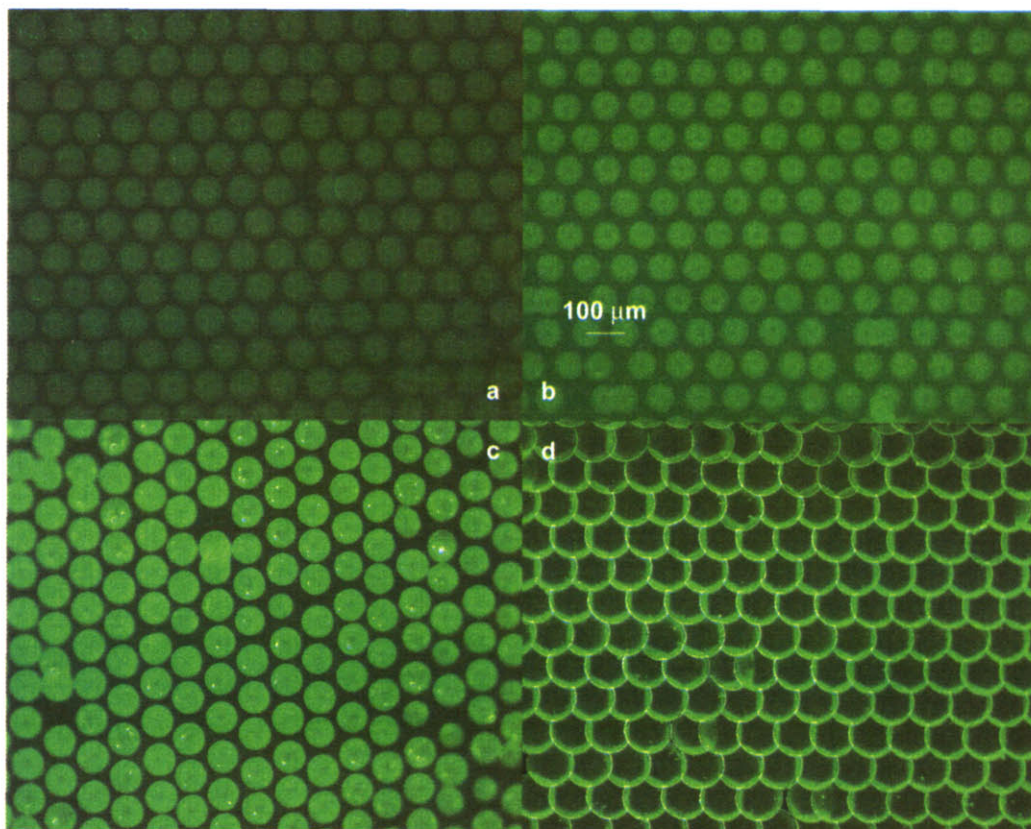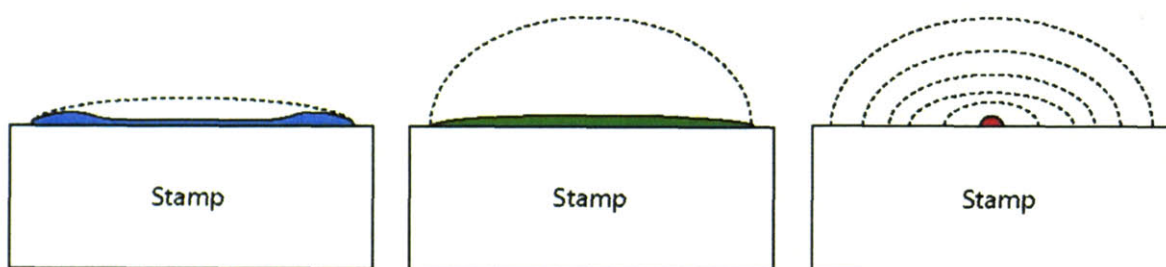

Figure 6-9. Printed patterns of Hexane based QD inks

Table 6-4. Experimental conditions of hexane:octane based QD inks on Parylene coated PDMS

Sample	Concentration (mg/mL)	Drop volume (pL)	Drop
a	1	1	1
b	1	5	1
c	5	5	1
d	5	10	1

Discussion

Figure 6-10. Ink drop volume reduction and pattern formation (a) coffee ring pattern; (b). more uniform pattern; (c). pattern totally dewetted from the stamp

Drying of an ink drop is non-trivial. In fact it is a very complicated process that has been studied extensively. As shown in **Figure 6-10**, three types of drying phenomena can be observed during our printing experiments. The coffee ring effect is most commonly seen in very dilute ink (QD in hexane) where the capillary outflow of solutes tends to enrich the QDs at the contact lines; Nearly flat pattern can form when the ink viscosity is high enough that the diffusive outward flow of solutes becomes largely suppressed (Alq3 in TFP ink); If the contact line is unpinned, as solvent evaporates, solutes will enrich to the center of the droplets and much smaller printed pattern will form (QDs in Ethanol + TFP).

Contact line pinning in dilute inks

PDMS stamps with or without parylene coating layer exhibits hysteretic effects in contact with ethanol or hexane. The first layer of the drop in direct contact with the stamp remain pinned by a surface friction force. Two ink edge advancing motions are competing with each other:

outward capillary flow of solutes to the pinned contact line and inflow retraction of ink due to surface tension (if the ink viscosity is low enough). Outflow of solute results in the "coffee ring pattern", while inflow of the ink will lead to the formation of "concentric pattern", where the ink solute is forced to "glide" on this pinned layer and enriches the rest of solute to the center (sample 3).

Formation of either the "coffee ring pattern" or the "concentric pattern" is a kinetic process that will terminate upon the drying of solvent. Therefore we can relate the pattern formation to the solvent evaporation rate and the ink "glide friction" (related to the viscosity and QD concentration). In an ideal scenario, small volume of very dilute, fast drying ink solution should produce uniform thickness profile. However, choice of fast drying (volatile) solvents is limited, as the solvent also needs to be fully compatible with the inkjet printer. Forced evaporation of solvent for example on a heated substrate can be helpful but might not be realistic in all cases, especially when the substrate is a poor thermal conductor (such as thick PDMS stamp).

Printing mixed OLED-QD materials

An interesting and prospective application of inkjet printer might be to pattern both OLED materials and QDs simultaneously. **Figure 6-11** shows an array of mixed TPD and Red CdSe QDs patterns printed undergoing photo bleaching.

189
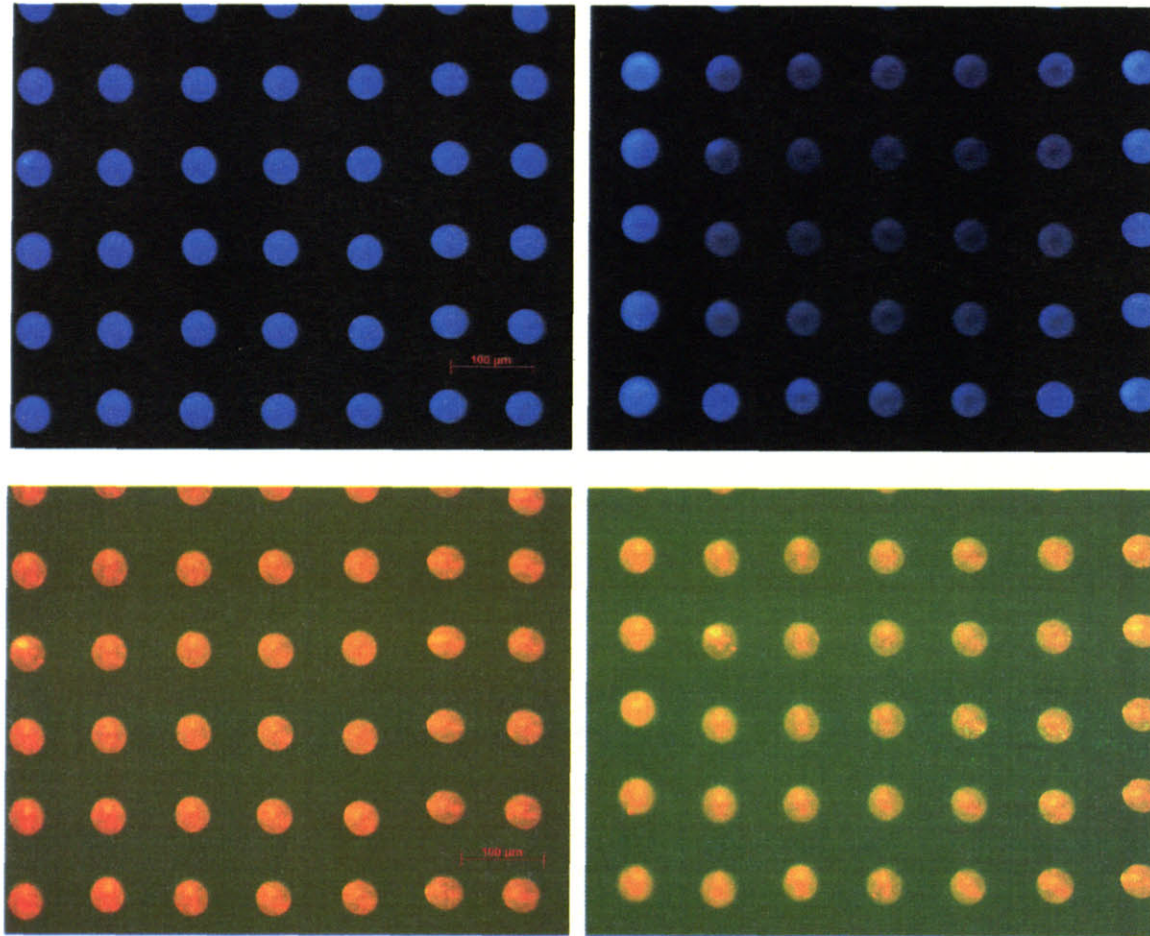
Figure 6-11. TPD + CdSe QD array under UV excitation

Inkjet print stamp transfer QD-LED

Given the experimental observations described above, directly printing a uniform monolayer of QDs on PDMS stamps still remains a challenge, with some technical hurdles to be overcome. Non-polar solvent hexane used as the ink vehicle shows better wettability on the stamp surface than alcohol based solvents. Although coffee-ring patterns is very non-uniform in terms of pattern thickness, the flat well can mimic a spin-coated film stretched by surface tension. Furthermore, since the rim of the pattern is much thicker than the flat bottom, when the QD pattern is incorporated into the OLED structure, charge recombination will preferentially take place at the thinner QD region and light will emit from the flat bottom region.
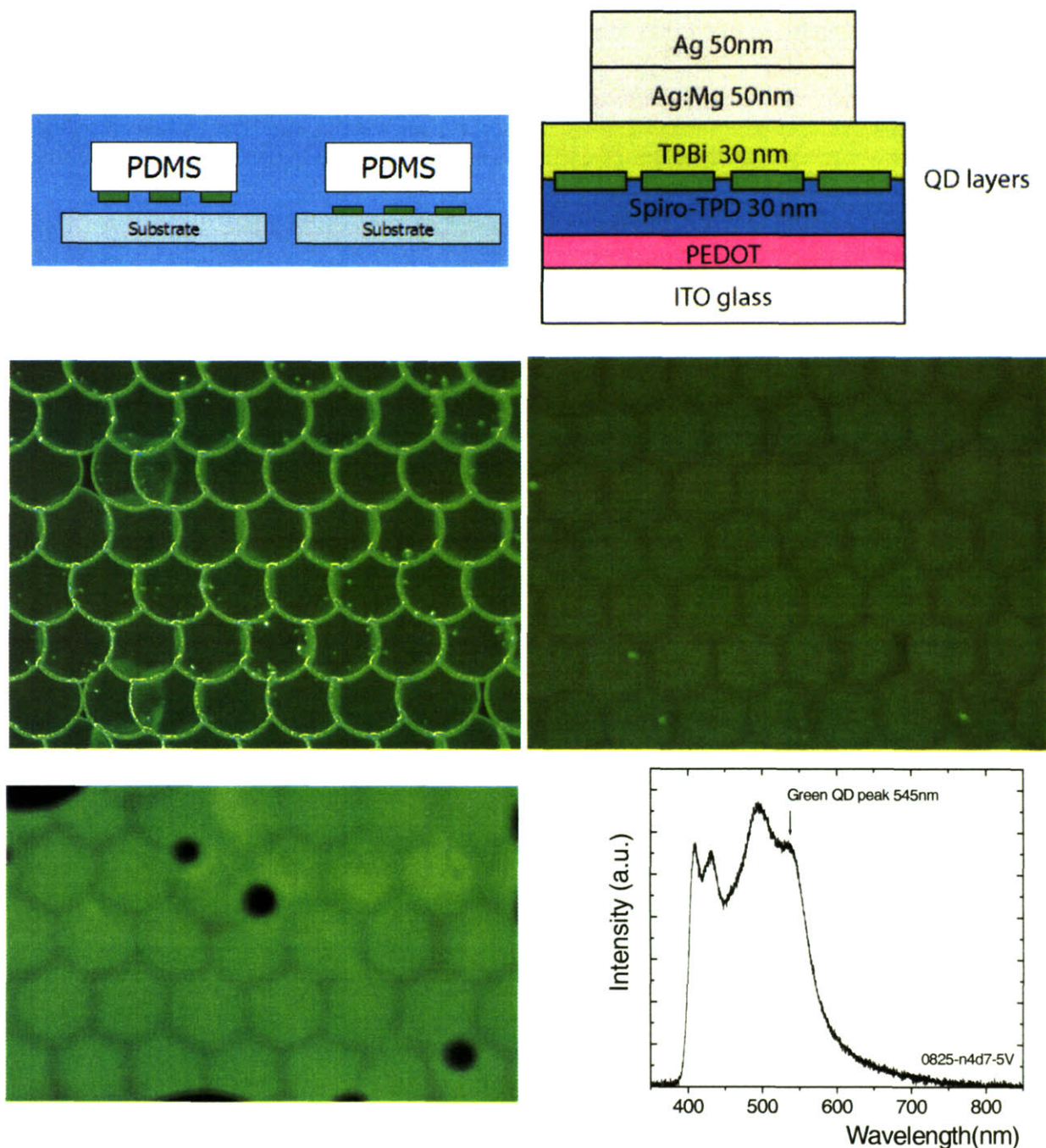
Figure 6-12. Inkjet assisted stamping transfer QD layer procedure and results. (a). Stamping QD layers by PDMS stamp. (b) QD-LED device structure. (c). PL microscope image of QD:hexane ink inkjet printed on PDMS stamp surface, pitch size = 100 μm. (d). Stamp transfer QD layer onto OLED half device (Spiro-TPD). (e). EL image of region of an active QD-LED by stamping. (d) EL spectrum of QD-LED showing QD peak at 545 nm and some organic emission background.

Figure 6-12 summarizes the procedure and results of a QD-LED fabricated by inkjet assisted stamping transfer method. The ink composition is identical to the sample in **Figure 6-9d**. The EL microscope image and the spectrum confine light emission from the stamp transferred QD layers. Some black spots are due to possible local surface defects (unclean surface regions) within the device. As the very first attempt, the results are quite promising that the concept of making QD-LED works by using inkjet to directly pattern QD inks then using stamp to transfer QD patterns.
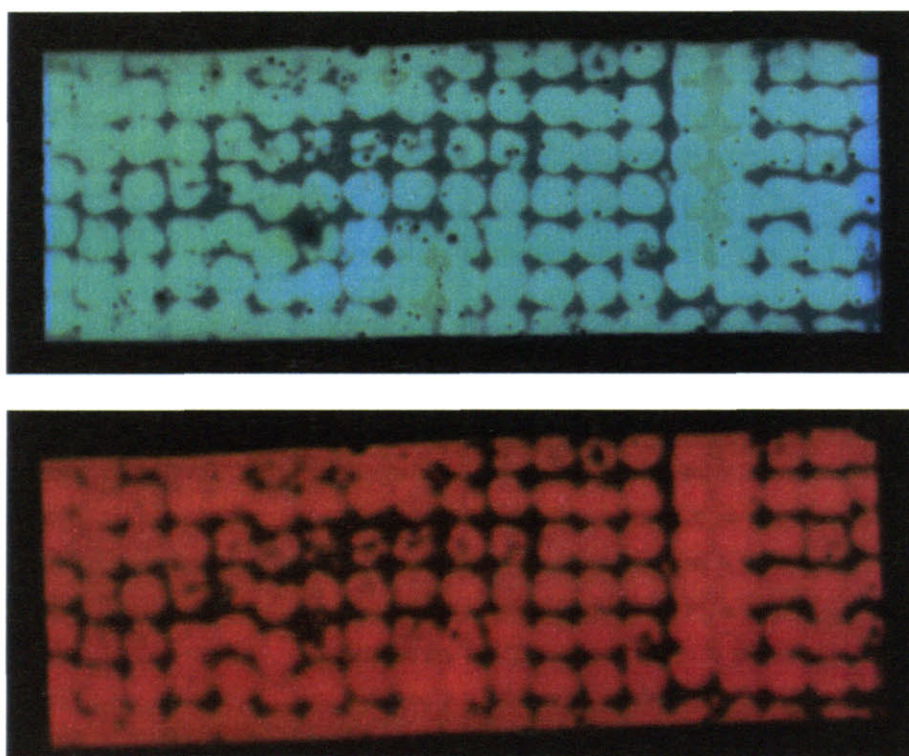
Figure 6-13. Inkjet assisted stamping red QD:EtOH (0.1%) ink, pitch size is 100 µm on parylene coated PDMS stamp. (a). QD-LED EL emission; (b). Image taken behind a yellow filter so that only red emission from QD layer is visible.

QD:EtOH ink is also successfully transferred into the same OLED structure by a parylene coated PDMS stamp, as shown in **Figure 6-13**. Although microscopically this ink doesn't wet the stamp surface as well as the hexane ink (please see **Figure 6-8**), the QD patterns still manage to transfer successfully. This could be related to the week binding nature between the QD ligands

that are surrounding the dots. The attraction between the dots (with ligands) and the organic film on the substrate exceeds the binding force between dots, leaving a layer (or perhaps more than a monolayer) attached to the organic film.

4. Summary

This work has demonstrated the capability of inkjet to pattern quantum dots and OLED patterns on micro-printing stamps. It has been shown that material use efficiency increases dramatically from less than 1% by spin coating to almost 100% by Inkjet. In this section, effects of both the stamp surface properties and the ink compositions are studies to improve uniform thickness profile across the printed patterns. Results from dynamic contact angle measurements have confirmed that 2000 Å parylene coating can promote the wettability of PDMS surface. The resolution of at least 50 um has been achieved.

Much more work however is still required to study the solvent drying that makes this method well controllable and consistent. There are still many important parameters yet need to be optimized, such as stamp making condition, applied pressures, ink concentration and choice of ink vehicle. The next step is to methodically measure and correlate those variables to the printed and transferred films, and to better understand the mechanisms involved. However, the preliminary results have been promising to observe the robustness of this process, despite the lack of detailed understanding of the relations between those parameters.

It will perhaps become a useful tool in fabricating the quantum dot or OLED patterns by providing good control over how and where they are deposited, without the process being time-consuming and costly. How solute interaction with the substrate will be an interesting exploration to follow. It will be more mature when more attempts are made on improving the control environment.

Reference

[1]. Seth Coe, PhD thesis, MIT 2005.

[2]. Seth Coe, Wing-Keung Woo, Moungi Bawendi‡ and Vladimir Bulovic, Electro-luminescence from single monolayers of nanocrystals in molecular organic devices, Nature, 420, 19/26 (2002).

[3]. Seth Coe-Sullivan, Wing-Keung Woo, Jonathan S. Steckel, Moungi Bawendi, Vladimir Bulovic, Tuning the performance of hybrid organic/inorganic quantum dot light-emitting devices, Organic Electronics, 4, 123 (2003).

[4]. Seth Coe-Sullivan, Jonathan S. Steckel, Wing-Keung Woo, Moungi Bawendi, Vladimir Bulovic, Large area quantum dot monolayers via phase separation during spin casting, Adv. Funct. Mater., 15, 1117 (2005).

[5]. Y. N. Xia and G. M. Whitesides. Soft lithography. ANGEWANDTECHEMIE INTERNATIONAL EDITION,, 37,551 (1998).

[6]. Y. N. Xia and George M. Whitesides. Soft lithography. Annual Review of Materials Science, 28, 153 (1998).

[7]. U.S. patent 7,037,380 Hayashi, et al. May 2, 2006.

[8]. http://www.usm.maine.edu/~newton/Chy251_253/Lectures/Solvents/Solvents.html

[9]. http://macro.lsu.edu/howto/solvents/Dipole%20Moment.htm

[10]. P.G. de Gennes, F. B. Wyart and D. Quere, Capillarity and wetting Phenomena, Springer, New York 2004.

[11]. A. Oron, S. H. Davis and S. G. Bankoff, Rev. Mod. Phys., 69. 931 (1997).

Appendix A. Growth of colloidal quantum dots

The most common method of chemically synthesizing II-VI quantum dots is achieved by using solution-phase colloidal synthesis; the general preparation scheme is based on reaction between chemical compounds containing metal ions (Cd^{2+}) and chalcogenide ions (S^{2-}, Se^{2-}). The synthesis typically proceeds in two steps: (1). super-saturation for nuclei formation and (2). subsequent grow. These are two competing processes. However, as long as the rate at which material adds to the nuclei is higher than the addition rate of new material into the solution, the solution will not exceed the critical saturation limit and the dots can continue to grow. It is essential to obtain uniform size and shape of quantum dots to study their optical and material properties, Bawendi and coworkers introduced a simple route for preparing such II-VI quantum dots (with <5% standard deviation in size) [1].

Seed formation and growth

The solvent is 50 g of trioctylphosphine oxide (TOPO), degassed by heating to 300 °C at 1atm of argon. The precursor is a mixture of two reacting solutions. Solution A is 1 mL of dimethylcadmium (Me_2Cd) in 25 mL of trioctylphosphine (TOP); and solution B is 10 mL of 1M trioctylphosphine selenide TOPSe in 15 mL TOP. The mixed solution is quickly injected into the reaction flask to form a yellow orange color, forming nucleation of initial quantum dot "seeds". Upon nucleation the solution concentration drops below the critical concentration for further nucleation. And this rapid injection also results in the solution a sudden decrease of temperature to hinder further growth of the nuclei. Heating of the solution is restored to gradually bring the temperature from 180 °C to 230-260 °C while the absorption spectra are constantly monitored from which the changes in the size distribution are estimated and the growth temperature is adjusted to accommodate the growth rate. When the desired absorption characteristics are

observed, the growth solution is transferred, cooled down and stored. This way a series of sizes can be produced and isolated from a single preparation of growth solution. The size distribution of the quantum dots is primarily controlled by the short time interval between the seed formation and growth.

Isolation and purification

The next step is to isolate and purify quantum dot crystals. Once the reaction solution is removed from the reactor, it is cooled down to slightly above TOPO's melting point. With additional methanol added into the solution to flocculate the nanocrystals, the mixture then goes through centrifugation to separate out the flocculate which will be redissolved in 1-butanol and will go through further centrifugation one more time to separate out clear solution that contains nanocrystals. The solution is further rinsed with methanol to remove excess TOPO and TOP and then is dried up in vacuum to produce nanocrystals powder. The resulting powder can be dispersed in a variety of alkanes, aromatics, long-chain alcohols, chlorinated solvents, and organic bases (amines, pyridines, furans, phosphines).

Size selective precipitation

To improve the dot size uniformity, the purified samples are dispersed in 1-butanol forming a clear solution, followed by adding methanol dropwise so that larger crystals will precipitate out. Separation of the larger crystals by centrifugation can sharpen the absorption spectrum of the produced solution. The process is repeated several times until no further sharpening in the absorption spectrum is observed. Different solvent pairs can be used in the size-selective precipitation, such as Chloroform/methanol.

Overcoating ZnS shell

CdSe bare dots dispersed in hexane is transferred into a mixture of 5 g TOPO and 0.5 mL TOP heated at 60 °C; Diethylzinc ($ZnEt_2$) and hexamethyldisilathiane ($(TMS)_2S$) are used as the

Zn and S precursors. Equal molar amounts of the precursors dissolved in TOP are added dropwise to the vigorously stirring reaction mixture over a period of 5-10 minutes. After the shell overcoating is complete, the mixture solution is cooled and later recovered in powder form by precipitating with methanol and redispersed into a variety of solvents including hexane, chloroform, toluene, THF, and pyridine [2].

Cap Exchange.

To be able to incorporate quantum dot crystal into different organic matrix, the crystal surface needs to be modified by repeated exposure to an excess of a competing capping group. This is realized by heating the TOPO/TOP capped nanocrystals to 60 °C and gradually adding pyridine (one of the many options available) in the mixture [**Figure A-1**]. Excess hexane is dispersed to flocculate the nanocrystals and then the solution is centrifuged to isolate the nanocrystals. The process is repeated a few times to produce crystallites which disperse readily in pyridine, methanol, and aromatics but no longer disperse in aliphatics.
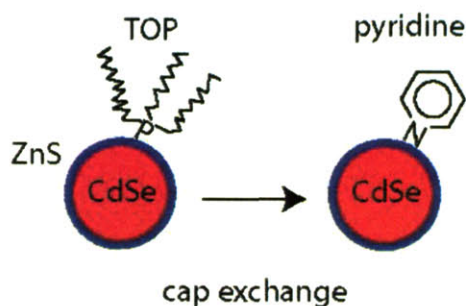
Figure A-1. Ligand exchange process to make nanocrystals dispersible in alcohols

Reference

[1]. C. B. Murray et al., Synthesis and characterization of nearly monodisperse CdE (E = sulfur, selenium, tellurium) semiconductor nanocrystallites, J. Am. Chem. Soc., 115, 8706 (1993).

[2]. B. O. Dabbousi et al., (CdSe)ZnS Core Shell Quantum Dots: Synthesis and Characterization of a Size Series of Highly Luminescent Nanocrystallites. J. Phys. Chem., 101, 9463 (1997).

Appendix B. Physics of QD Quantum Confinement: Particle-in-a-spherical-box model

The various optical properties of QD involve solid-state physics that have been studied for decades. The following paragraphs will review the physics basis of quantum dots.

The electron wavefunction and the potential field in space/solids are related, the Hamiltonian is simply written as:

$$\hat{H}\varphi(r) = [-\frac{\hbar^2}{2m}\nabla^2 + V(r)]\varphi(r) = E\varphi(r), \text{ where } \vec{r} = \vec{x} + \vec{y} + \vec{z} \qquad \text{(B-1)}$$

When the potential field is zero, the free electron wavefunction is:

$\varphi = A\exp(ikr)$ or $\varphi = A\exp(ikx)$ if the motion is simplified to one-dimension, here k is the wave number, which defines the energy state of the electron:

$$E = \frac{\hbar^2 k^2}{2m} \qquad \text{(B-2)}$$

This result shows that the energy of the free electron is continuous and in a parabolic shape versus the wave number.

In bulk crystalline solids, the potential field is periodic for the underlying Bravais lattice:

$V(r) = V(r + R)$, R is the lattice vector.

The eigenstates of the Schrödinger equation for an electron in such a periodic potential field are composed of $\psi(r) = \exp(ikr)u_{n,k}(r)$, a plane wave $\exp(ikr)$ and a periodic function $u_{n,k}(r)$,

and $u_{n,k}(r) = u_{n,k}(r + R)$. Here n is the band index and k the wave vector. This is the well-known Bloch theorem.

The energy eigenstates are given again by:

$$E = \frac{\hbar^2 k^2}{2m^*},$$

(B-3)

with m* represent the effective mass of the electron or the hole.

$$m^* = \frac{\hbar^2}{\partial^2 E(k)/\partial k^2}$$

(B-4)

In the case of electron as a quasi-free party being confined in a three dimensional potential field, namely an electron in a "box", the Schrödinger equation and the potential function can be written as:

$$\hat{H}\psi(r) = [-\frac{\hbar^2}{2m^*}\nabla^2 + V(r)]\psi(r) = E\psi(r)$$

(B-5)

$$V(x,y,z) = \begin{cases} 0 & x < a, y < b, z < c \\ \infty & x \geq a, y \geq b, z \geq c \end{cases}$$

(B-6)

One can proceed immediately that the amplitudes of wavefunction are zero at the boundaries and find the wavefunction and the energy of electron associated with the solutions to be given by:

$$\psi_{n_x,n_y,n_z} = \sqrt{\frac{8}{abc}} \sin(\frac{n_x \pi x}{a}) \sin(\frac{n_y \pi y}{b}) \sin(\frac{n_z \pi z}{c})$$

(B-7)

$$E_{n_x, n_y, n_z} = \frac{\hbar^2 \pi^2}{2m*} \left[(\frac{n_x}{a})^2 + (\frac{n_y}{b})^2 + (\frac{n_z}{c})^2 \right], \text{ with } n_i = 1, 2, 3 \ldots \tag{B-8}$$

When a = b =c =L, the system is degenerated because of the system symmetry:

$$E_{n_x, n_y, n_z} = \frac{\hbar^2 \pi^2}{2m* L^2} (n_x^2 + n_y^2 + n_z^2) \tag{B-9}$$

And the spacing between the discrete energy levels will be inversely proportional to the square of cube dimension $\Delta E \propto \frac{1}{L^2}$.

Suppose now the case turns into the electron-hole pair inside a spherical potential field, as a simple example, a semiconductor dot is surrounded by an infinitely high potential barrier. Neglecting the perturbation of the potential barrier to the electron (hole)'s parabolic energy band (approximation) and the Coulomb interaction between the electron – hole pair, the Hamiltonian is given by:

$$\hat{H} = \left[-\frac{\hbar^2}{2m_e} \nabla_e^2 - \frac{\hbar^2}{2m_h} \nabla_h^2 + V_e(r_e) + V_h(r_h) \right] \text{ with the potential being:}$$

$$V_i(r_i) = \left\{ \begin{array}{ccc} 0 & for & r_i < R \\ \infty & for & r_i \geq R \end{array} \right\} \ R \text{ is the radius of the quantum dot.} \tag{B-10}$$

Since we neglect the interaction between the electron and the hole, the envelop wavefunction can be separated to independent wavefunctions of electron and hole. $\psi = \phi_e(r_e) \cdot \phi_h(r_h)$

201

The derivation of this model yields the normalized wavefunctions for electrons (or holes) [1, 2]:

$$\phi_{nlm}^{i}(r) = Y_{lm}\sqrt{\frac{2}{R^3}}\frac{J_l(\chi_{nl}\frac{r}{R})}{J_{l+1}(\chi_{nl})}, \text{ with } -l \leq m \leq l; l = 0(s),1(p),2(d)...; n = 1,2,3.... \tag{B-11}$$

Y_{lm} is the spherical harmonic; J_l is the Bessel function;

Following the requirement of zero amplitude of wavefunction at the boundary:

$$J_l(\chi_{nl}\frac{r}{R})|_{R=r} = 0,$$

The energy eigenvalue is determined to be: $E_{nl}^{e.h} = \frac{\hbar^2}{2m_{e.h}}\frac{\chi_{nl}^2}{R^2}$ χ_{nl} is the nth zero of the

spherical Bessel function of order l. $\chi_{1s}=\pi$; $\chi_{1p}=4.493$; $\chi_{1d}=5.763$; $\chi_{2s}=2\pi$ and χ_{nl} increases when

n and l increase. The quantization of confined energy is easily seen here, for example, the lowest

1s energy state is shown as:

$$E_{1s}^{e.h} = \frac{\hbar^2}{2m_{e.h}}\frac{\pi^2}{R^2} \tag{B-12}$$

The energy of a particle in a spherical potential field discretely scales with the inverse of

radius square R^2.

A more precise model of one-electron-hole-pair in a confine system should include the

Coulomb interaction between the electron and the hole.

$$\hat{H} = \left[-\frac{h^2}{2m_e} \nabla_e^2 - \frac{h^2}{2m_h} \nabla_h^2 + V_e(r_e) + V_h(r_h) - \frac{e^2}{\varepsilon |r_e - r_h|} \right]$$ (B-13)

Unlike the bulk material where the Hamiltonian is separatable, inside a confined quantum dot, this dipole interaction acts as a perturbation to the symmetry of the system. There is no simple approach to get the exact analytical solutions. One relatively simple treatment takes into account that the Coulomb energy scales with $\frac{1}{R}$, while the kinetic energy scales with $\frac{1}{R^2}$. Let R_B denote the exciton Bohr radius. The strength of the Coulomb interaction can be justified by comparing the quantum dot radius R to the exciton radius R_B. In the so-called strong confinement range ($R \ll R_B$), the Coulomb interaction can be neglected, and the problem reduces to the non-interacting electron-hole pair described in the previous paragraphs. Alternatively when the quantum dot size is much larger than the Bohr radius ($R \gg R_B$), the case is analog to the particle in a box problem, where the electron-hole pair (exciton) is considered as single particle with the confining potential acting only on the center of mass motion. This is the so-called weak confinement.

An improved model that is one step closer to the reality is to replace the infinite barriers in the confining potentials with finite barriers. This approach has been adopted in the calculation of exact wavefunctions inside the quantum dots. Since the electron or hole wavefunctions can now penetrate into/ through the barriers, their wavefunctions are no longer identical. The once before dipole forbidden transitions can then occur with finite possibilities. Further discussion on this approach can be referred to other literature [2].

Reference

[1]. A. S. Davydov, Biology and Quantum Mechanics, Pergamon, Oxford (1982).

[2]. U.Woggon, *Optical Properties of Semiconductor Quantum Dots*, Springer, Berlin (1996).

Appendix C. Procedure flow of printing power phosphors EL layer

1. Select a wide-mouth jar of about 200 mL volume with a tight-fitting cap

2. Add liquid binder and phosphor powder to the jar in the ratio of 40 parts binder to 60 parts phosphor. Add the binder first.

3. Use a spatula to mix the phosphor and binder together. Make sure that no dry clumps remain.

4. Place the cap on the jar, and then start the jar on a slow rotation, about 4 to 8 revolutions per minute for 50 minutes.

5. When ready to print the phosphor layer, inspect the contents first. All the phosphor powders should be wetted and not any dry powder in the corners of the jar. Now the phosphor paste is ready for printing. Blade casting method is used to print a single layer (**Figure C-1**). A single printing of phosphor is usually sufficient.

6. Dry the phosphor layer in a convection oven at a temperature of 120 to 130 °C for 15 to 20 minutes.

7. The printing screen can be cleaned with an absorbent wiper wetted with ethylene glycol diacetate solvent.

8. The dielectric (insulating) layer can be applied in the same way. Normally it will need to print two or possibly three layers of dielectric with a drying step in between each layer.
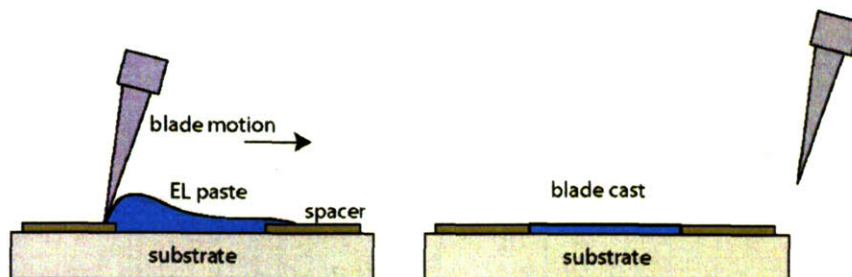
Figure C-1. Illustration of blade casting to form a thin layer of phosphors on top of the printed QD layer. The thickness of the phosphor layer is determined by the spacer.